TIME - DEPENDENT SEISMIC HAZARD ASSESSMENT FOR THE NORTH AND EAST ANATOLIAN FAULTS

by

Cem Koca

B.S., Civil Engineering, Yıldız Technical University, 2018

Submitted to Kandilli Observatory and Earthquake Research Institute
in partial fulfillment of
the requirements for the degree of
Master of Science

Graduate Program in Earthquake Engineering
Boğaziçi University
2022

TIME - DEPENDENT SEISMIC HAZARD ASSESSMENT FOR THE NORTH AND EAST ANATOLIAN FAULTS

DATE OF APPROVAL: 28.07.2022

ACKNOWLEDGEMENTS

I have learned a lot through this thesis, which is my first academic work in my education life. What I have gained in this process is not limited to academic knowledge. I deeply appreciate that a person cannot cope with such difficult periods of life alone. Therefore, it is a duty of loyalty to express my gratitude to the people who supported me in bringing this thesis to life.

First of all, I would like to express my gratitude to my thesis advisor, Asst. Prof. Karin Şeşetyan, for her help and patience within this period. However, these cliché expressions are quite inadequate to express the role of my thesis supervisor. I am grateful to her for giving me a place of free thought and expression. This has also gave me a "researcher mentality" and self-confidence to take the initiative. It is thanks to her that I am now excited to conduct new academic studies. Apart from these, the fact that my thesis advisor is such a good person deserves respect and gratitude per se.

I dedicate this paragraph to my invaluable friend Ph.D. candidate Gamze Canlı. I could not have carried out such a study without her moral support. I am grateful for sharing all her experiences and knowledge with me without any hesitation. Her presence during this period is a happy chance for me.

I also want to sincerely thank Prof. Eser Çaktı, and Prof. Ayşegül Askan for their valuable comments on my thesis.

I am also grateful to the Scientific and Technological Research Council of Turkey (TÜBİTAK) for granting me within the scope of 2211 - Domestic Graduate Scholarship Program and thereby providing financial support during my graduate education.

Finally, I would like to express my profound gratitude to my precious mother and father, Beyaz Koca and Adıgüzel Koca. I could not have completed my graduate studies without their understanding and support. I am very lucky to have such parents.

ABSTRACT

TIME - DEPENDENT SEISMIC HAZARD ASSESSMENT FOR THE NORTH AND EAST ANATOLIAN FAULTS

Until now, many probabilistic seismic hazard assessment (PSHA) studies have been performed for Turkey. However, except in a limited number of cases, characteristic fault source modeling was not used. Since the North and East Anatolian Faults (NAF and EAF) have a tendency for rupturing in characteristic earthquakes, the first objective of this research is to develop a sound hybrid characteristic recurrence model for the NAF and EAF. The so-called hybrid model involves a composite characteristic model (i.e., an exponential part for the smaller and a characteristic part for larger magnitudes) developed for each segment combined with a characteristic recurrence proposed for multi-segment ruptures. Two different hybrid earthquake recurrence models with time - independent (or Poissonian) and time – dependent (or renewal) characteristics are developed. By means of the renewal hybrid model, the effect of some seismic gaps along the NAF and EAF on seismic hazard is assessed, which is the primary purpose of the thesis. On the other hand, these two models have also given the opportunity to evaluate the results of the fully exponential model of the NAF and EAF. The comparison between different earthquake recurrence models developed for the NAF and EAF yields interesting results. Fully exponential model usually produces overestimated seismic hazard compared to the Poissonian hybrid – characteristic model. Slip deficits on some fault segments can increase the seismic hazard dramatically if the results of renewal hybrid model are considered. Although the overestimated results of fully exponential fault source model can compensate the high hazard based on renewal hybrid model, depending on the amount of slip deficit, the time – dependent hazard may exceed the hazard obtained by the fully exponential model. In cases where there is a considerable amount of slip deficit on a fault, a time - dependent seismic hazard model should be developed to deal with the worst-case scenario.

ÖZET

KUZEY VE DOĞU ANADOLU FAYLARININ ZAMAN BAĞIMLI DEPREM TEHLİKESİNİN DEĞERLENDİRİLMESİ

Türkiye için birçok olasılıksal sismik tehlike modeli geliştirilmiştir. Ancak az sayıdaki birkaç örnek dışında bu çalışmalarda karakteristik fay modellemesi yöntemi benimsenmemiştir. Kuzey Anadolu (KAF) ve Doğu Anadolu (DAF) faylarında karakteristik depremlerle kırılma eğilimi gözlemlenmesi nedeniyle, bu araştırmanın öncelikli amacı KAF ve DAF için akla yatkın hibrit karakteristik deprem tekerrür modelleri geliştirmektir. Önerilen hibrit model, fay segmentlerinin herbiri için küçük magnitüdlerde üstel, büyük magnitüdlerde ise karakteristik tekerrür modelini birleştirmekte, ve bunlara ek olarak çoklu segment yırtılmaları için de ayrı bir karakteristik tekerrür modelini kapsamaktadır. Bu tez çerçevesinde zaman bağımsız ve zaman bağımlı niteliklerde iki farklı hibrit deprem tekerrür modeli geliştirilmiştir. Zaman bağımlı hibrit model aracılığıyla KAF ve DAF boyunca kimi sismik boşlukların sismik tehlike üzerindeki etkisi değerlendirilmiştir. Öte yandan bu iki hibrit model, KAF ve DAF için tam üstel tekerrür modeli sonuçları ile karşılaştırma olanağı sunmaktadır. KAF ve DAF için geliştirilen farklı deprem tekerrür modellerinin kıyasından ilginç sonuçlar elde edilmiştir. Zaman bağımsız hibrit karakteristik modele kıyasla tam üstel model yüksek sonuçlar vermektedir. Zaman bağımlı hibrit modelin sonuçları dikkate alındığında, bazı segmentlerdeki kayma açığının sismik tehlikeyi çarpıcı bir şekilde arttırdığı görülmektedir. Her ne kadar tam üstel modelin yüksek sonuçları zaman bağımlı modelden elde edilen sismik tehlikeyi karşılayabilse de bazı durumlarda kayma açığına bağlı olarak zaman bağımlı tehlike, tam üstel modelden elde edilen tehlikeyi aşabilmektedir. Dolayısıyla bir fay üzerinde ciddi bir kayma açığı olduğu durumlarda en kötü senaryo ile baş edebilmek adına böylesi bir fay için zaman bağımlı sismik tehlike modeli geliştirilmelidir.

TABLE OF CONTENTS

LIST OF FIGURES

LIST OF TABLES

LIST OF SYMBOLS

a	The absolute seismicity level of the magnitude probability density function curve
A	Area
A_f	Total fault plane area
b	The slope of the magnitude probability density function curve
L	Length
M	Magnitude
Mmin	Minimum magnitude
Mchar	Characteristic magnitude
Ms	Surface wave magnitude
Mw	Moment magnitude
m°	Arbitrary reference magnitude
m^u	Upper bound magnitude
M_0^u	Moment for the upper bound magnitude
P_{cond}	Conditional probability
R	Source-to-site distance
T	Natural period
Vs30	The average velocity of shear waves in the top 30 m of soil
α	Aperiodicity
λ, λ_m or N	Mean annual rate of earthquake occurrence
μ	Mean earthquake recurrence interval
μ_Y	The shear modulus
σ	Standard deviation

LIST OF ACRONYMS/ABBREVIATIONS

AFAD	Disaster and Emergency Management Authority of Turkey
Ave	Average
BPT	Brownian Passage Time
CA	Cyprus Arc
CoV	Coefficient of variation
Char.	Characteristic
DSF	Dead Sea Fault
EAF	East Anatolian Fault
eq.	Earthquake
Exp.	Exponential
EAFZ	East Anatolian Fault Zone
GMIM	Ground motion intensity measure
GMM	Ground motion model
G-R	Gutenberg - Richter
km	kilometer
KMZ	Kyrenia–Misis Zone
Max.	Maximum
MFD	Magnitude frequency distribution
Min.	Minimum
MLE	Adjusted maximum likelihood estimation
mm	Milimeter
MTA	The institue of Mineral Research And Exploration
NAF	North Anatolian Fault
NAFZ	North Anatolian Fault Zone
PDF	Probability density function
PGA	Peak Ground Acceleration (in g)
PGV	Peak Ground Velocity (in m/s)
PSA	Pseudo-spectral Acceleration (in g)

PSHA	Probabilistic seismic hazard assessment
RA	Rupture area
RP	Return period
SA	Spectral Acceleration (in g)
SoF	Style-of-faulting
SC	Site class
Sr, S	Slip rate
SRL	Surface rupture length
TI	Time - Independent
TR	Recurrence interval
UDAP-Ç-13-36	The Revision of Turkish Seismic Hazard Map Project
yr, yrs	year, years

1. INTRODUCTION

The Alpine-Himalayan orogenic system is one of the planet's seismically most active regions. Turkey is situated in the Eastern Mediterranean portion of this system. As asserted by Kadirioğlu et al. [12], in a period of 113 years between 1900 and 2012, the number of earthquakes with Mw$\geq$6.0 occurred in Turkey and its near vicinity is 203. While the death of even one person is unacceptable, more than 90 thousand people died due to the most destructive 72 of these earthquakes. Earthquakes per se are not the cause of these casualties since they don't kill people, buildings do [13]. Moreover, Turkish economy has had to shoulder a financial burden of more than 50 billion dollars in total because of such earthquakes [14]. Leaving aside the material effects, the destruction caused by earthquakes has crippling psychological effects on people, which is the most profound one for me. A lot of research (e.g., [15–18]) has demonstrated that earthquakes cause some psychological problems in children, adolescents and adults. Şalcıoğlu and Başoğlu [19] have indicated that loss of control that is brought on by exposure to unpredictable and uncontrollable earthquakes seems to be a mediator of traumatic stress. Hence, if the subject is seismic hazard analysis, all earthquake occurrence models should be evaluated and the most suitable one(s) for the studied faults should be chosen, which is a rational approach to deal with the earthquake hazard in the best possible way.

The history of seismic hazard analysis in Turkey dates back to the 1940s. A multitude of seismic zonation maps were drawn to depict the earthquake hazard in Turkey [3]. The first attempt to perform seismic hazard analysis of the region was made in 1980 by Yarar et al. [20]. Nevertheless, the first national earthquake hazard project in Turkey was launched in 1985 by Erdik et al. [21]. After this date, many research projects on national or international-scale probabilistic seismic hazard assessment were set up for Turkey and its surroundings. Few of these projects used fault source as seismic source characterization [3]. When fault sources were incorporated in these large-scale projects, fully exponential magnitude recurrence relationship was used in all of them, including the latest Turkish Seismic Hazard Map. To illustrate, SHARE (Seismic

Hazard HARmonization in Europe [22]) Project has used Anderson and Luco [23] exponential recurrence relationship for the North Anatolian Fault (NAF) and the East Anatolian Fault (EAF). On the other hand, within the scope of EMME (Earthquake Model of the Middle East [24]) Project, Youngs and Coppersmith [25] exponential earthquake occurrence model is adopted for fault sources. Consequently, seismic hazard analyses involving the characteristic and/or hybrid fault source modeling has been limited to a number of local studies (e.g., [26] for the Eastern Marmara region and [27]).

The presence of some seismic gaps along NAF and EAF (e.g., Yedisu segment on the NAF and Pazarcık segment on the EAF) implies the construction of time – dependent seismic hazard models. This is because the seismic gaps can cause unforeseen ground motion levels around the related faults. Contrarily, overestimated ground motion intensity measures (GMIMs) can be used in the design of structures to be built in the central and western North Anatolian Fault Zone (NAFZ), which discharged its stored seismic energy with major events in the 20th century. Undoubtedly, this will have economic consequences. All these questions cannot be answered without building a robust time - dependent model for the NAF and EAF. However, the lack of characteristic fault source models for the entire length of these two faults is a chief obstacle in developing renewal models. Therefore, the time – dependent seismic hazard analysis has not been performed for the whole NAF and EAF yet.

In this study, instead of fully characteristic recurrence model, a hybrid characteristic - exponential recurrence modeling approach parallel to the model proposed by Youngs and Coppersmith [25] is adopted. That is, while the recurrence of major earthquakes has been modelled by characteristic recurrence, earthquakes with smaller magnitude are represented through exponential magnitude recurrence relationship in the same model. This is because it has been detected that fully characteristic recurrence model does not possess coherence with observed seismicity (i.e. recurrence intervals (TR) determined by paleoseismic investigations). In this sense, 6% of the total seismic moment rate accumulated on the fault is assigned to exponential tail and the remaining part is given to the characteristic recurrence.

The difference with the composite characteristic model of Youngs and Coppersmith [25] is that multi-segment ruptures are also allowed in the recurrence. The model includes three components:

(i) An exponential part covering the recurrence of earthquakes from Mmin to Mchar - 0.1 units for each segment,

(ii) A characteristic recurrence at Mchar of each segment, considering that the segments may rupture individually,

(iii) A multi-segment rupturing characteristic recurrence model, which accounts for very large magnitude earthquakes such as 1939 Erzincan earthquake.

Another overwhelming advantage of this time – independent hybrid model is that it can be adapted to a renewal one. Thus, the effect of time – dependency on seismic hazard in the NAFZ and EAFZ is assessed in this research.

Other earthquake recurrence models (e.g., fully characteristic, classical Youngs and Coppersmith's composite model [25]) have also been used to validate the obtained hybrid model. After the hybrid model has proven its rationality, background – smoothed seismicity and the secondary faults are also included. Thus, in content, our hybrid model becomes comparable to fully exponential model constructed by Demircioğlu et al. [28].

Seismic hazard analyses have been performed for mean peak ground acceleration (PGA) and 5% damped spectral acceleration (SA) at T=0.2 and 1 s for rock conditions (Vs30 = 760 m/s). The probabilities of exceedance of these GMIMs in the next 50 years presented herein are 10% and 2%. OpenQuake Software [29] is operated to do the analyses. The results are shown as both GMIM values on selected sites along the faults and seismic hazard distributions within the buffer zone of the faults.

1.1. Objectives and Scope of the Thesis

That segmented individual faults like the Wasatch fault zone are predisposed to rupturing in characteristic earthquakes has been ascertained by Schwartz and Coppersmith [30]. This has led to the construction of Youngs and Coppersmith's characteristic earthquake model [7].

Since the North and East Anatolian Faults are also well-developed strike-slip faults with segmentation, they show a tendency for characteristic rupture behavior. In this study, we aim to develop a characteristic fault source model for the NAF and EAF and to analyze the effects of characteristic modeling in the determination of the seismic hazard in the region. While some segments of both fault zones have been recently ruptured, some of them have remained silent for several centuries. As such, we also aim to examine the effect of time dependency on the seismic hazard estimations.

Another objective of the study is to compare results of time - dependent vs independent models as well as characteristic/hybrid vs. fully exponential fault source modeling. Instead of building fully exponential earthquake recurrence models for the NAF and EAF, the results of the research done by Demircioğlu et al. [28] are directly used to make such a comparison.

Within the scope of the research, we examine the whole EAF while evaluating the central and eastern sections of the NAF, starting from the segments ruptured in the 1944 Bolu – Gerede earthquake. Thus, we excluded the part of the NAF in the Marmara region from the study as it is illustrated in Figure 1.1. This is because many studies even involving time - dependency have already been undertaken for the Marmara region (e.g., [7, 26, 27]). The fault segmentation model used herein is based on the research done by Emre et al. [14] in terms of both geometry and kinematic properties.

Figure 1.1. The NAF and EAF's segments studied in this thesis

2. LITERATURE SURVEY: PSHA HISTORY AND CURRENT HAZARD MAP IN TURKEY

Humankind has endeavored to make sense of the occurrence of earthquakes since ever since it entered on the stage of history. Earthquakes have even attributed to the righteous anger of God [31], which is consistent with the argument known as the “The God of the Gaps”, a perspective filling in gaps in the explanation of the phenomena of nature with Gods [32]. When we look at the history of mankind’s struggle with earthquakes, the first estimation of seismic hazard with respect to ground motion intensity measures (e.g., PGA) is carried out by C. Allin Cornell [33]. This is the foundation for modern Probabilistic Seismic Hazard Analysis (PSHA) [34].

As for Turkey in terms of the history of PSHA, seismic hazard studies, only in the form of an earthquake zonation map, have started in the first half of the 1930s. As it would be estimated, such studies could only be performed using earthquake catalogs and macroseismic intensity at that time. The first attempts to analyze probabilistic seismic hazard in the region was made in the late 1970s (e.g., [20, 35]). It is worth emphasizing that until the late 1990s, the use of seismic zoning map to define design spectrum was a worldwide tradition. Namely, this was not a situation specific to Turkey [3].

In 1932, the first seismic zoning map of Turkey, shown in Figure 2.1, was drawn by Sieberg [1] using sharply limited data and studies. However, it has not been officially approved. In addition to seismic zones, the map also includes faults, rivers, lakes and the names of important settlements. Showing Konya and Ankara within the earthquake zone and the absence of the NAF are the striking features of the map [2].

After the 1939 Great Erzincan Earthquake, caused 32962 casualty and destroyed or damaged 116720 dwellings, earthquake risk mitigation brought to the fore in Turkey. Until 1945, this severe event was followed by another destructive earthquake series (i.e.,

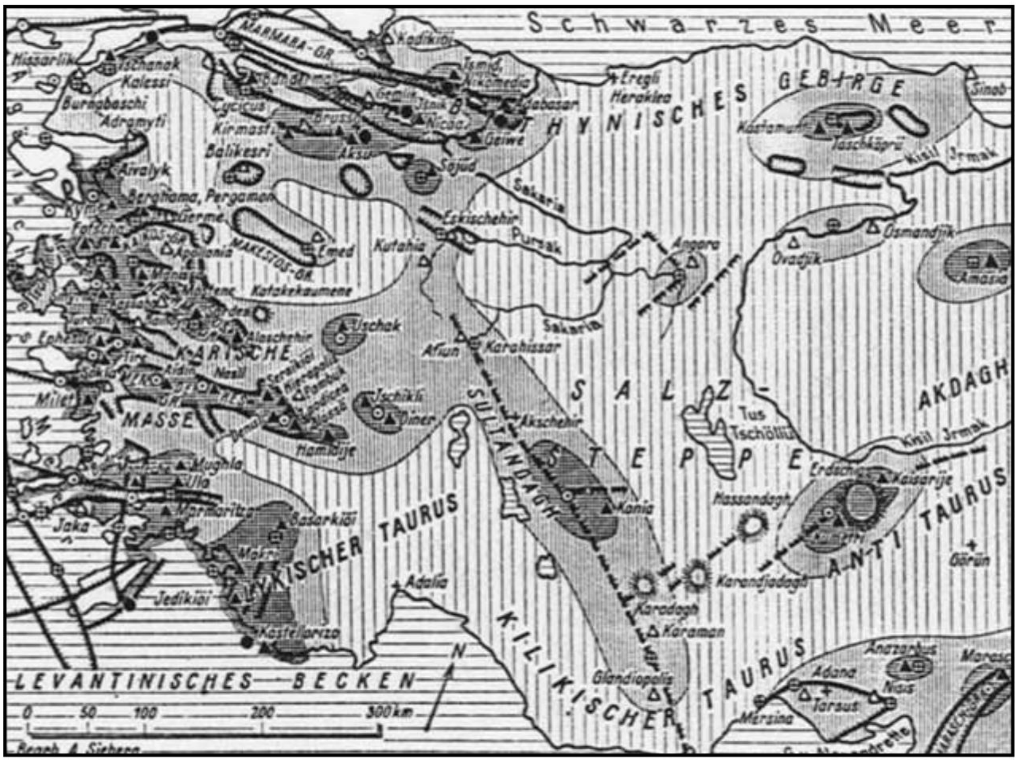

Figure 2.1. Earthquake zonation map prepared by Sieberg [1](Figure from the research done by Özmen [2])

1942 Erbaa - Niksar, 1943 Tosya - Ladik, 1944 Bolu - Gerede earthquakes) along the NAF. Eventually, Turkey's first official earthquake zonation map was produced and published in 1945. This map splitted the country up three seismic regions. As is shown in Figure 2.2, while the first zone (dark red) is representing high earthquake hazard level, the second (light red) and the third ones (white) are depicting less and no hazard level, respectively. Since 1945, numerous official or unofficial earthquake hazard maps have been declared for Turkey as it is explained in meticulous details by Özmen [2] and Akkar et al. [3]. In those maps, it is necessary to dwell on the one produced in 1996. Up to this date, all seismic zonation maps were based on ground motion-induced structural damage or macro-seismic intensity. In this sense, the map arranged in 1996, seen in Figure 2.3, is the first one originated in a PSHA, undertaken by Gülkan et al. [36]. On the other hand, the seismic zonation concept is valid for all but the latest Turkish Seismic Hazard Map.

Figure 2.2. The first official earthquake zonation map of Turkey [2]

Within the framework of the National Earthquake Strategy and Action Plan-2023, Disaster and Emergency Management Presidency (AFAD) launched a project in 2013. The purpose was to develop a state-of-the-art earthquake hazard map at the national level for the first time after the study conducted by Gülkan et al. [36] and to use it in Turkish seismic design code for buildings. Another primary motivation behind this project is to create contour maps to use in the design spectrum calculations of the revised Turkish earthquake-resistant design specification. The necessary consequence of this intention is to leave behind the seismic zonation concept for defining lateral and vertical seismic loads [3].

The latest version of Turkish Seismic Hazard Map demonstrates the continuous change of PGA, peak ground velocity (PGV) or SA (i.e., ground motion intensity measure) for a chosen period by taking into consideration the position of the relevant site with reference to the seismic source. It should be reminded that seismic zoning maps has no such property; that is, these maps assign a fixed value to a selected ground motion intensity parameter within the same seismic zone. The seismic zone concept primarily illustrates the typical characteristics of prominent seismotectonic provinces and their activity within the region. Actually, for a pre-delineated earthquake zone, the total change of a ground motion intensity measure through contour lines is shown

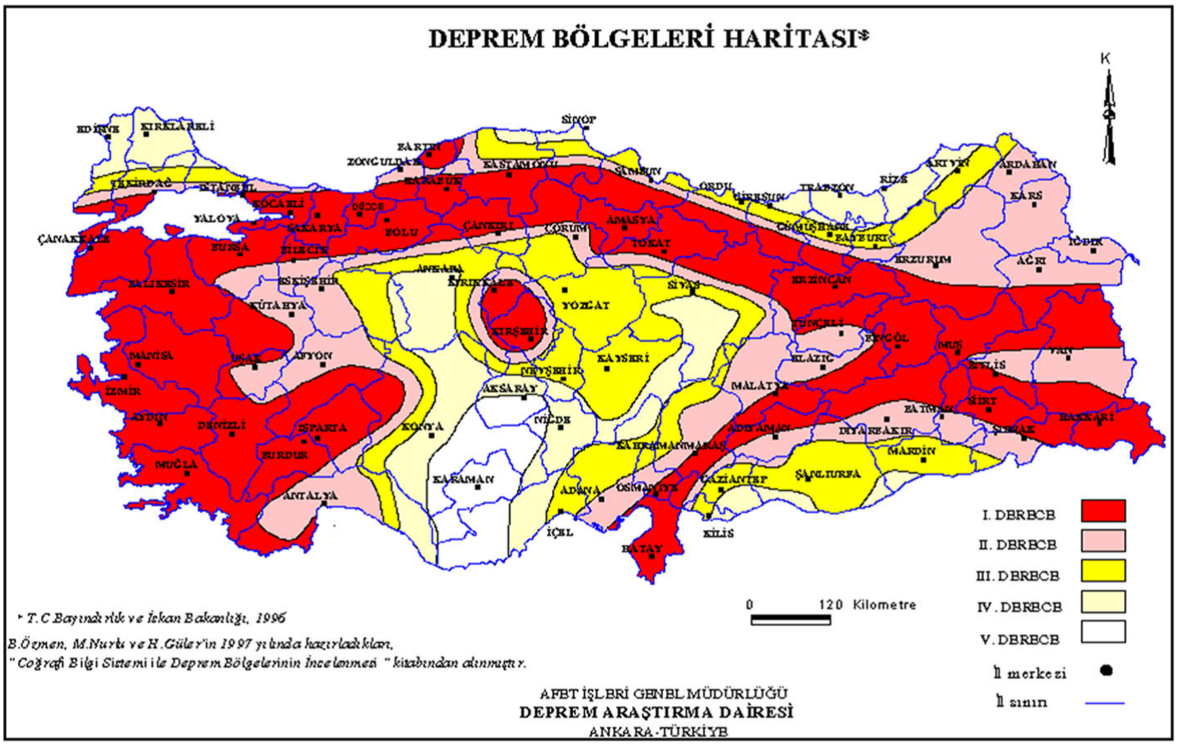

Figure 2.3. Seismic Zoning Map that was produced in 1996 [3]

by the features of the constant value proposed in the zonation map. In this respect, earthquake zonation maps correspond to the simple form of seismic contour maps. The reason why seismic zonation maps were widely used in estimating earthquake loads until the early 2000s was the lack of well-developed geographic information systems. In other words, the geographical distribution of the ground motion parameters could not be shown. Compared to the zonation map, the contour based one is more realistic to display the amplitude of PGA, PGV or PSA values for a chosen return period (RP) because the constant value offered by zonation maps disregards the uniform distribution of the target return period in the relevant seismic zone. Since this is not the case for contour maps, the uniformity in the target return period is the sine qua non for these maps [3].

Even though the initiation of seismic design code dates back to 1949 in Turkey, the first PSHA project that intended to draw an earthquake hazard map for Turkey was run by Yarar et al. [20]. After 1980, such PSHA projects have been carried out in a small quantity not exceeding the number of fingers on both hands. These national or international studies are listed chronologically below:

- Yarar et al. [20];
- Erdik and Öner [37]
- Erdik et al. [21]
- Onur [38]
- Bommer et al. [39]
- Jimenez et al. [40]
- Demircioglu et al. [41]
- Woessner et al. [22]
- Şeşetyan et al. [24] and Danciu et al. [42]

Among these projects carried out on a national scale ([20–22, 24, 37–41]) concentrated only on the prediction of target hazard levels.

Here, the salient characteristics of the aforementioned national and international seismic hazard projects will be highlighted so as to develop the awareness of the evolution of seismic source modeling, ground-motion characterization and PSHA implementation (see Akkar et al. [3]), the principal source of this chapter, to get further information). It should also be indicated that although the study made by Yarar et al. [20] is the first PSHA, it is not a large-scale PSHA project (i.e., as its authors state, it is a preliminary study). This research, therefore, is not going to be mentioned in the following paragraphs.

The noteworthy features of the projects to be discussed will be presented in brief information.

(i) Erdik et al. [21]
  - Regions studied in the project: Turkey
  - Seismic source delineation: Area sources
  - Ground motion characterization: While Erdik et al. [43] is used for macro-

seismic intensity, Schnabel and Seed [44] with near field adjustments from Campbell [45] is employed for PGA.

- Distinctive qualities:

  Selected ground motion intensity measure: PGA and macroseismic intensity

  Return periods: 225, 475 and 10000 years

  Logic tree: There is no logic tree.

  Reference site: Reference site is rock. However, there is not any specific metric to define its circumstances.

(ii) Gülkan et al. [36]

- Regions studied in the project: Turkey
- Seismic source delineation: Area sources
- Ground motion characterization: Joyner and Boore [46]
- Distinctive qualities:

  Selected ground motion intensity measure: PGA

  Return periods: 100, 225, 475 and 1000 years

  Logic tree: It is not included.

  Reference site: Reference site is stiff soil.

(iii) SESAME (Unified Hazard Model for the European - Mediterranean Region [40])

- Regions studied in the project: Turkey including Europe
- Seismic source delineation: Area sources
- Ground motion characterization: Ambraseys et al. [47]
- Distinctive qualities:

  Selected ground motion intensity measure: PGA and PSA at T = 0.3 and 1.0 s (5% damping ratio)

  Return periods: 475 years

  Logic tree: It is not included.

  Reference site: Reference site is rock. However, there is not any specific metric to define its circumstances.

(iv) TEFER (Turkish Emergency Flood and Earthquake Recovery Programme [39])

- Regions studied in the project: Turkey
- Seismic source delineation: Area sources
- Ground motion characterization:

  Active shallow crust: While Campbell [48], Boore et al. [49], Sadigh et al. [50] are used for PGA, Boore et al. [49]), Sadigh et al. [50] are applied for PSA.
- Distinctive qualities:

  Selected ground motion intensity measure: PGA and PSA at T = 0.3 and 1.0 s (5% damping ratio)

  Return periods: 475 and 2475 years

  Logic tree: Identical weights are assigned to the aforementioned ground motion models (GMM).

  Reference site: Reference site is rock. However, there is not any specific metric to define its circumstances.

(v) DLH (Demircioğlu et al. [41])

- Regions studied in the project: Turkey
- Seismic source delineation: Area and fault sources
- Ground motion characterization:

  Active shallow crust: While Campbell [48], Boore et al. [49], Sadigh et al. [50] are used for PGA, Boore et al. [49]), Sadigh et al. [50] are applied for PSA.
- Distinctive qualities:

  Selected ground motion intensity measure: PGA and PSA at T = 0.2 and 1.0 s (5% damping ratio)

  Return periods: 475 and 2475 years

  Logic tree: Identical weights are assigned to the aforementioned GMMs.

  Reference site: Reference site is rock and VS30 equals to 760 m/s.

(vi) SHARE (Seismic Hazard HARmonization in Europe [22])

- Regions studied in the project: The entire Europe, including Turkey
- Seismic source delineation: Area source model (uses Guttenberg - Richter occurrence model), Kernel smoothed seismicity, Fault and background seis-

micity (adopt Anderson and Luco [23] recurrence relationship)

Tectonic regionalization: Stable regions (shield and continental crust), oceanic crust, active shallow crust (compression, extension, strike - slip, mid - oceanic ridges), subduction zones, deep seismicity regions and volcanos

- Ground motion characterization:

  For active shallow and oceanic crust: Zhao et al. [51] (0.1), Cauzzi and Faccioli [52] (0.35); Chiou and Youngs [53] (0.2); Akkar and Bommer [54] (0.35)

  For stable continental regions: Toro [55] (0.2), Campbell [56] (0.2), Cauzzi and Faccioli [52] (0.2), Chiou and Youngs [53] (0.2), Akkar and Bommer [54] (0.2)

  For stable (shield): Toro [55] (0.5), Campbell [56] (0.5)

  For subduction inslab and interface: Youngs et al. [57] (0.2), Atkinson and Boore [58] (0.2); Zhao et al. [51] (0.4), Lin and Lee [59] (0.2)

  For volcano: Faccioli et al. [60] (1.0)

  For deep seismicity: Lin and Lee [59] (0.5), Youngs et al. [57] (0.5)

- Distinctive qualities:

  Selected GMIMs: PGA and PSA until T = 10 s (5% damping ratio)

  Return periods: 225, 475 and 10000 years

  Logic tree: For the source model, the weights of logic tree branches change with the return periods:

  For the return periods smaller than 475 years, the area source, Kernel smoothed seismicity and the fault source with background seismicity weights are 0.45, 0.45, and 0.10, respectively. For the return periods between 475 and 2475, the weights equal to 0.50, 0.30 and 0.20. For the return periods greater than 2475 years, corresponding weights are 0.60, 0.10 and 0.30.

  On the other hand, as for the ground motion models, presented in "ground motion characterization" part, the weights of logic tree branches have been shown in parenthesis next to each GMM name.

  Reference site: Reference site is rock and VS30 equals to 800 m/s. Kappa modification is made to Toro [55] and Campbell [56] GMMs for reference rock circumstances.

(vii) EMME (Earthquake Model of the Middle East [24, 42])

- Regions studied in the project: Middle East, Caucuses and Pakistan
- Seismic source delineation: Area source model and fault source model that incorporates smoothed seismicity are used. While area source and smoothed seismicity employ Guttenberg - Richter earthquake occurrence relationship by using historical and instrumental earthquake datasets, for faults, Youngs and Coppersmith exponential earthquake occurrence model [25] is established by using slip rates based on geologic findings. Shallow crust, stable regions, deep seismic sources, subduction interface and inslab sources depict tectonic regions.
- Ground motion characterization:

  For active shallow crustal regions: Akkar and Cagnan [61] (0.2), Akkar et al. [62] (0.35), Chiou and Youngs [53] (0.35), Zhao et al. [51] (0.1)

  For stable shallow crustal regions: Atkinson and Boore [63] (0.4), Toro [55] (0.25), Campbell [56] (0.35)

  For subduction interface and inslab: Atkinson and Boore [58], Lin and Lee [59] (0.2), Youngs et al. [57] (0.2), Zhao et al. [51] (0.4)

  For deep seismicity: Lin and Lee [59] (0.5), Youngs et al. [57] (0.5)
- Distinctive qualities:

  235 area and 778 fault sources are used within the scope of this study.

  Selected ground motion intensity measures: PGA and PSA at T = 0.10, 0.15, 0.20, 0.25, 0.30, 0.50, 0.75, 1.0 and 2.0 s (5% damping ratio)

  Return periods: 72, 475, 975, 2475 and 4975 years

  Logic tree: Branch weights of the area and fault source models, mentioned in "seismic source delineation" section, are chosen as 0.6 and 0.4, respectively. Logic tree weights of the ground motion prediction models, presented in "ground motion characterization" part, have been shown in parenthesis next to each GMM name.

  Reference site: Reference site is rock and VS30 equals to 800 m/s.

(viii) T-SHM (The Revised Turkish Seismic Hazard Map Project [3])

This is the final project in which Turkey's probabilistic seismic hazard is analyzed. It is supported by AFAD with the project code of UDAP-Ç-13-36.

- Regions studied in the project: Turkey
- Seismic source delineation: Area source model [64] and fault source model that incorporates smoothed seismicity [28] are used. While the area sources and smoothed seismicity employ Guttenberg - Richter earthquake occurrence relationship by using historical and instrumental earthquake datasets, for faults, Youngs and Coppersmith exponential earthquake occurrence model [25] is developed. Shallow crustal, subduction interface and in - slab sources are the tectonic regions of area source model.

  The fault and background smoothed seismicity source models are based on the active fault database produced by Emre et al. [14, 65] and Duman et al. [66]. Earthquakes with magnitudes greater than 6, whose epicenter is within the 15 km buffer zone surrounding the relevant main fault line (e.g., the NAF or EAF), are related to fault sources. On the other hand, the hazard contribution of the earthquakes with moment magnitude between 4.5 and 6 is calculated through smoothed seismicity [67]. It is thought that such earthquakes do not occur directly on the faults; therefore, they are represented in the background as point sources.
- Ground motion characterization:

  PGA and PSA:

  For active shallow crustal regions: Akkar et al. [62] (0.30), Chiou and Youngs [53] (0.30), Akkar and Cagnan [61] (0.30), Zhao et al. [51] (0.10)

  For subduction interface and inslab: Zhao et al. [51] (0.40), Atkinson and Boore [58] (0.20), Youngs et al. [57](0.20), Lin and Lee [59] (0.20)

  PGV:

  For active shallow crustal regions: Akkar et al. [62] (0.33), Chiou and Youngs [53] (0.33), Akkar and Cagnan [61] (0.33)

  For subduction interface and inslab: Megawati and Pan [68] - interface (1.0), Garcia et al. [69] - inslab (1.0)

- Distinctive qualities:

  235 area and 778 fault sources are used within the scope of this study.

  Selected ground motion intensity measures: PGA, PGV and PSA at T = 0.20 and 1.0 s (5% damping ratio)

  Return periods: 43, 72, 475, 975, and 2475 years

  Logic tree: Logic tree weights of the area and fault source models are equal with respect to each other.

  Branch weights of the ground motion prediction models, presented in “ground motion characterization” part, have been shown in parenthesis next to each GMM name.

  Reference site: Reference site is rock and VS30 equals to 760 m/s.

The summary of these projects:

- While a limited number of ground-motion predictive models is used to obtain ground motion intensity measures (primarily PGA) in early projects, TEFER and its successor studies employ many GMMs.
- Until the study undertaken by Demircioğlu et al. [41], area source model was necessarily the only option to identify seismic sources because there was a rudimentary knowledge of faults. Furthermore, the broad tendency toward characterization of seismic sources and ground-motions is to ignore epistemic uncertainty.
- In addition to the notable advancements in constructing reasonable models to typify seismic sources and ground-motions, immensely complex application of PSHA have begun with SHARE and EMME projects. That is, area and fault sources with background smoothed seismicity are integrated through a complicated logic tree to decrease epistemic uncertainty. These two serious studies also encouraged T-SHM project in terms of the modeling method they adopted and background research they conducted.

3. THE DISTINCTIVE CHARACTERISTICS OF THE NAF AND EAF

The NAF and EAF, which are at the focal point of this study, are home to most of the devastating earthquakes in mainland Turkey. This is why the typical features of the NAF and EAF are examined in this chapter, respectively.

The Anatolian microplate, accommodating the NAF and EAF, and its surrounding plates are illustrated in Figure 3.1. Anatolia can be divided into three tectonic provinces [70]. The western one is the extensional province, colored in yellow, the central one is the "Ova" province, colored green, and the eastern one is the contractional province, colored red in Figure 3.1. The Anatolian block is located in an intricate tectonic system governed by collisions [4]. The movement of the Arabian plate toward the north causes the Anatolian microplate to move counterclockwise, which leads to internal deformation in the Anatolian block itself [71]. The counterclockwise rotational movement of the Anatolian block, demonstrated by Reilinger et al. [72], results in that the direction of motion becomes perpendicular to the Hellenic Arc and the amount of movement hits its maximum value in the west. Besides, the internal deformations of the Anatolian block in central Turkey and the Eastern Anatolian zone are detected by Aktuğ et al. [28, 73–75]. The NAF, the northern border of the Anatolian block, is one of the gigantic active strike-slip faults not only in Turkey but also in the world. It follows the route from the Gulf of Saros, located in the northern Aegean Sea, to the Karlıova triple junction. This fault line is approximately 1200 km long between the mentioned locations [5,6]. The NAF holds most of the deformation along the northern boundary of the westward moving Anatolian microplate, which molds predominantly dextral strike-slip motion [4].

As for the geologic time at which the NAFZ has begun to take shape, there is a consensus on that it is between the late Miocene and the early Pliocene [5].

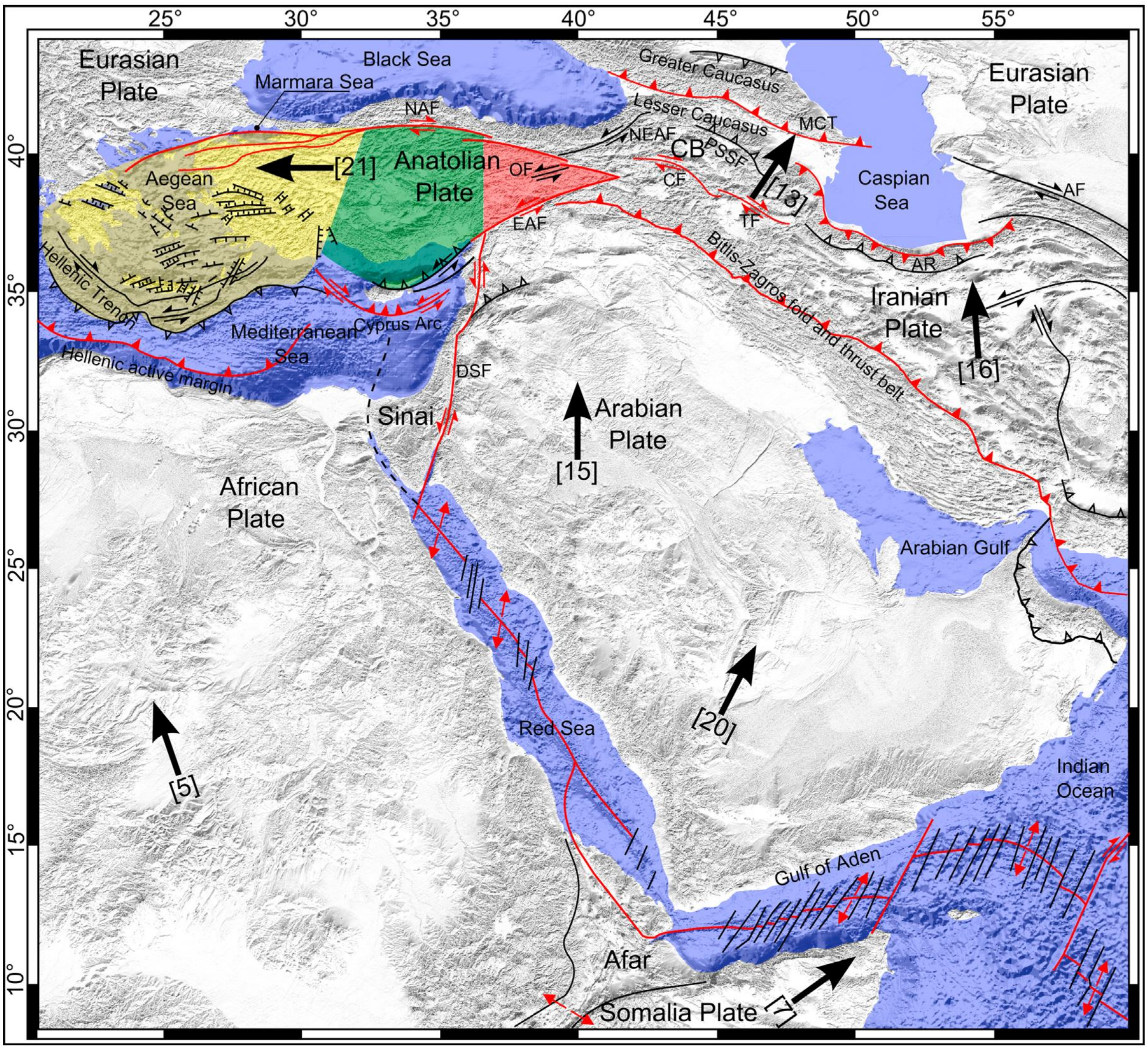

Figure 3.1. Anatolian microplate region [4]

A multitude of interpretations were made to understand the structure of the NAFZ until 1948. However, a distinctly different explanation was proposed by İhsan Ketin [76]. He indicated that surface ruptures occurred during massive earthquakes generally exhibit east-west-striking, right-lateral behavior. Ketin's declaration was the first authentication of the existence of a sizable and active strike-slip fault across the globe. Furthermore, the NAFZ's recognition as a great strike-slip fault has been started by Prof. İhsan Ketin [6].

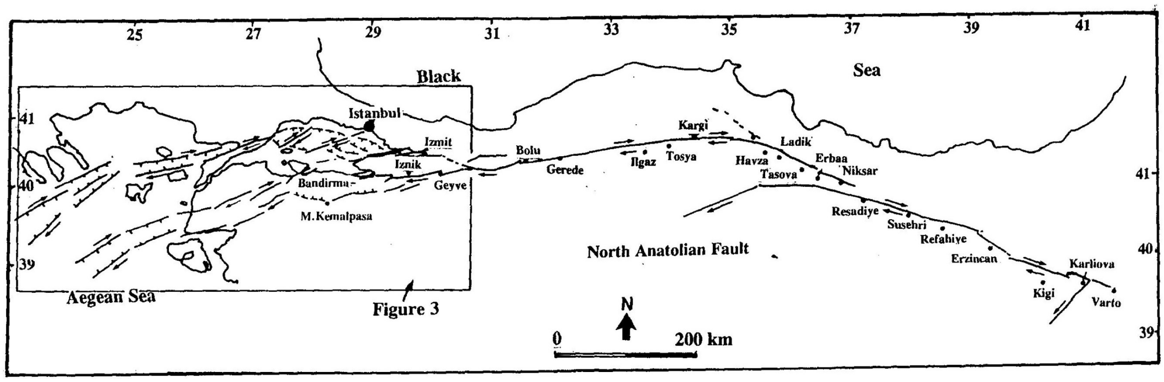

Figure 3.2. Three main parts of the NAF [5]

The NAFZ can be subdivided into three large sections: the Eastern part, from Karlıova to Niksar, the Central part, from Niksar to the west of Bolu, and the Western part, roughly shown in a rectangle in Figure 3.2. While a limited deformation zone typifies the Eastern and Central NAFZ, the Western part is an example of a broad deformation zone. It should be noted in advance that while the Western section is ignored in the scope of this study, fault segments that was ruptured during the 1957 and 1967 earthquakes are not considered as a portion of the Central section (i.e., only the part of this section extending up to Bolu has been examined).

The Eastern NAF covers a length of approximately 430 km between the Karlıova triple junction and the Niksar releasing stepover. Along this part, the Erzincan pull-apart basin is the foremost jog. 1939 Erzincan earthquake with Ms 7.9 broke the 330 km-long western part of this section, including the Ezinepazarı segment. Fraser et al. [4] have asserted that the behavior of the NAF in the Eastern section is sometimes similar to that in the central translational part. Namely, many fault segments can be ruptured all together as in the case of 1939 great Erzincan earthquake; nevertheless, the NAF may also rupture with shorter segments in the Eastern section. Yedisu segment, which has a considerable slip deficit, is also located in the east of this section. Contrary to complicated fault geometries in the Karlıova triple-junction region, a much more straightforward fault formation is observed in the west of Erzincan [14].

On the other hand, the Central NAF is placed between Niksar, a district of Tokat province, and Dokurcun, a neighborhood of Akyazı district of Sakarya. It starts at the north of the Niksar releasing stepover and extends as a convex arc, which is approximately 525 km long and has a north-vergent characteristic. The west end of the Dokurcun valley, where the fault trace splits into 2 branches, is the end point for the central section of the NAF. Other than the segment boundaries, this section is noticed along a narrow deformation zone, identified via a regional scale restraining bend with respect to large bend geometry. The NAF serves a crucial function in the development of the final morphology of the region because tectonic valleys and troughs outside the stepover zones are shaped by the NAF. For example, it is the reason for approximately 17 and 25 km diversion of the Yeşilırmak and Kızılırmak rivers, respectively. Apart from these, from east to west, 1942 Erbaa–Niksar earthquake with Ms 7.1, 1943 Tosya – Ladik earthquake with Ms 7.4, 1944 Bolu– Gerede earthquake with Ms 7.3, 1957 Abant earthquake with Ms 7.1 and 1967 Mudurnu earthquake with Ms 7.2 are the examples of multi-segment ruptures on the Central section of the NAF [14]. It can be said that the Central section exhibits the simplest behavior and appears to commonly rupture in rapid succession or in unison [4].

According to Şengör et al. [6], the NAF doesn't display a characteristic regular or cyclical behavior for all times. On the other hand, a succession of earthquakes appear to have happened in the 17th, 18th and 19th centuries to the west of the estimated rupture of the 1668 earthquake. It can be asserted that there is a cycle not different from the 20th century cycle despite a longer time frame. This situation provides a rational basis for the construction of the characteristic earthquake recurrence model of the NAF.

Au contraire, it is almost impossible to find any regular behavior of the NAF before the 17th century. In every century between the 11th and 16th centuries, there was a great earthquake between Refahiye and Karlıova. Besides, there is no records going back to the 7th century. This is probably because the time span cited was a chaotic chapter in the episodic social history of Anatolia. This asesimic period is termed the Paphlagonian Temporal Seismic Gap, illustrated in Figure 3.3.

As it is appreciated, it is devilishly difficult to describe the characteristics of the events occurred in the first five Christian eras [6].

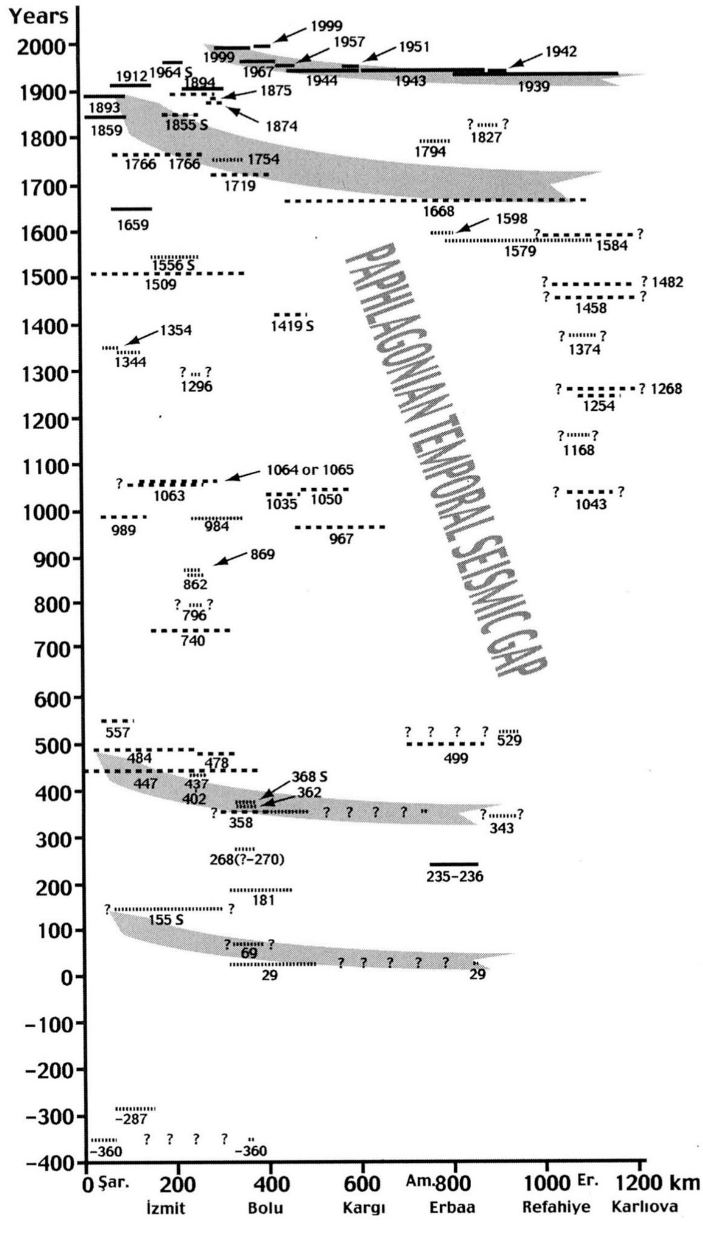

Figure 3.3. Historical seismicity of the NAF [6]

It has been stated above that the eastern end of the NAF is the Karlıova triple junction. Here, the NAF merges with the EAF, which is illustrated in Figure 3.4. As it is seen in Figure 3.1, the EAFZ is formed by relative movement between the Anatolian and Arabian plates, a northward-moving block. This relative drift causes a left-lateral strike slip fault mechanism. The fault zone follows a line from Karlıova triple junction towards the Mediterranean. As it has been ascertained by many studies (e.g., [70, 77–82]), the EAF houses the westward extrusion of the Anatolian block simultaneously with the NAF [4].

Figure 3.4. The assumed geometry of the EAFZ in this study (The circle represents Karlıova triple junction region)

Although the EAF was discovered by Esen Arpat, İhsan Ketin had previously predicted the existence of this fault. Ketin indicated that since interior Anatolia was not widely seismic, the westward movement of the entire Anatolian block is necessary along the strike-slip fault he defined. The inevitable consequence of this is the existence of another left-lateral fault to compensate such a motion. His prediction was confirmed by the discovery of the EAF in 1972 [70].

The discovery history of the EAF has been elucidated in minute detail by Arpat [83]. After the 22nd May 1971 Ms 6.8 Bingöl earthquake, Arpat was commissioned by the institute of Mineral Research and Exploration (MTA) to examine the causes of this earthquake and to draw up a report on findings [84]. On the other hand, there were already discussions and speculations in the literature about the existence of a fault zone in eastern Anatolia as mentioned in the previous paragraph. For example, while Ketin [85] attributed the seismicity of this region to the Muş-Bingöl collapse basin, Allen [86] asserted that there is a fault, starting from Karlıova and connected to the Dead Sea fault system over Bingöl-Hazar Lake. Since the fieldwork that was conducted by Arpat confirms Allen's opinion, a study was published by Arpat and Şaroğlu [87], and thus, this fault was given a name. That research is the first one declaring the left-lateral strike slip characteristic of the EAF [88]. Then, a detailed map of the EAF was drawn by Arpat and Şaroğlu [89]. While the aforementioned studies did not encounter any scientific opposition before, various reactions arose when it was understood that the Karakaya Dam was designed without taking the EAF into account. This is because it would have a serious cost in the construction of the dam.

With the discovery of the EAFZ, it has been the subject of a tremendous amount of research about its seismotectonics and characteristics, directly or indirectly (e.g., [11, 77, 78, 81, 82, 90–94]). According to Westaway and Arger [95], there is a consensus on that the age of the EAFZ is 2-3 Ma (e.g., [96, 97]) [88].

3.1. Segmentation of the NAFZ

Even though there are a lot of studies conducted on the segmentation of the NAF (e.g., [98–100]), the study that was published by Barka and Kadinsky - Cade [71] is an authoritative source for the segmentation of the NAF. According to this study, segmentation of fault zones is often described in two ways. The first one is to use geometric discontinuities along the faults. The other one is rupture based segmentation. If a fault section is separated by a clean break (stepover $\geq$ 1 km, bends $\geq 5°$), it is classified as "fault segment". On the other hand, some segments might systematically rupture in concert with adjacent segments. Fault sections ruptured by great earthquakes are named "rupture segments". Therefore, rupture segments might involve several fault segments [5, 71]. Such segments correspond "combined ruptures" in the characteristic earthquake occurrence model developed in this thesis. Based on geometry, rupture segments formed during the earthquakes that happened between 1939 and 1967 are characterized and divided into individual fault segments by Barka [98]. Understanding the temporal continuity of this type of segments is imperative to grasp the behavior of the North Anatolian Fault. Consequently, in total, Barka and Kadinsky - Cade [71] describe 69 fault segments, 26 of which are the central and eastern sections of the North Anatolian Fault (approximately east of Bolu) and the other 43 are along the western section of the NAF [4].

In this study, the definitions, boundaries and names of the NAF's segments between Bolu and Karlıova are taken from the research carried out by Emre et al. [14]. The Figure 3.5 shows the NAF's segments considered in this thesis.

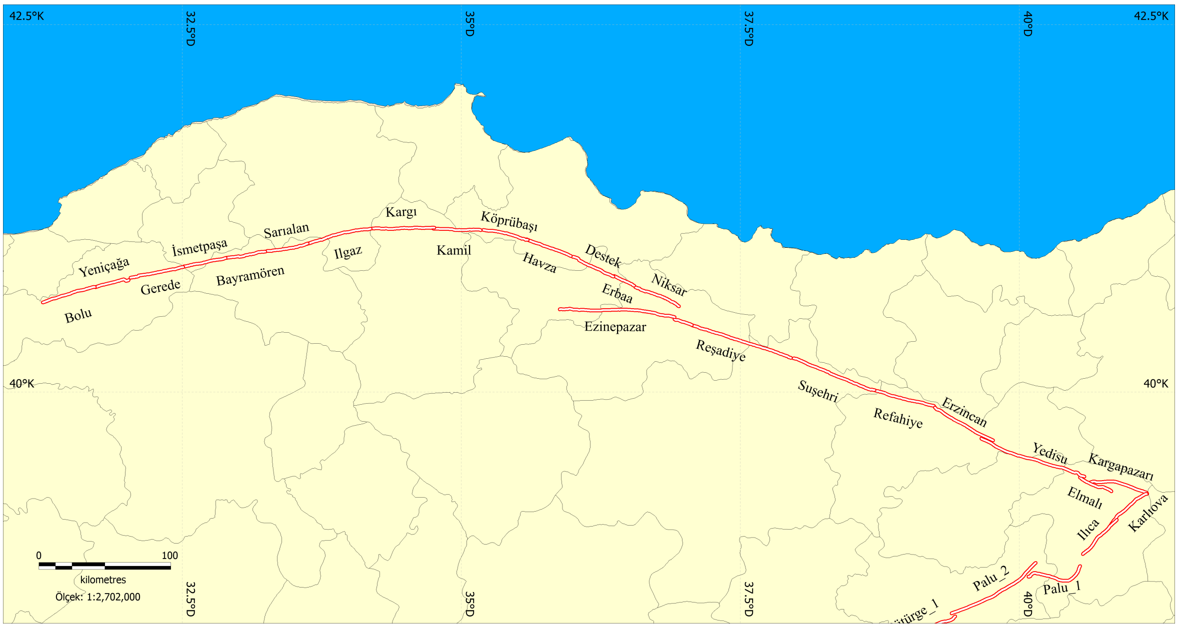

Figure 3.5. The segments of the NAF

3.2. Segmentation of the EAFZ

With the study that was published by Arpat and Şaroğlu [87], comments on the segmentation of it have started on a modest scale (i.e., between Karlıova - Bingöl and Palu - Hazar lake). Then, Arpat and Şaroğlu [89] have evaluated and mapped the Palu - Sincik part of the EAF. Hempton et al. [101] divided the EAF, which they claims to be 450 km long (the length of the EAF is actually equal to 560 - 600 km), into five segments listed below with respect to along strike variations in geometry:

- Karlıova – Bingöl
- Bingöl – Palu
- Palu – Pütürge
- Pütürge – Çelikhan
- Çelikhan - Türkoğlu

As it can be easily noticed, the Amanos segment, located approximately between Türkoğlu and Antakya, is not included in this classification. Barka and Kadinsky - Cade [71], on the other hand, divided the same part of the EAF, between Karlıova-Türkoğlu, into 14 segments by means of bends and stepovers. For the first time, the Amanos segment has been recognized by Şaroğlu et al. [97] as a part of the EAF. In this study, the EAF has been characterized as 6 individual fault segments from Karlıova to Antakya. For the same length of the EAF, the number of segments has been increased to 11 by Herece [88, 102].

In literature, there is a debate over the relationship between the EAF and the other fault systems in the region (e.g., Dead Sea Fault Zone (DSFZ), the Cyprus Arc (CA) and the Kyrenia–Misis Zone (KMZ)). While some studies (e.g., [103–106]) have accepted that Maraş triple junction is a connection point between DSF and EAF, others (e.g., [87, 89, 107]) have regarded Amanos segment as a part of the EAF. Thus, the EAF is located between the Karlıova and Amik triple junctions [88].

Within the scope of this thesis, it is acknowledged that the EAF is comprised of seven main segments based on Duman and Emre [88] and Emre et al. [14]. These segments are illustrated in Figure 3.6. Although the Hacıpaşa segment belongs to the DSFZ, it has been accepted as an extension of the EAF. This is because a part of the Hacıpaşa segment, named as Hacıpaşa 1, is located in Hatay province and there is a seismic gap on the whole segment [108]. Since high time - dependent hazard may occur in Hatay province and surrounding area, it is reasonable to take account of Hacıpaşa fault section.

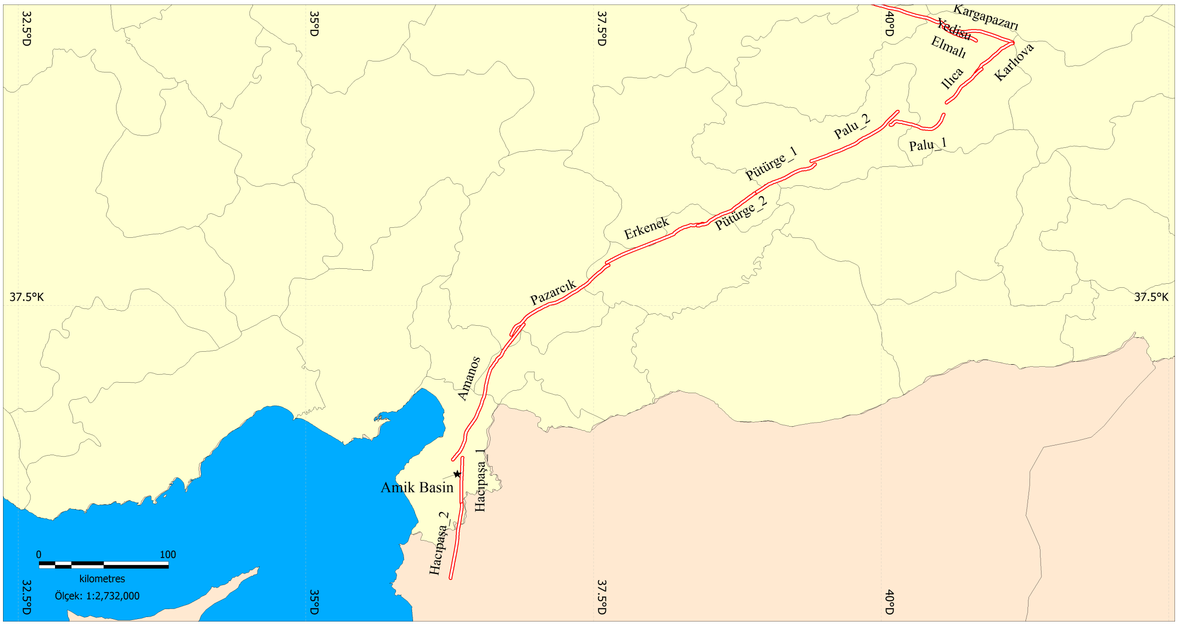

Figure 3.6. The EAF's segments considered in this study

It is also worth noting that Palu segment is divided into two parts: Palu 1 and Palu 2. This is due to the fact that its geometrical shape and slip rate value differ in the section denoted as Palu 1. The reason why the Pütürge and Hacıpaşa segments are divided into two sections is that these segments were not ruptured as a whole during related historical characteristic earthquakes. This is detailed in the fifth chapter.

4. SEISMIC HAZARD ANALYSIS: PRINCIPLES AND TIME – INDEPENDENT AND TIME – DEPENDENT MODELS

Traditionally two approaches are adopted for seismic hazard analyses. One of them is the probabilistic seismic hazard assessment, which takes into account almost all fault rupture scenarios that may affect the site. These scenarios pose hazard that is described via ground motions intensity parameters at reference site conditions, such as PGA and SA. In other words, PSHA for a definite site gives the intensity of a strong ground-motion parameter (e.g., PGA) exceeding a particular level during the exposure period (e.g., 50 years) [109]. The other approach is the deterministic seismic hazard assessment. It covers the decision on the scenario earthquake, characterization of appropriate GMMs and the thorough evaluation of site response [8].

PSHA is generally carried out prior to the deterministic one because the earthquake scenario with the major contribution to hazard must be found for the deterministic assessment. This scenario forms the basis for the deterministic seismic hazard assessment [7].

PSHA basically consists of 5 steps explained below:

(i) All seismic sources that can produce strong ground motion should described.
(ii) The distribution of earthquakes of different magnitude expected to happen is determined.
(iii) Source-to-site distances related to potential earthquakes are defined.
(iv) Ground motion models are employed to foresee the possible distribution of GMIMs with respect to magnitude, distance, and so on.
(v) With the help of the total probability theorem uncertainties in earthquake size, location and ground motion intensity are integrated [110].

The first three steps are also known as earthquake rupture forecast (ERF). Over a given period of time, an earthquake rupture forecast designates the probability of occurrence of different magnitude, locations, and faulting types for all seismic sources in an area. For an earthquake with a certain magnitude happening near the site, a ground motion model governs the probability distribution of assorted intensity measurements at that site [8].

Earthquake rupture forecast and ground motion models are the principal components of PSHA. These inputs are numerically combined by means of a suitable probabilistic model to attain the probability of exceedance of various GMIMs in the relevant territory [7].

Generally, the basic way to integrate the first three steps for fault sources (i.e., a fault-based ERF) consists of several phases. Firstly, the fault structures and the corresponding fault segmentation are characterized with respect to geologic findings. Secondly, with the help of geologic slip rates and paleoseismic studies, the long-term rate for each segment or multi-segment rupture, a rupture scenario that unfolds the probability of many segments rupturing together, is determined. Fault slip rates can be obtained from measured geologic offsets (e.g.kozacıya atıf) or calculated by using geodetic measurements (e.g. [72]). Lastly, the earthquake occurrence relationship of related faults is developed [8].

The third or last phase of ERF is usually taken into account time - independently (i.e., as a homogeneous Poisson process). The fundamental premise is that past earthquakes have no memory. Namely, inter-event times are independent and fairly distributed exponential random variables [8]. Notwithstanding, a homogeneous Poisson process cannot properly represent the long-term time dependency of major events on definite fault segments. As the time elapsed since the last major earthquake exceeds the mean recurrence interval of such events, seismic hazard increases [111]. This disadvantage of the PSHA can be removed through constructing time - dependent occurrence models [112]. On the other hand, for broad seismic zones and tectonic systems with missing information for the time - dependent modeling, time - independent models are constructed [7].

The probability of occurrence of the next earthquake does not depend on the time passed since the previous one in the time - independent models. The probability of occurrence at least one characteristic event on a fault or segment within the time interval (ΔT) for a homogeneous Poisson model is expressed as follows:

$$P[N \geq 1] = 1 - exp(-R\Delta T), \tag{4.1}$$

where R is the annual rate of earthquake recurrence of the segment. It is the reciprocal of the recurrence period. This process is called Poissonian because R is independent of time.

The widespread use of the Poisson model is based on several reasons according to Cornell and Winterstein [111] and Iacoletti et al. [8]. Firstly, this model only needs the annual rate of occurrence (i.e., the average recurrence time), which is associated with the coefficient a in the familiar Gutenberg-Richter MFD [113]. Secondly, the use of non-Poissonian models requires further information as to characteristic tectonic features. Thirdly, the sum of non-Poissonian processes could approximately become Poissonian. Fourthly, Poissonian assumptions are genuinely useful to set basic and computationally efficient mathematical equations to be worked out in PSHA.

The assumption of that there is no memory of past earthquakes, the basic premise in a homogeneous Poisson process, is not physically motivated for individual fault sources. This is because the process of stress buildup and its release is innately time - dependent [114], based on the elastic rebound theory [115]. This theory asserts that faults periodically store elastic strain energy, which is discharged when it exceeds the shear strength of the fault rocks. This energy naturally resets to zero after a major earthquake. The whole process is a "renewal" process because it suggests that there is time - dependency between characteristic events. On the other hand, there are some critics of elastic rebound theory. They have rightly pointed out a lot of controversial and fault segmentation-related assumptions needed in applying the models. Two of them are the appropriate choice of renewal (time - dependent) model, and aperiodicity [112]. Notwithstanding, some studies have ascertained that ignoring elastic rebound causes unrealistic aftershock statistics [8, 116].

According to Cornell and Winterstein [111], if a fault behaves characteristically (i.e., in keeping with the elastic rebound theory), the Poisson estimate may be inadequate. As explained above, this is the case in situations which the mean recurrence period of a fault is smaller than the elapsed time since the last characteristic event occurred on the fault. Such faults need to be modeled time - dependently.

The renewal (time - dependent) model is primarily based on the presumption that characteristic events take place repeatedly. If an earthquake has not happened in the last T years, the conditional probability of the occurrence of it in the next ΔT years is given by [7]:

$$P(T, \Delta T) = \frac{\int_{T}^{T+\Delta T} f(t)\, dt}{\int_{T}^{\infty} f(t)\, dt}, \tag{4.2}$$

where $f(t)$ is the probability density function (PDF) for the recurrence interval, T is the time passed since the last characteristic event and ΔT is the exposure period usually taken as 50 years. The nominator of this expression is equal to the hatched area, and the denominator corresponds to the total shaded area under the lognormal PDF as is shown in Figure 4.1.

The Weibull [117], lognormal [118], and Brownian Passage Time (BPT) [119, 120] distributions are the most famous PDFs that have been used in time - dependent occurrence models [8].

In time - dependent models, the log-normal distribution for PDF is delineated with 2 parameters: the mean earthquake recurrence interval of the fault, μ and the coefficient of variation, “CoV”, which is a measure of the periodicity of the recurrence interval. “CoV” usually takes values between 0.3 and 0.7 [121]. It also decreases with

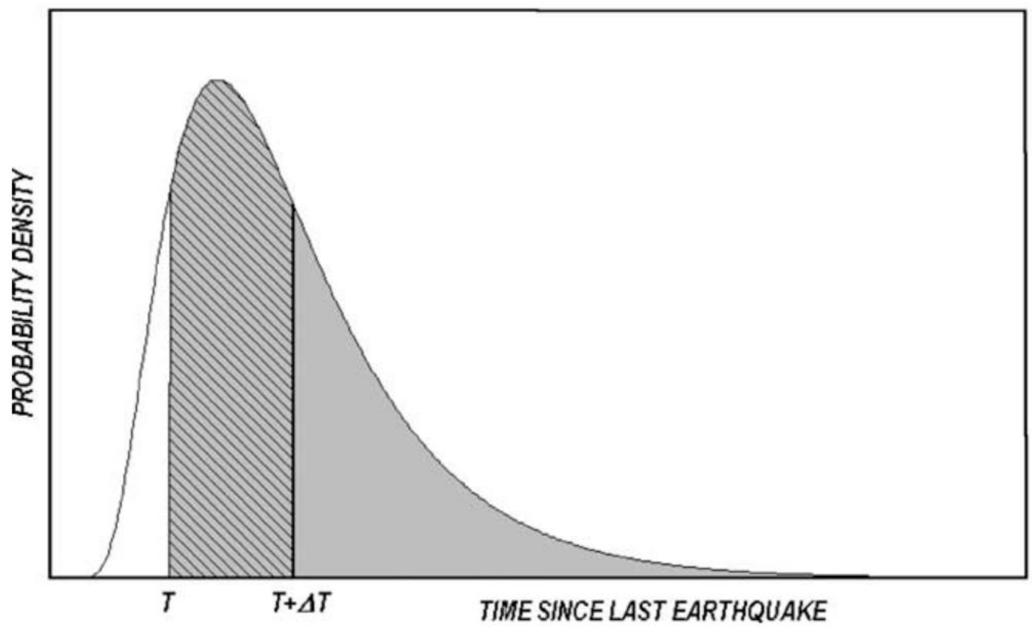

Figure 4.1. The relationship between the probability density function and conditional probability [7]

higher periodicity. Nishenko and Buland [118] have ascertained that the lognormal distribution is the most compatible with the observed seismicity compared to the others (It should be indicated that at that time BPT had not yet been discovered). The PDF of the log-normal distribution is as follows:

$$PDF = \left(\sqrt{2\pi}\sigma t\right)^{-1} exp\left[-\frac{(logt-\mu)^2}{2\sigma^2}\right], \tag{4.3}$$

where μ is the mean recurrence period, σ is the standard deviation and t is the time elapsed since previous earthquake [7].

The mean time between events (μ) and the aperiodicity of the mean time (α), equivalent to the coefficient of variation (CoV), distinguish a Brownian passage - time distribution [122].

The PDF of the BPT is as follows:

$$PDF = \left(\frac{\mu}{2\pi\alpha^2 t^3}\right)^{1/2} exp\left[-\frac{(t-\mu)^2}{2\alpha^2\mu t}\right] \tag{4.4}$$

As for Weibull distribution, its PDF is written below:

$$f(t) = \frac{\beta}{\alpha}\left(\frac{t-\mu}{\alpha}\right)^{\beta-1} exp\left[-\left(\frac{t-\mu}{\alpha}\right)^{\beta}\right] \text{for } t \geqslant \mu;\ \beta,\ \alpha > 0, \tag{4.5}$$

where α, β and μ represent scale, shape and local parameters, respectively.

For the same $\mu = 250$ yrs and CoV $= 0.5$, the PDFs of the distributions, including exponential (i.e., Poissonian or time - independent) one, have been compared in Figure 4.2 [8].

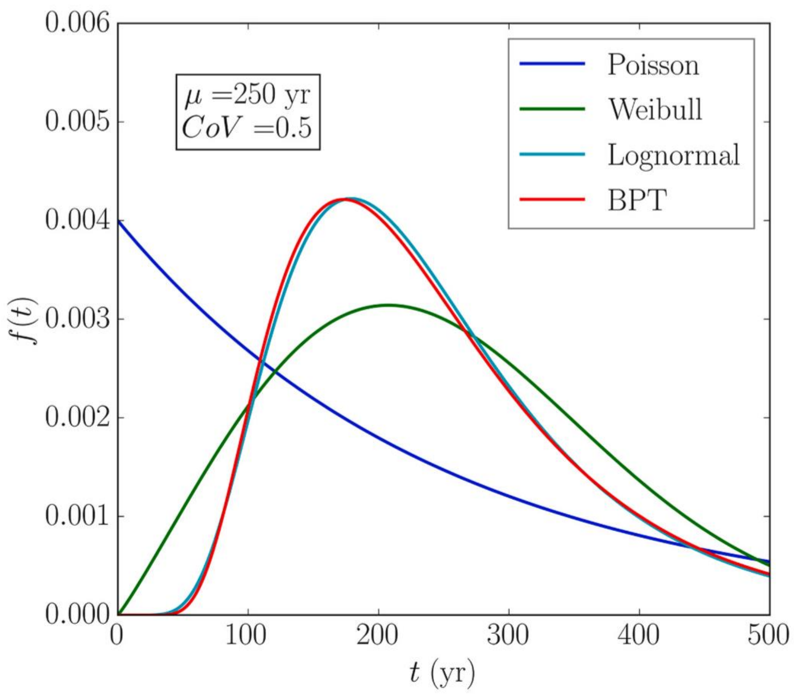

Figure 4.2. Including Poissonian distribution, the comparison of the most popular PDFs used in renewal models for the same recurrence interval and aperiodicity [8]

The Poisson process is identified by a constant hazard function. Namely, the conditional probability of happening an earthquake in a rigid time interval is independent from the time elapsed since the last event (i.e., time - independent). On the other hand, the probability of occurrence of the next earthquake is affected by the features of the preceding earthquakes in time - dependent models. It could increase with elapsed time since the last event according to a large class of statistical models. Furthermore, time - dependent models like the Weibull, the lognormal, and the BPT determine a lower (or zero) probability of occurrence for faults in the beginning of the seismic cycle compared to time - independent ones, which is also in great harmony with Reid's theory. On the other hand, for faults in the late period of the seismic cycle, they compute a higher probability for the next earthquake [122].

Even though there is not any empirical proof encouraging to choose one model of time - dependent occurrence relationships over another, there is a general agreement on applying the BPT model compared to the other renewal recurrence models [8, 112, 123]. The reasons for the choice of BPT over Weibull and lognormal distributions are as follows:

(i) BPT model is a physically motivated time - dependent model for earthquake occurrence. It has a connection between the typical features of the stress and strain accumulation process of the elastic rebound theory and the noticeable distribution of the genuine inter-event data [119, 120, 122]

(ii) For the BPT model, after long time since the last event, the hazard function places a fixed value. That is, the probability of occurrence of earthquakes becomes time - independent. Whereas, the lognormal distribution converges to zero and the Weibull distribution with shape parameter greater than 1 goes to infinity. Besides, as time converges to infinity, the hazard function hits zero for the lognormal distribution and the Weibull distribution with shape parameter smaller than 1. This is why some researchers regard these distributions as obsolete, which is particularly plausible if the mechanism of earthquake occurrence is ascribed to the process of ever-increasing load on the fault [122].

5. DEVELOPMENT OF RECURRENCE MODELS OF THE NAFZ AND EAFZ

5.1. Methodology

In this thesis, the prime purpose is to develop an earthquake occurrence relationship which reflects the intrinsic behavior of the NAF and EAF properly. The first step towards this goal is to determine historical or observed seismicity of the fault zones. Nature acts without being aware of the scientific models attributed to its behavior patterns. Therefore, the first step implies that a fully exponential or characteristic model cannot be built. The development of a hybrid earthquake occurrence model for related faults is inevitable in this sense. Then, which earthquake recurrence relationships should this hybrid model consist of? The hybrid model basically involves an exponential tail for smaller earthquakes and a characteristic part for major earthquakes. This model seems as if it is same as Youngs and Coppersmith's composite model [25], but it is not. It also incorporates into the probability of happening multi-fault rupture. Here, the issue to be addressed is the amount of seismic slip to be assigned to exponential tail or combined - characteristic part (the term "combined - characteristic" represents the characteristic part that includes the probability of occurring multi-segment or combined rupture). Since only fault sources are used for seismic source characterization, slip rate of related faults is manipulated to achieve consistency with the observed seismicity, which procedure is also known as moment balancing in literature.

In that case, the next step is to determine observed seismicity (i.e., recurrence parameters of the NAF and EAF) by using the earthquake catalogue compiled by Kadirioğlu et al. [12]. Then, slip partitioning has been done. Based on the observed seismicity, the percentage of slip rate to be allocated to exponential part of the model is determined.

Another stage is to calculate characteristic magnitude and recurrence intervals of the individual and combined rupture segments. The remainder of the slip rate is assigned to the combined - characteristic part. In order to compute recurrence intervals, there is needed a further slip partitioning process between individual and combined ruptures of the fault segments. At this stage, the reference point representing the observed seismicity is paleoseismic studies (e.g., [4]). Based on such studies, it is decided what percentage of the remainder slip rate will be allocated to characteristic and combined ruptures. With these slip rates, the recurrence periods of both individual and combined segments are computed. The calculated recurrence intervals are compared with those suggested by paleoseismic studies, and the amount of slip rate shared between two parts is calibrated. In short, we are trying to develop a hybrid earthquake occurrence model such that its exponential tail and combined - characteristic part are in a perfect harmony with the observed seismicity separately.

6% and 94% of the total slip rate which is assigned manually to the exponential tail and combined - characteristic part, respectively, has ensured a reasonable consistency with the observed seismicity. However, we have built another earthquake recurrence model for the NAF and EAF so as to investigate the reliability of the first model. In this model, 94% of the slip rate would not be divided between individual and combined ruptures and all of it would be assigned to individual ruptures. The hazard curves of this model have been compared with those obtained using the classical Youngs and Coppersmith composite model [25] in OpenQuake software [29]. In this software, total seismic moment rate is automatically distributed over the exponential and characteristic parts when Youngs and Coppersmith model tool is used. Eventually, almost the same results have been achieved from the two models. Thus, it is justified once again that the total seismic slip rate is allocated between the exponential tail and combined - characteristic part at a rate of 6% and 94%, respectively.

Finally, the hybrid earthquake occurrence model, which provides a remarkable insight into the distinctive seismic nature of the NAF and EAF, is constructed. This model displays a time - independent (i.e., Poissonian) characteristic. However, the hybrid model demonstrates an overwhelming superiority over its counterparts: it can be easily converted a time - dependent one. By means of the research carried out by Demircioğlu et al. [28], information on the other (secondary) faults in the studied region and background smoothed seismicity has also been added to the hybrid model, which makes it possible to compare the results of the hybrid model and the latest Turkish Seismic Hazard Map in terms of ground motion intensity parameters (e.g., PGA and SA). It should be indicated that "the latest Turkish Seismic Hazard Map" refers to the fully exponential fault source model built by Demircioğlu et al. [28]. Whether the results of the Poissonian hybrid model is overestimated or underestimated has also been evaluated by comparing them with the results of time - dependent version. Moreover, the results of the fully exponential model and the time - dependent model have been compared. The purpose of this comparison is to judge the results of the fully exponential model, which is widely used in practice, based on the results of the renewal model, which enables a more realistic seismic hazard assessment.

5.2. Identification of Seismic Sources

Fault sources are the main seismic sources within the framework of this study. The "fault" term can be defined as a geologic characteristic creating a potential seismic hazard for a region under consideration. As for "fault segment", it suggests distinctive seismic sources within a fault. Fault segments make contribution to hazard en masse. Although the geometry of them is generally simplified according to the map geometry, it possesses internal coherence with observable features of the entire fault. The rake angle of the fault is an example of such features of the original fault. The mentioned fault segments, which are reduced, is adopted straightforwardly for PSHA studies [8].

The configuration of the Database of Individual Seismogenic Sources (DISS) [9] has been used for the consideration of the fault source model. In Figure 5.1, an Individual Seismogenic Source is simply illustrated. The active fault characterization database (AFCD), produced by Emre et al. [65], is used in order to build the fault source model. The AFCD has been re-categorized after the characterization of Individual Seismogenic Sources. They have been identified through a whole set of geometric, kinematic (rake angle), and seismological parameters. While strike, dip, length, width and depth of sources delineate geometric parameters, single event displacement, magnitude, slip rate and recurrence interval symbolize seismological properties. Parameters missing in the features of AFCD have been assigned with respect to the available literature with some presumptions [14]. Minimum and maximum values have been assigned to each separate seismogenic source entity for the overwhelming majority of the parameters [28].

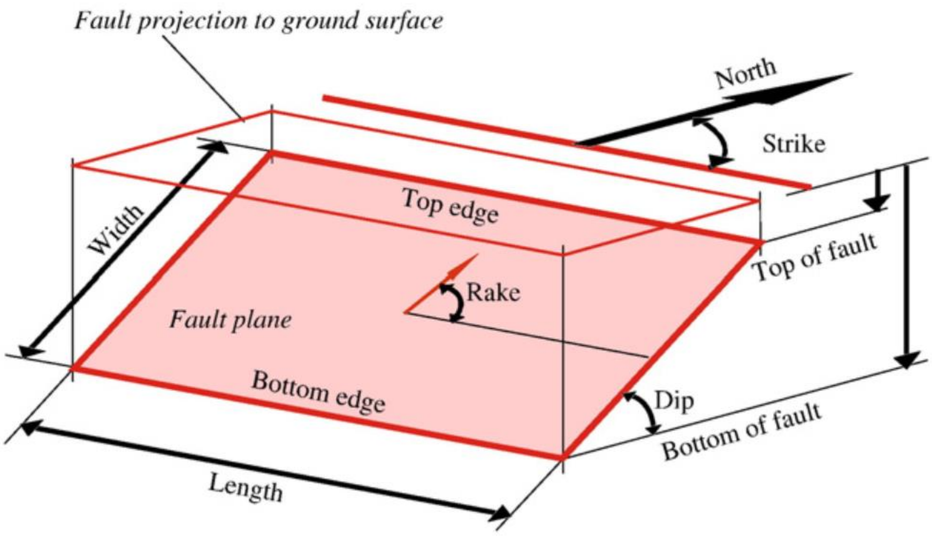

Figure 5.1. Simple illustration of an Individual Seismogenic Source and its typical features [9]

All information about the NAFZ and EAFZ is taken from Emre et al. [14] and UDAP-Ç-13-06 Project.

5.2.1. Fault Source Information of the NAFZ

Here, all the necessary information for the fault source modeling is given in Table 5.1. However, the lengths of the fault segments are specific to this study because some adjustments have been made to some of them.

Table 5.1. Fault source characteristics of the NAF.

Segments	MAP Length (km)	Min. Sr (mm/yr)	Max. Sr (mm/yr)	Min. Depth (km)	Max. Depth (km)	Rake Angle	Min. Dip Angle	Max. Dip Angle
Kargapazarı	45.58	17	18	0	18	180	87	90
Elmalı	27.03	1	2	0	18	180	87	90
Yedisu	85.62	18	19	0	18	180	87	90
Erzincan	51.49	22	23	0	18	180	87	90
Refahiye	47.83	22	23	0	18	180	87	90
Suşehri	66.59	22	23	0	18	180	87	90
Reşadiye	94.11	22	23	0	18	180	87	90
Ezinepazar	88.04	2	2.1	0	18	180	87	90
Niksar	37.32	21	22	0	18	180	87	90
Erbaa	19.95	21	22	0	18	180	87	90
Destek	34.71	21	22	0	18	180	87	90
Havza	35.85	21	22	0	18	180	87	90
Köprübaşı	34.66	21	22	0	18	180	87	90
Kamil	37.03	21	22	0	18	180	87	90
Kargı	47.23	21	22	0	18	180	87	90
Ilgaz	49.69	21	22	0	18	180	87	90
Sarıalan	31.55	21	22	0	18	180	87	90
Bayramören	30.38	23	24	0	18	180	90	90
İsmetpaşa	32.53	23	24	0	18	180	90	90
Gerede	40.95	23	24	0	18	180	90	90
Yeniçağa	26.59	23	24	0	18	180	90	90
Bolu	41.40	23	24	0	18	180	90	90

5.2.2. Fault Source Information of the EAFZ

The lengths of the EAF's segments may also differ from those given by Emre et al. [14] and UDAP-Ç-13-06 Project.The necessary information is provided in Table 5.2

Table 5.2. Fault source characteristics of the EAF.

Segments	MAP Length (km)	Min. Sr (mm/yr)	Max. Sr (mm/yr)	Min. Depth (km)	Max. Depth (km)	Rake Angle	Min. Dip Angle	Max. Dip Angle
Karlıova	37.26	8	8.1	0	18	0	90	90
Ilıca	37.29	8	8.1	0	18	0	90	90
Palu 1	48.42	6	7	0	18	0	85	90
Palu 2	76.96	9	10	0	18	0	85	90
Pütürge 1	51.25	9	10	0	18	0	85	90
Pütürge 2	50.92	9	10	0	18	0	85	90
Erkenek	82.94	6.5	7	0	18	0	85	90
Pazarcık	93.77	6.5	7	0	18	0	85	90
Amanos	120.00	6	7	0	18	0	85	90
Hacıpaşa 1	35.48	4.5	5	0	18	0	87	90
Hacıpaşa 2	57.64	4.5	5	0	18	0	87	90

5.3. Estimation of Recurrence Parameters of the NAF and EAF

To characterize the exponential magnitude distribution of the NAF&EAF with the Youngs and Coppersmith's exponential model [25], region -or fault zone- specific b values are needed. As is schematically represented in Figure 5.2, buffer zones of 15 kilometers were drawn around the surface projections of the fault zones. By using the declustered earthquake catalog of Kadirioğlu et al. [12], earthquakes whose epicenters fall within the buffer zone are detected. Characteristic earthquakes are excluded in this process because they have been used in the development of combined - characteristic part of our hybrid earthquake occurrence model. Completeness periods of the NAFZ and EAFZ are taken from Şeşetyan et al. [64]. Then, the recurrence parameters are calculated via Weichert's method [124] for the both fault zones. The values are presented in Table 5.3

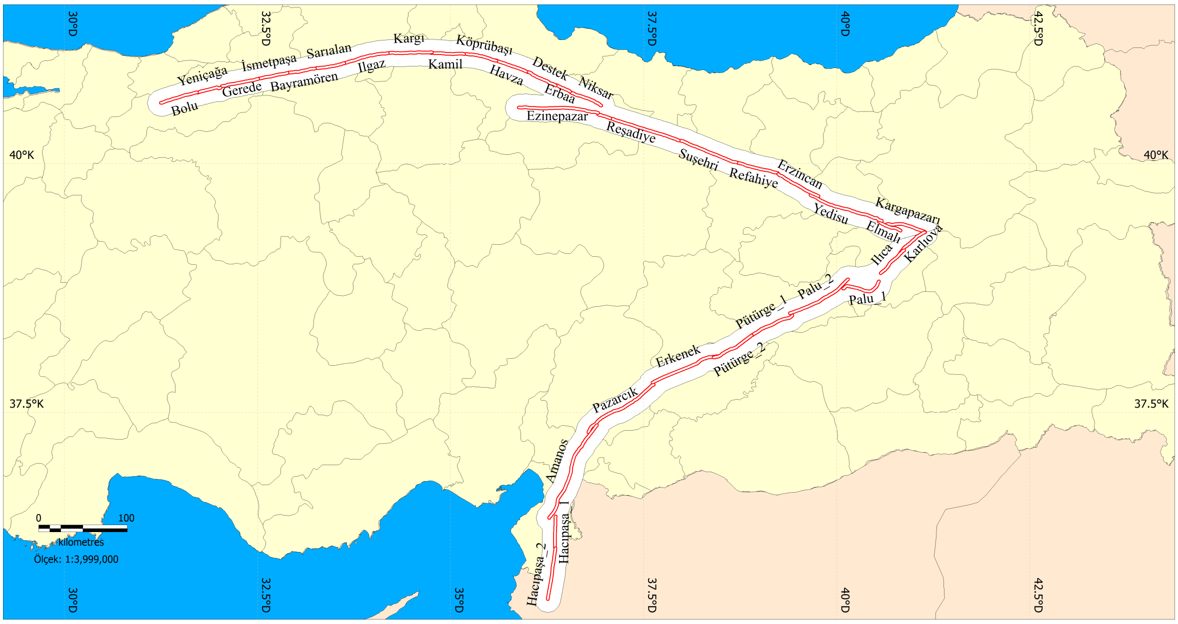

Figure 5.2. The buffer zone drawn around faults

With the estimated recurrence parameters, the truncated (bounded) Gutenberg and Richter [113] magnitude - frequency distribution (MFD) has also been drawn for the NAF and EAF in Figure 5.3 and 5.4, respectively. The bounded G-R magnitude - frequency distribution is calculated with the following equation:

$$\lambda_m = \nu \frac{exp\left[-\beta\left(M - M_{min}\right)\right] - exp\left[-\beta\left(M_{max} - M_{min}\right)\right]}{1 - exp\left[-\beta\left(M_{max} - M_{min}\right)\right]}, \tag{5.1}$$

where $\nu = exp\left(\alpha - \beta M_{min}\right)$, $\alpha = 2.303a$ and $\beta = 2.303b$

Table 5.3. Recurrence parameters for the both fault zones.

Recurrence Parameters	NAF	EAF
a	3.95	4.74
b	0.87	1.08

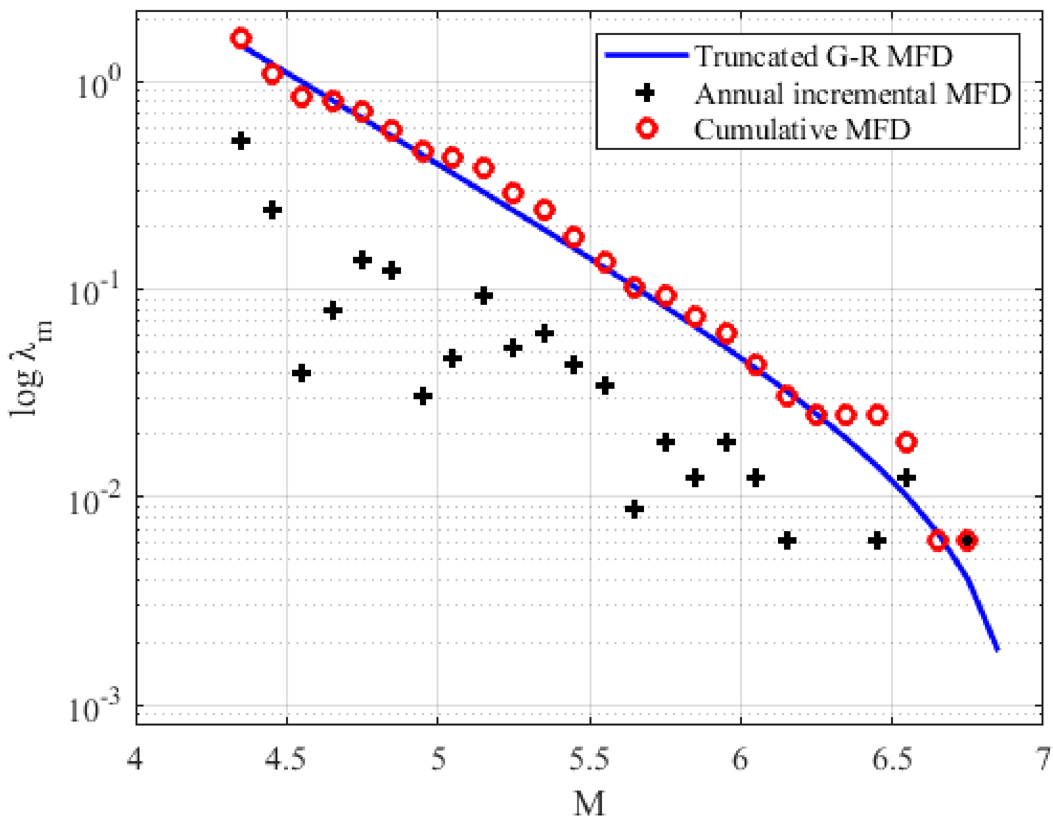

Figure 5.3. Earthquake recurrence relationship of the NAFZ

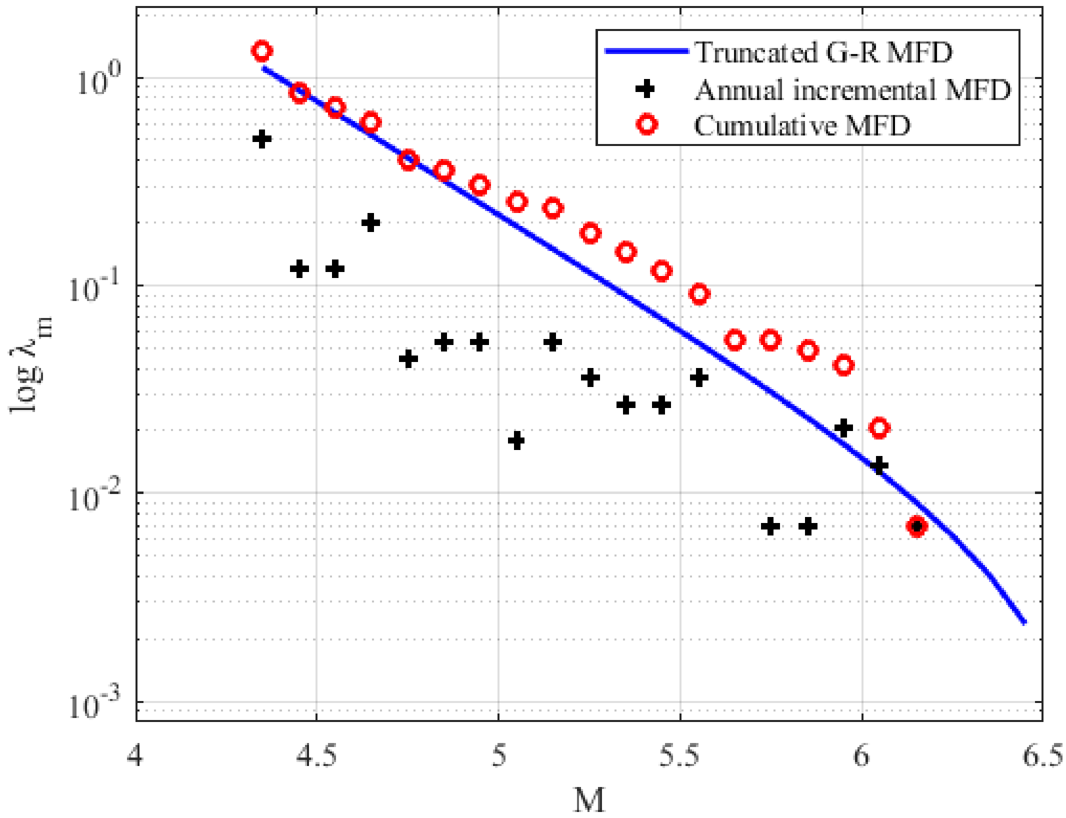

Figure 5.4. Earthquake recurrence relationship of the EAFZ

The red and black dots in these graphs symbolize the observed seismicity.

5.4. Slip Rate Constraints on Exponential Magnitude Recurrence Relationships for the NAF and EAF

In order to model and characterize active faults as individual seismogenic sources with respect to their dimensions and slip rates, seismotectonic knowledge is used. Here, it should be pointed out that slip rate is an essential parameter controlling the calculation of seismic moment and recurrence interval [28, 125–127]

Slip rate is also used to follow the seismic moment balancing method. According to this approach, the seismic moment released by an earthquake is directly proportional to the strain accumulation along an active fault during an inter-event time. The seismic moment must be converted to moment magnitude domain associated with the choice of magnitude recurrence model when it is calculated for each fault source. In this study, it was declared that a hybrid earthquake occurrence model is constructed instead of the fully characteristic [30] or fully exponential one [25]. The small magnitude events that occur around the faults are also taken into account; nevertheless, some researchers (e.g. [128, 129]) are in opposition the combination of a regional background and faults. In their opinion, this eventuates an increased number of earthquakes with small and moderate magnitude. To surmount this difficulty, occurrence rates of small to moderate-sized and moderate to large-sized earthquakes have been combined as it was exemplified by Demircioğlu et al. [28]. While recurrences for small to moderate magnitude events, which are accounted for background seismicity, are obtained from earthquake catalog published by Kadirioğlu et al. [12], the occurrence rates of moderate to large-sized earthquakes are calculated for individual segments. These two recurrence models are separated by a threshold magnitude, restricting the minimum magnitude on the segments through a value somewhat greater than the maximum one considered for a background zone. In the 2003 European Mediterranean source model [22] and in the 2014 Middle East Earthquake Source Model [42], the threshold value was chosen as Mw 6.5 and Mw 5.5, respectively [28]. In the scope of this research, a threshold value of 6.00 Mw is assigned to segregate the seismicity of background from the occurrence rates originated from individual fault segments. The exponential magnitude recurrence relationship (i.e., Gutenberg–Richter distribution) is used to obtain recurrences in both the exponential tail of the hybrid fault source model and the background seismicity.

Bungum [130] has argued that seismic activity and crustal deformation rates have a basic relationship. Therefore, for quantifying earthquake activity on fault sources, the activity rate $N(M_{min})$ and the integration of the MFD must be multiplied by each other [28].

Anderson and Luco [23] have outlined three categories of fault recurrence models to establish a magnitude recurrence relationship from the geological slip [131]. Bungum [130] demonstrates the distinctions between the recurrence relationships developed Anderson and Luco [23] and Youngs and Coppersmith [25]. The difference is mainly due to the behavior of the recurrence distribution at the vicinity of upper bound magnitude. While the exponential magnitude recurrence relationship built by Youngs and Coppersmith is rooted in the constant moment energy release along a fault, the amount of moment release near the maximum magnitude is larger in Anderson and Luco's models, and thereby, ending up with a higher activity rate [28]. This and the high level of earthquake activity in Turkey are considered in tandem, the winner of the comparison will be Youngs and Coppersmith's truncated exponential model. Therefore, it is chosen to calculate recurrences for each individual fault segment rather than the Anderson and Luco model. Besides, Demircioğlu et al. [28] have examined the differences between the first two model of Anderson and Luco and Youngs and Coppersmith's exponential model in terms of a value along the fault sources. They have concluded that Youngs and Coppersmith's exponential magnitude recurrence relationship is more applicable since the annual slip rates of the faults in Turkey are mostly high as previously mentioned.

Youngs and Coppersmith's exponential model [25], used in this study as a part of hybrid model, is formulated as:

$$\mu_Y A_f S = \frac{bN(m^\circ)M_0^u \; exp[-\beta(m^u - m^\circ)]}{(c-b)\left\{1 - exp[-\beta(m^u - m^\circ)]\right\}}, \tag{5.2}$$

where m° is an arbitrary reference magnitude, $\beta = b \times ln10$. A_f is the total fault plane area. The term M_0^u is the moment for the upper bound magnitude m^u. Hanks and Kanamori [132] have determined $c = 1.5$. μ_Y is shear modulus. For Turkey, this value can be taken as 30 GPa (or 3×10^{11} $dyne/cm^2$) [133]. b value of each fault segment is assumed to be equal to the overall b value calculated for both fault zone.

With the fault zone specific recurrence parameters obtained in the previous chapter, the truncated exponential tail of the hybrid earthquake occurrence model is calculated for both fault zones. The b value of each fault segment is assumed to be equal to the b value of the fault zone in which the segment is located. If the characteristic magnitude value of each segment is called "Mchar", the magnitude range is determined from the threshold magnitude (Mw 6.00) to "Mchar - 0.1". This is because characteristic earthquakes will be subsequently taken into account in the combined - characteristic part of the hybrid model.

Youngs and Coppersmith's exponential magnitude recurrence relationship are calculated and illustrated for the NAF and EAF's segments in Figure 5.5 and 5.6, respectively. As minimum and maximum slip rates assigned to individual segments display a very small variability, the central value of the range was adopted for the activity rate computation. "Cumulative" and "Truncated Exp" values in the graphs correspond to "Cumulative MDF" and "Truncated G-R MDF", respectively, which were calculated in the previous section and represent the observed seismicity. As is can be noticed that when 6% of the total seismic moment rate is allocated to fault each segment, the total annual rate of earthquake occurrences, shown as "TOTAL" in the graphs, converges the observed seismicity. This means 6% of the total seismic moment rate is enough for the exponential tail of the hybrid model to achieve consistency with the observed seismicity.

5.5. Time – Independent Recurrence Relationship of Combined – Characteristic Part of the Hybrid Model

The term "combined - characteristic" means the characteristic earthquake model that includes the probability of occurring combined rupture. Hence, the key objective of this chapter is to develop characteristic earthquake occurrence model for the NAF and EAF.

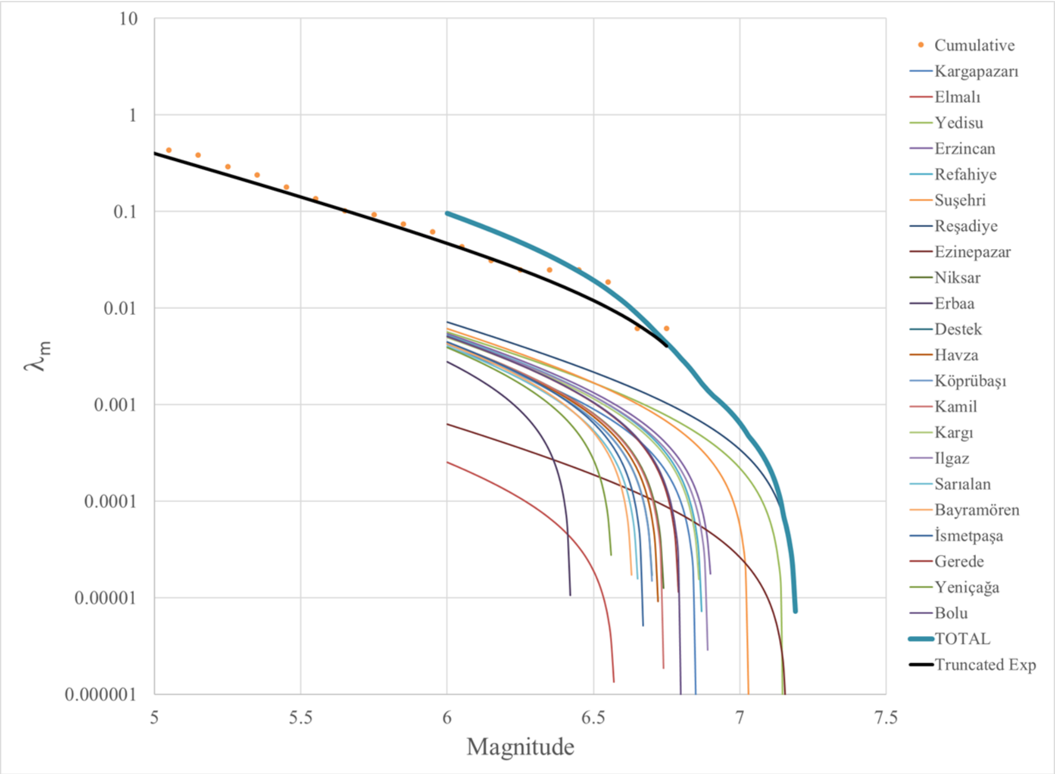

Figure 5.5. Exponential magnitude recurrence relationship for the NAF's segments

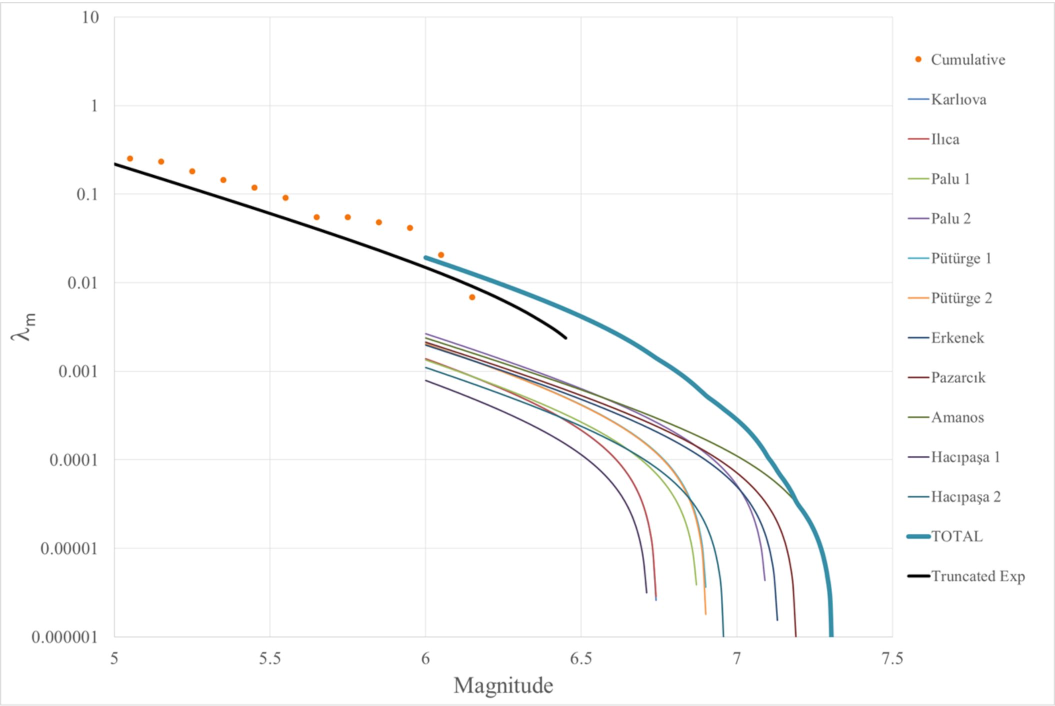

Figure 5.6. Exponential magnitude recurrence relationship for the EAF's segments

The characteristic earthquake model was suggested for the first time by Wesnousky et al. [129] and Schwartz and Coppersmith [30]. Afterwards, it has gained general acceptance in the earthquake science community, and therefore, in many fault - based PSHA studies (e.g., [134]), the implementation of the characteristic earthquake model has been achieved. While a vehement opposition to the basis of this model has been put up by some studies (e.g., [135–137]), Ishibe and Shimazaki [138, p. 1054] have ascertained that "the characteristic earthquake model offers a more appropriate description of the magnitude – frequency distribution around the individual late Quaternary active fault zone in Japan during one seismic cycle." Ultimately, in many studies (e.g., [28, 123, 139]), characteristic earthquake MFDs in relation to Gutenberg - Richter MFDs has been used extensively [8].

The segmented fault source model is usually incorporated in probabilistic seismic hazard analysis through the seismic moment balancing technique. This approach considers that the total amount of the seismic moment is directly proportional to the strain accumulation along a fault segment during interevent time. The moment magnitude of the earthquakes generated by probable rupture scenarios is computed via the seismic moment calculated for each segment. This computation is based on a selected MFD and the presumptions concerning possible rupture scenarios between the segments (e.g., [26]). The kind of ruptures taken into account in fault - based ERF is controlled by the preference of MFD [8].For example, the selection of a characteristic MFD for each segment has two meanings. Firstly, fault segments are regarded as individual seismic sources [140, 141], which means they don't depend on each other. Secondly, during characteristic earthquakes, surface rupture is observed on roughly the whole segment [30, 134, 140]. On the other hand, in order to account for the occurrence of ruptures shorter than the entire segment surface, the exponential magnitude recurrence relationship, where fault segments are considered independent seismic sources, or a combination of different magnitude frequency distributions can be used. This kind of rupture models are also known as "floating ruptures" [142, 143].

Strict fault segmentation models in which fault segments are considered independently (i.e., there is no interaction between them) don't reflect the contribution of medium-to-large earthquakes on seismic hazard properly [144, 145]. Geologic findings suggest that along - strike bends cannot always consistently halted earthquake ruptures [146], and therefore, rupture may propagate one segment to another as in the case of 1939 Erzincan earthquake, which is the basis for including the possibility of multi-rupture occurrence in our hybrid model. Naturally, when ruptures are confined to individual segments, the probability of the occurrence of multi-fault rupture is neglected in a fault - based PSHA [8]. Nevertheless, in many studies, multi-ruptures that will probably occur are not incorporated in fault models (e.g., [28, 134]).

The modeling of multi-fault rupture is based on the assumption that several great adjacent fault segments might rupture as a group due to a severe earthquake (e.g., [143, 147]). Nonetheless, describing all possible rupture combinations for a given fault system is not always achievable. This is because the interpretation of paleoseismic or geologic findings is tough. Moreover, such findings may not even exist for the region under consideration [8]. Another difficulty is adjustment of the occurrence rates for multi-fault ruptures. The inevitable consequence of these reasons is that there is no consensus over the selection of the type of ruptures and the application of fault segmentation models in seismic hazard analyses.

As has been said above, segments of the faults are not always ruptured by earthquakes with characteristic magnitude. The term cascade refers the rupturing of segments one after another. Thus, it causes larger rupture areas and magnitude. Although fault segments can be delineated independently at the surface, they can be associated with a single structure at depth, and thereby, combined. To include this phenomenon in the hazard model, two rupture scenarios are painted. The first one is that segments rupture independently, and thus, cause characteristic earthquakes to happen. The second one is that fault segments rupture collectively as a cascade, which produces earthquakes with magnitude greater than in the first model [7]. Since the annual slip rates and depths of the segments that form the combined rupture scenario are identical, a detailed cascading process is not required in the development of our combined rupture model.

First of all, the combined rupture scenario is constructed and characteristic earthquake magnitude values are calculated for both individual and combined rupture scenarios. Then, 94% of the total seismic moment budget will be distributed between the individual and combined ruptures, which is necessary for moment balancing. Finally, annual rate of occurrences (i.e., recurrence periods) of each scenario are computed.

5.5.1. Combined Rupture Scenarios

In the drawing of combined rupture scenario for the NAF, the earthquakes that occurred in the 20th century occupy a decisive role. That is, the segments ruptured by the earthquakes which occurred on the NAF in the 20th century, which are shown in Figure 5.7, are considered as segment groups that can cause a combined rupture. Since the last characteristic earthquake in the Yedisu region occurred in 1784 [5], Kargapazarı and Yedisu segments have also been included in the combined rupture scenario named "1784 EQ Rupture ". In Table 5.4, the component segments of combined ruptures are listed in groups. Except for "1784 EQ Rupture" scenario, the slip rate and maximum depths of the component segments are identical within the same group. This is why even though Ezinepazar segment was ruptured during the 1939 Erzincan earthquake, it is not included the combined rupture scenario. The annual slip rate value of Ezinepazar segment is quite low (2 mm/yr) compared to its counterparts.

As for the EAF, there is a limited number of combined rupture scenario. This is because large - scale geometric discontinuities are more closely spaced along the EAF than compared to the NAF. This can be the reason for that the statistics of combined ruptures and thereby major earthquakes that were occurred along the NAF are higher. In other words, ruptures occurred during earthquakes along the NAF is more likely to jump to the adjacent segment [71].

The fault segments shown as Pütürge 1 and Pütürge 2 in Figure 5.8 were ruptured during the 2020 and 1905 earthquakes, respectively [71, 148]. This is the reason for that Pütürge segment presented as a single fault segment in by Emre et al. [14] is cut into two sub-sections within the scope of this study. Then, the possibility of

Table 5.4. Details of combined rupture scenarios for the NAF.

Combined Rupture Scenario	**Segments**	**Mean Slip Rate (mm/yr)**	**Max. Depth (km)**
1784 EQ Rupture	Kargapazarı	17.5	18
	Yedisu	18.5	18
1939 EQ Rupture	Erzincan	22.5	18
	Refahiye	22.5	18
	Suşehri	22.5	18
	Reşadiye	22.5	18
1942 EQ Rupture	Niksar	21.5	18
	Erbaa	21.5	18
1943 EQ Rupture	Destek	21.5	18
	Havza	21.5	18
	Köprübaşı	21.5	18
	Kamil	21.5	18
	Kargı	21.5	18
	Ilgaz	21.5	18
	Sarıalan	21.5	18
1944 EQ Rupture	Bayramören	23.5	18
	İsmetpaşa	23.5	18
	Gerede	23.5	18
	Yeniçağa	23.5	18
	Bolu	23.5	18

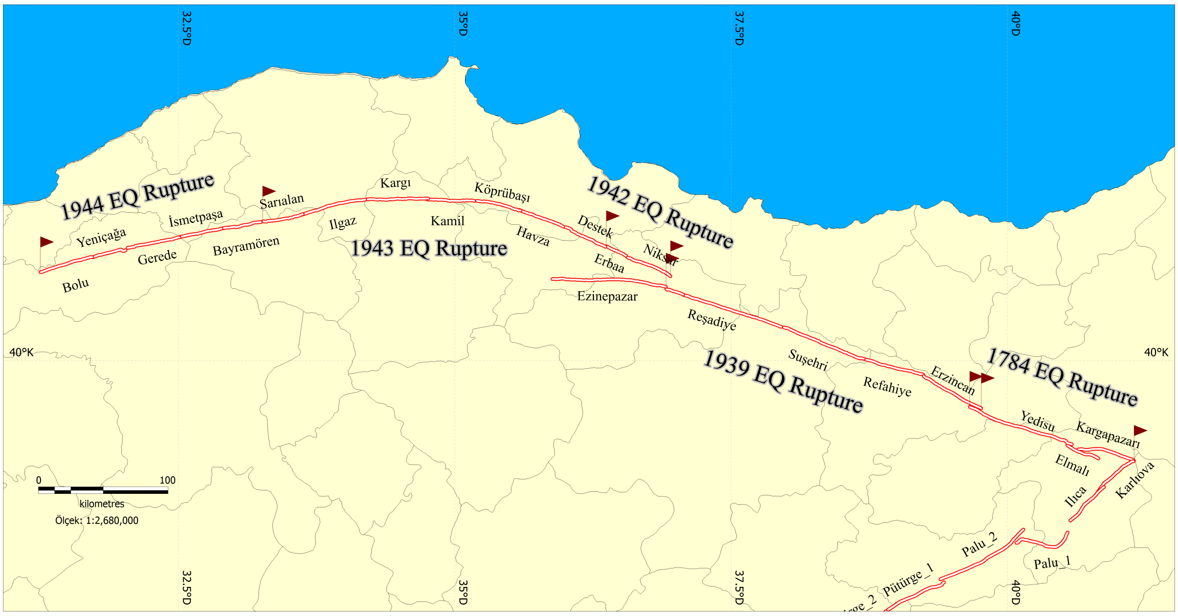

Figure 5.7. Combined rupture scenarios for the NAF

these two sub-section rupturing together has been evaluated with a combined rupture scenario called “Pütürge” in Table 5.5. The same is also valid the segment defined as Hacıpaşa by Emre et al. [14]. According to Akyüz et al. [108], while the north of the Hacıpaşa segment, called Hacıpaşa 1 in this study, was ruptured during 1872 earthquake, the whole Hacıpaşa segment was ruptured during 1408 earthquake. This is why Hacıpaşa segment is also divided into two sub-sections. The combined rupture scenario called “Hacıpaşa” takes into account the possibility of these two sub-segments rupturing together just like during the 1408 earthquake. In this sense, the reason why a combined rupture scenario was not created by using the Palu 1 and Palu 2 segments is that it is not quite possible. While Palu 1 is also delineated by thrusting, Palu 2 predominantly has strike slip morphology.

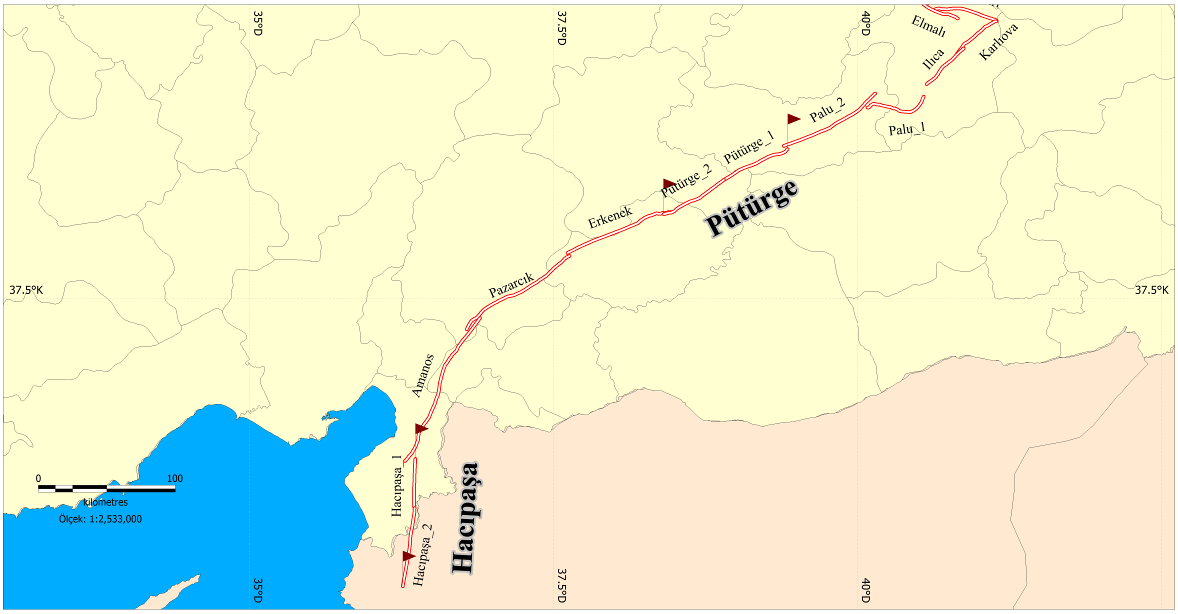

Figure 5.8. Combined rupture scenarios for the EAF

Table 5.5. Details of combined rupture scenarios for the EAF.

Combined Rupture Scenario	**Segments**	**Mean Slip Rate (mm/yr)**	**Max. Depth (km)**
Pütürge	Pütürge 1	9.50	18
	Pütürge 2	9.50	18
Hacıpaşa	Hacıpaşa 1	4.75	18
	Hacıpaşa 2	4.75	18

5.5.2. Source Scaling Relationships

Fault rupture parameters, which are associated with the magnitude of an earthquake, are usually used to determine the potential of a fault to produce earthquakes in the future [149]. In order to estimate characteristic earthquake magnitude of the segments three different source scaling relationships given below have been used.

(i) Wells and Coppersmith [149]
(ii) Leonard [150]
(iii) Hanks and Bakun [151]

When the relationships of Wells and Coppersmith and Leonard are taken into account, both surface rupture length and rupture area equations are used. On the other hand, when Hanks and Bakun is considered, only fault area based equation is used. At the end of the calculations, the mean of the results of these five equations is calculated to represent the characteristic magnitude of the segments. The results are shown in Table 5.6 and 5.7 for individual ruptures. On the other hand, for combined rupture scenarios, characteristic magnitude values are presented in Table 5.8 and 5.9.

Table 5.6. The calculation of the characteristic earthquake magnitude of the NAF's segments.

Segments	**Length (km)**	**Mw(SRL) (W&C94)**	**Mw(RA) (W&C94)**	**Mw(A) (H&B14)**	**Mw(L) (L10)**	**Mw(A) (L10)**	**Mw Mean**
Kargapazarı	45.6	7.0	7.0	7.0	6.9	6.9	6.95
Elmalı	27.0	6.8	6.7	6.7	6.5	6.7	6.68
Yedisu	85.6	7.3	7.2	7.3	7.2	7.2	7.25
Erzincan	51.5	7.1	7.0	7.0	7.0	7.0	7.01
Refahiye	47.8	7.0	7.0	7.0	6.9	6.9	6.97
Suşehri	66.6	7.2	7.1	7.2	7.1	7.1	7.13
Reşadiye	94.1	7.4	7.3	7.4	7.2	7.2	7.30
Ezinepazar	88.0	7.3	7.2	7.3	7.2	7.2	7.26
Niksar	37.3	6.9	6.9	6.8	6.8	6.8	6.84
Erbaa	20.0	6.6	6.6	6.5	6.3	6.5	6.52
Destek	34.7	6.9	6.8	6.8	6.7	6.8	6.81
Havza	35.9	6.9	6.8	6.8	6.8	6.8	6.82
Köprübaşı	34.7	6.9	6.8	6.8	6.7	6.8	6.81
Kamil	37.0	6.9	6.9	6.8	6.8	6.8	6.84
Kargı	47.2	7.0	7.0	7.0	6.9	6.9	6.97
Ilgaz	49.7	7.1	7.0	7.0	7.0	6.9	6.99
Sarıalan	31.6	6.8	6.8	6.7	6.7	6.7	6.76
Bayramören	30.4	6.8	6.8	6.7	6.6	6.7	6.74
İsmetpaşa	32.5	6.9	6.8	6.8	6.7	6.8	6.77
Gerede	41.0	7.0	6.9	6.9	6.9	6.9	6.89
Yeniçağa	26.6	6.8	6.7	6.7	6.5	6.7	6.67
Bolu	41.4	7.0	6.9	6.9	6.9	6.9	6.90

Table 5.7. The calculation of the characteristic earthquake magnitude of the EAF's segments.

Segments	**Length (km)**	**Mw(SRL) (W&C94)**	**Mw(RA) (W&C94)**	**Mw(A) (H&B14)**	**Mw(L) (L10)**	**Mw(A) (L10)**	**Mw Mean**
Karlıova	37.26	6.9	6.9	6.8	6.8	6.8	6.84
Ilıca	37.29	6.9	6.9	6.8	6.8	6.8	6.84
Palu 1	48.42	7.0	7.0	7.0	6.9	6.9	6.98
Palu 2	76.96	7.3	7.2	7.3	7.1	7.1	7.20
Pütürge 1	51.25	7.1	7.0	7.0	7.0	7.0	7.01
Pütürge 2	50.92	7.1	7.0	7.0	7.0	7.0	7.00
Erkenek	82.94	7.3	7.2	7.3	7.2	7.2	7.23
Pazarcık	93.77	7.4	7.3	7.4	7.2	7.2	7.29
Amanos	120	7.5	7.4	7.5	7.3	7.3	7.41
Hacıpaşa 1	35.48	6.9	6.8	6.8	6.7	6.8	6.82
Hacıpaşa 2	57.64	7.1	7.1	7.1	7.0	7.0	7.06

Table 5.8. Characteristic magnitude values of the combined rupture scenarios for the NAF.

Segments	**Length (km)**	**Mw(SRL) (W&C94)**	**Mw(RA) (W&C94)**	**Mw(A) (H&B14)**	**Mw(L) (L10)**	**Mw(A) (L10)**	**Mw Mean**
1784 EQ Rupture	131.2	7.5	7.4	7.6	7.4	7.4	7.45
1939 EQ Rupture	260.0	7.9	7.7	8.0	7.7	7.7	7.78
1942 EQ Rupture	57.3	7.1	7.1	7.1	7.0	7.0	7.06
1943 EQ Rupture	270.7	7.9	7.7	8.0	7.7	7.7	7.80
1944 EQ Rupture	171.9	7.7	7.5	7.7	7.5	7.5	7.58

Table 5.9. Characteristic magnitude values of the combined rupture scenarios for the EAF.

Segments	Length (km)	Mw(SRL) (W&C94)	Mw(RA) (W&C94)	Mw(A) (H&B14)	Mw(L) (L10)	Mw(A) (L10)	Mw Mean
Pütürge	102.2	7.4	7.3	7.4	7.3	7.3	7.33
Hacıpaşa	93.1	7.4	7.3	7.4	7.2	7.2	7.29

5.5.3. Moment Balancing between Individual and Combined Rupture Scenarios

The remaining amount of slip rate (94%) is split between individual and combined rupture scenarios. The main objective is to achieve coherence between recurrence intervals of the rupture scenarios and observed seismicity revealed by paleoseismic studies.

Paleoseismic investigations use geological and geomorphological data as well as Quaternary dating techniques to identify the estimated timing of surface - rupturing events. The spatiotemporal understanding of earthquakes can be achieved via harmonizing historical and paleoseismological data. This offer us deep insight into long - term fault behavior [4]. The study conducted by Fraser at al. [4] has classified paleoseismic data sets of the NAF and interpreted the results by means of historical earthquake catalogs. At the end of the research, some recurrence intervals have been proposed for trenches located along the NAF. By following a method, these recurrence periods are matched with the combined rupture scenarios in our model.

According to the aforementioned method, the positions of the trenches are determined, and thus, the relationship between these trenches and NAF's segments is clarified. As it can be discerned in Figure 5.9, while some trenches are located on the same segment, there is no trenches on some fault segments. In Table 5.10, the segments where trenches are located, the proposed recurrence intervals for trenches by Fraser et al. [4] and the corresponding combined rupture scenarios are given. Since these recurrence periods differ significantly even within the same fault segment, the related recurrence periods have been averaged to estimate recurrence interval of each scenario.

Figure 5.9. Positions of trenches studied by Fraser et al. [4]

In Table 5.11, the remaining slip rate (94%) is distributed between combined rupture models and their component segments, which also refer individual rupture models or scenarios. Since the main purpose is to achive harmony with recurrence intervals proposed by Fraser et al. [4], there is no fixed percentage of slip partitioning between scenarios. While the study carried out by Fraser et al. [4] is used to do moment balancing between two rupture scenarios for the NAF, the slip partitioning ratio of 50% is directly selected to do it for the EAF. This is because such a comprehensive paleoseismic study has not been made for the EAF yet. Slip partitioning has not been performed for the fault segments not included in the combined rupture scenarios (e.g., Ezinepazar on the NAF and Karlıova on the EAF), and thus, the remaining slip rate (94%) has been allocated to these segments for only individual rupture scenarios.

Table 5.10. The relationship between trenches' locations, recurrence intervals and combined rupture scenarios.

Combined Rupture Scenario	**Segments**	**Trenches**	**Proposed TR (yr)**	**Mean TR (yr)**
1784 EQ Rupture	Kargapazarı			~260
	Yedisu	EEB	202-306	
1939 EQ Rupture	Erzincan			~560
	Refahiye	YAY, CUK	349–387, 495–570	
	Suşehri	GUN	646–688	
	Reşadiye	RSA	667–702	
1942 EQ Rupture	Niksar			—
	Erbaa			
1943 EQ Rupture	Destek	DTK	362–407	~450
	Havza	HAV, AYA(AYB)	601–789, 329–488	
	Köprübaşı			
	Kamil	ELM	470–529	
	Kargı			
	Ilgaz			
	Sarıalan			
1944 EQ Rupture	Bayramören			~520
	İsmetpaşa			
	Gerede	GDT	478–576	
	Yeniçağa			
	Bolu			

Table 5.11. Slip partitioning between combined and individual rupture models.

Scenario	Combined Rupture Model	Individual Rupture Model
1784 EQ Rupture	50%	50%
1939 EQ Rupture	40%	60%
1942 EQ Rupture	50%	50%
1943 EQ Rupture	45%	55%
1944 EQ Rupture	30%	70%
Pütürge	50%	50%
Hacıpaşa	50%	50%

5.5.4. Recurrence Intervals of the Individual and Combined Rupture Scenarios

The recurrence periods and annual rate of occurrences obtained as a result of the process of the moment balancing are given in Tables 5.12, 5.13, 5.14, and 5.15.

Although we have not any paleoseismic research suggesting recurrence intervals along the EAF, Barka and Kadinsky - Cade [71] have asserted that the recurrence interval of the EAF could be up to 1000 years as in the "Hacıpaşa" combined rupture scenario. Çetin et al. [106] have proposed a recurrence period of 100 - 360 years for the Palu - Lake Hazar segment, corresponding Palu 2 segment in our model. On the other hand, Hubert - Ferrari et al. [94] have determined the recurrence period for the same region to be approximately 190 years. As for the southern end of the EAF, Akyüz et al. [108] have suggested a recurrence interval of approximately 500 years for the segment called Hacıpaşa 1 in our model. In the light of this information, it can be said that recurrence intervals of the EAF, obtained as a result of the moment balancing procedure, also achieve reasonable harmony with the observed seismicity.

Table 5.12. Recurrence intervals of the NAF's segments for the individual rupture scenario.

Segments	**Length (km)**	**Mw Mean**	**N (Ave) (eq/year)**	**TR (Ave) (year)**
Kargapazarı	45.6	6.95	0.0060	166
Elmalı	27.0	6.68	0.0016	631
Yedisu	85.6	7.25	0.0045	223
Erzincan	51.5	7.01	0.0086	116
Refahiye	47.8	6.97	0.0090	111
Suşehri	66.6	7.13	0.0073	137
Reşadiye	94.1	7.30	0.0058	171
Ezinepazar	88.0	7.26	0.0009	1079
Niksar	37.3	6.84	0.0087	114
Erbaa	20.0	6.52	0.0142	70
Destek	34.7	6.81	0.0102	98
Havza	35.9	6.82	0.0099	101
Köprübaşı	34.7	6.81	0.0102	98
Kamil	37.0	6.84	0.0097	103
Kargı	47.2	6.97	0.0080	125
Ilgaz	49.7	6.99	0.0077	130
Sarıalan	31.6	6.76	0.0111	90
Bayramören	30.4	6.74	0.0159	63
İsmetpaşa	32.5	6.77	0.0150	67
Gerede	41.0	6.89	0.0124	81
Yeniçağa	26.6	6.67	0.0176	57
Bolu	41.4	6.90	0.0123	82

Table 5.13. Recurrence intervals of the combined rupture scenarios for the NAF.

Scenarios	**Length (km)**	**Mw (Mean)**	**N (Ave) (eq/year)**	**TR (Ave) (yr)**	**Paleoseismic TR (Ave) (yr)**
1784 EQ Rupture	131.2	7.45	0.0031	327	260
1939 EQ Rupture	260.0	7.78	0.0020	493	560
1942 EQ Rupture	57.3	7.06	0.0064	156	-
1943 EQ Rupture	270.7	7.80	0.0021	470	450
1944 EQ Rupture	171.9	7.58	0.0021	482	520

Table 5.14. Recurrence intervals of the EAF's segments for the individual rupture scenario.

Segments	**Length (km)**	**Mw (Mean)**	**N (Ave) (eq/year)**	**TR (Ave) (year)**
Karlıova	37.26	6.84	0.0066	153
Ilıca	37.29	6.84	0.0065	153
Palu 1	48.42	6.98	0.0043	232
Palu 2	76.96	7.20	0.0047	214
Pütürge 1	51.25	7.01	0.0030	329
Pütürge 2	50.92	7.00	0.0031	328
Erkenek	82.94	7.23	0.0032	315
Pazarcık	93.77	7.29	0.0029	341
Amanos	120.00	7.41	0.0024	415
Hacıpaşa 1	35.48	6.82	0.0020	496
Hacıpaşa 2	57.64	7.06	0.0014	710

Table 5.15. Recurrence intervals of the combined rupture scenarios for the EAF.

Combined Rupture	**Length (km)**	**Mw (Mean)**	**N (Ave) (eq/year)**	**TR (Ave) (year)**
Pütürge	102.2	7.33	0.0020	512
Hacıpaşa	93.1	7.29	0.0010	965

5.6. Time – Dependent Recurrence Relationship of Combined – Characteristic Part of the Hybrid Model

In order to convert the Poissonian hybrid model to time - dependent one, the last characteristic earthquakes occurred along the fault segments should be determined.

5.6.1. The Last Characteristic Earthquakes on the NAF and EAF

The epicenter locations of recent major earthquakes occurred along the NAF are shown in Figure 5.10 and further information about these earthquakes is provided below. As it is noticed through Figure 5.10 and also indicated by Barka and Kadinsky - Cade [71], the epicenters of characteristic earthquakes are usually located at the start and end points of the fault segments.

- 1784 Earthquake

  This earthquake with magnitude of Ms 7.6 [152] has been associated with the Kagapazarı and Yedisu segments. Only if these two segments are ruptured together (Mw 7.45) will such a magnitude occur.
- 1949 Earthquake

  Both Nalbant et al. [153] and Emre et al. [154] have asserted that Elmalıdere segment, corresponding Elmalı segment in our model, was ruptured during 1949 earthquake (Ms 6.9).

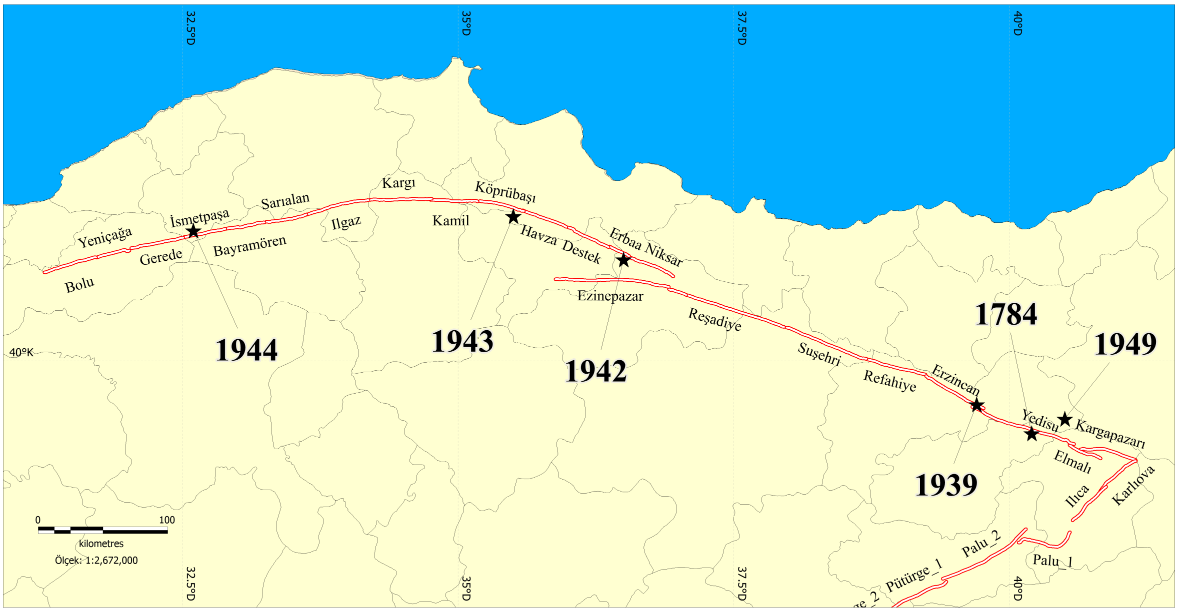

Figure 5.10. The last characteristic earthquakes along the NAF

- 1939 Erzincan Earthquake

  During this earthquake (Ms 7.8) [152], Erzincan, Refahiye, Suşehri, Reşadiye and Ezinepazar segments were ruptured all together.

- 1942 Niksar - Erbaa Earthquake

  This earthquake with magnitude of Ms 7.1 [152] ruptured only Niksar and Erbaa fault segments.

- 1943 Tosya - Ladik Earthquake

  Destek, Havza, Köprübaşı, Kamil, Kargı, Ilgaz, and Sarılan segments ruptured en masse during the earthquake with Ms 7.4 [152].

- 1943 Tosya - Ladik Earthquake

  Destek, Havza, Köprübaşı, Kamil, Kargı, Ilgaz, and Sarılan segments ruptured en masse during the earthquake with Ms 7.4 [152].

- 1944 Bolu - Gerede Earthquake

  Bayramören, İsmetpaşa, Gerede, Yeniçağa and Bolu segments are the segments that were ruptured during this earthquake with magnitude of Ms 7.3 [152]

In Figure 5.11, the epicenter locations of the recent characteristic earthquakes related to the EAF are illustrated. Contrary to the NAF, only a few characteristic earthquakes have occurred in 20th century along the EAFZ such as 1905 and 1971 earthquakes [71]. Therefore, it is not a straightforward procedure to associate the characteristic earthquakes with EAF's segments. General information on the last major earthquakes and the segments that were ruptured during these earthquakes is given below.

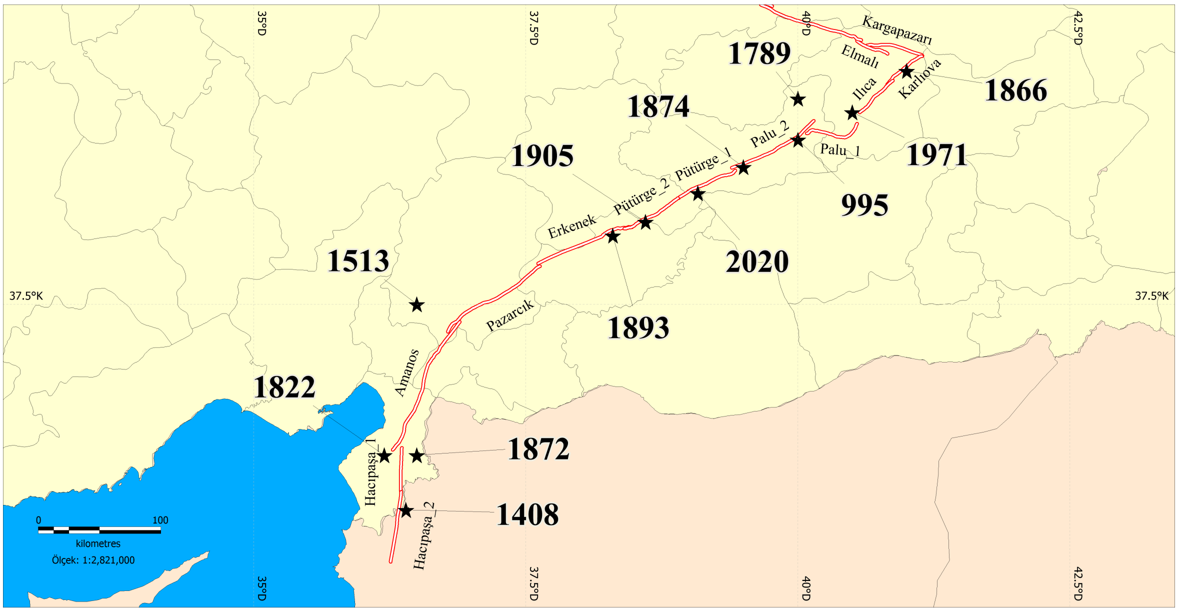

Figure 5.11. The last characteristic earthquakes along the EAF

- 1866 Earthquake

  The magnitude of this earthquake is Ms 7.2 [153]. When the damage distribution of this earthquake is analyzed, a uniform distribution is noticed around the Karlıova segment as it is presented in Figure 5.12. Therefore, 1866 earthquake has only been associated with Karlıova segment.

- 1971 Bingöl Earthquake

  According to information gotten by Barka and Kadinsky - Cade [71] and Seymen and Aydın [155], it can be inferred that this earthquake with a magnitude Ms 6.8 [11] ruptured only Ilıca segment. This is sensible when the characteristic magnitude of Ilıca segment (Mw 6.84) is considered.

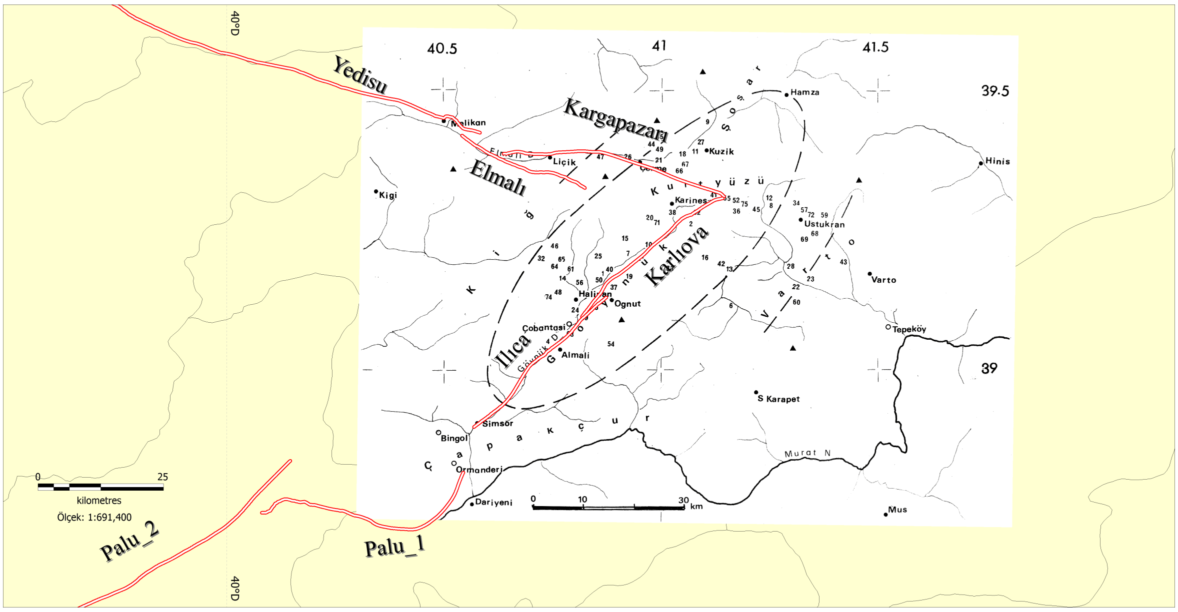

Figure 5.12. The damage distribution of 1866 earthquake [10]

- 1789 Earthquake

  This earthquake with a magnitude Ms>7 [11] is associated with Palu 1 segment, which is nearly compatible with the characteristic magnitude of Palu 1 segment (Mw 7).

- 995 Earthquake

  It is assumed that this earthquake, whose magnitude is given by Ambraseys and Jackson [152] in the range of Ms 7-7.8, is the last major earthquake to rupture Pütürge 1 and 2 segments together, corresponding “Pütürge” combined rupture scenario.

- 1874 Earthquake

  Ambraseys [11] has suggested that the surface-wave magnitude of this earthquake is greater than 7.1. In this study, it is accepted that 1874 earthquake is the last characteristic one that ruptured Palu 2 segment.

- 2020 Elazığ Earthquake

  This earthquake with a magnitude Mw 6.75 ruptured Pütürge 1 segment [148].

- 1905 Earthquake

  By means of information gained from Nalbant et al. [153], it can be said that 1905 Malatya earthquake with Ms 6.8 ruptured Pütürge 2 segment. The felt area of this earthquake, shown in Figure 5.13, also rationalizes this assumption.

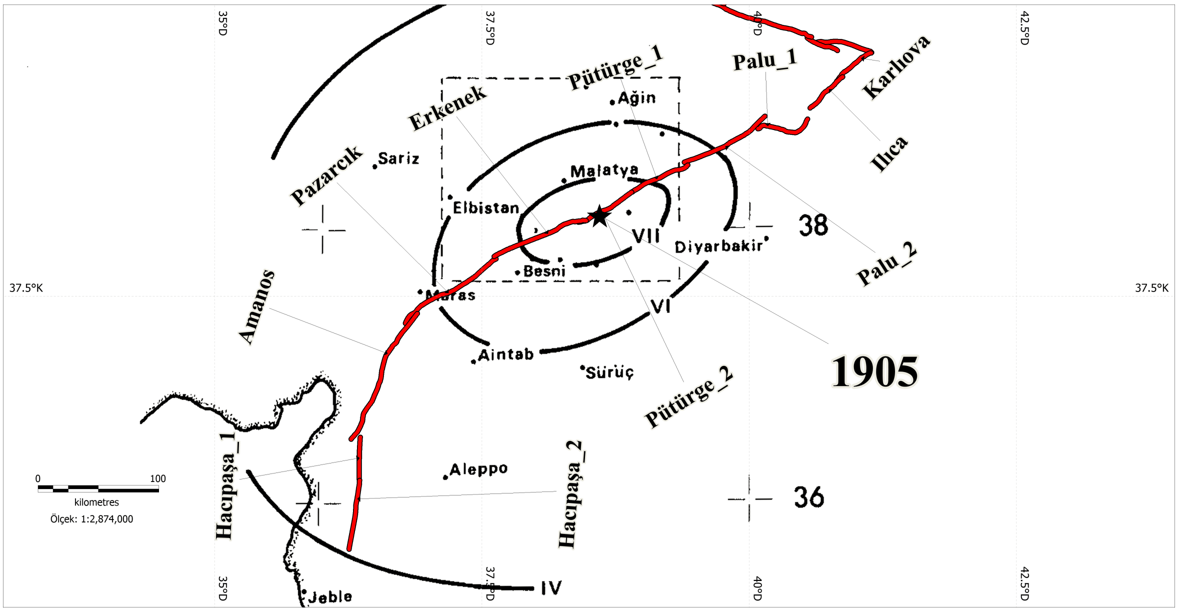

Figure 5.13. Felt area of 1905 earthquake [11]

- 1893 Earthquake

  When the felt area, seen in Figure 5.14, and epicenter location of this earthquake with a magnitude Ms>7.1 is considered, it can be inferred that this earthquake is the last major earthquake to rupture Erkenek segment.

- 1513 Earthquake

  According to Karabacak et al. [93] and Aktuğ et al. [156], this earthquake with a magnitude Ms>7.4 [11] is the last characteristic one that was occurred on Pazarcık segment. Therefore, there is a seismic gap on this segment.

- 1822 Earthquake

  While Ambraseys [11] has asserted that the magnitude of this earthquake is Ms>7.4, Karaki [157] has proposed the magnitude of Ml 7.1. Akyüz et al. [108] have stated this event took place in the Karasu valley. Therefore, it is accepted that 1822 earthquake is the last characteristic event of Amanos segment.

- 1872 Earthquake

  Based on the paleoseismic research done by Akyüz et al. [108], only the segment named Hacıpaşa 1 within the framework of this study was ruptured during 1872 Lake Amik earthquake with Ms 7.2 [11].

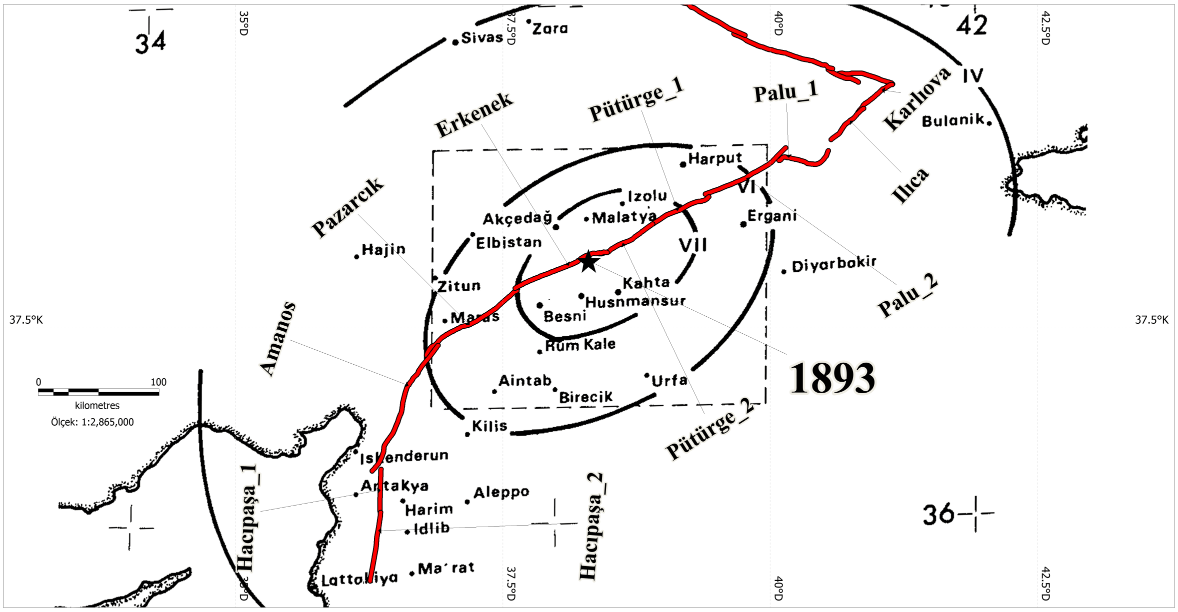

Figure 5.14. Felt area of 1893 earthquake [11]

- 1408 Earthquake

  There is no detailed information on this historical major event in literature as in the case of 1513 earthquake. The epicenter location is taken from Ambraseys and Jackson [152]. The magnitude of this event has been proposed as Ms 7.2 by Khair et al. [158]. Akyüz et al. [108] have declared that this is the last characteristic event that ruptured Hacıpaşa 1 and 2 segments as a whole, corresponding "Hacıpaşa" combined rupture in our model. Hence, there has been a tremendous amount of seismic gap especially on Hacıpaşa 2 segment since 1408 because the other segment was ruptured during 1872 major earthquake.

5.6.2. Time – Dependent Annual Rate of Occurrences of the NAF and EAF

For the determination of time – dependent annual rate of occurrences, the conditional probabilities of each rupture scenario are computed. These probabilities are called conditional because they depend on the time elapsed since the last characteristic earthquake. Both the lognormal and BPT probability density functions have been used to calculate conditional probabilities. However, only results of the BPT model are adopted in the seismic hazard calculations. The rationale on which this decision is based has been explained in minor details in chapter 4.

The mean earthquake recurrence interval (μ) and CoV or aperiodicity (α), identifying renewal models, can be approximated in a variety of methods depending on the information provided. In case of the presence of a substantial amount of data regarding historical past event dates, for model calibration, the adjusted maximum likelihood estimation (MLE) method can be employed. In the other case, the principle of the conservation of total seismic moment rate accumulated on segments is applied to calibrate the mean recurrence interval of the renewal recurrence model, which requires the use of a set of values generally preferred such as 0.3, 0.5, and 0.7 for the CoV [8, 123]. Hence, aperiodicity (α) and/or the coefficient of variation (CoV) are chosen 0.5 in the calculation of conditional probabilities because this value reflects the moderate periodic behavior of the NAF and EAF.

The 50 year conditional probabilities obtained are translated to Poissonian ones by using following formula [7]:

$$\lambda = \frac{-ln\,(1 - P_{cond})}{T} \tag{5.3}$$

In Table 5.16 and 5.17, the calculation results of the conditional probabilities and corresponding annual rate of occurrences are listed for the each rupture scenario of NAF and EAF, respectively. The results of the time – independent model are also provided to make a comparison between time – dependent and independent models possible.

Table 5.16. Conditional probabilities for the rupture scenarios of the NAF.

Scenarios	The Last Char. Eq.	μ (yr)	Lognormal		BPT		TI	
			P_{cond}	λ	P_{cond}	λ	λ	P_{cond}
1784 EQ Rupture	1784	330	0.22934	0.00521	0.22790	0.00517	0.0030	0.1406
Elmalı	1949	630	0.00063	0.00001	0.00023	0.00000	0.0016	0.0764
1939 EQ Rupture	1939	490	0.00559	0.00011	0.00411	0.00008	0.0020	0.0970
1942 EQ Rupture	1942	160	0.34830	0.00856	0.35263	0.00870	0.0063	0.2684
1943 EQ Rupture	1943	470	0.00600	0.00012	0.00447	0.00009	0.0021	0.1010
1944 EQ Rupture	1944	480	0.00506	0.00010	0.00361	0.00007	0.0021	0.0988
Ezinepazar	1939	1080	0.000014	0.00000	0.0000006	0.00000	0.0009	0.0454

Table 5.17. Conditional probabilities for the rupture scenarios of the EAF.

Scenarios	The Last Char. Eq.	μ (yr)	Lognormal		BPT		TI	
			P_{cond}	λ	P_{cond}	λ	λ	P_{cond}
Karlıova	1866	150	0.51438	0.01445	0.50401	0.01402	0.0067	0.2836
Ilıca	1971	150	0.25884	0.00599	0.26718	0.00622	0.0067	0.2836
Palu 1	1789	230	0.36929	0.00922	0.36069	0.00895	0.0044	0.1955
Palu 2	1874	220	0.31922	0.00769	0.31779	0.00765	0.0046	0.2035
Pütürge 1	2020	330	0.00012	0.00000	0.00002	0.00000	0.0030	0.1406
Pütürge 2	1905	330	0.09120	0.00191	0.09578	0.00201	0.0030	0.1406
Pütürge	995	510	0.20025	0.00447	0.20238	0.00452	0.0020	0.0934
Erkenek	1893	320	0.11990	0.00255	0.12561	0.00268	0.0031	0.1449
Pazarcık	1513	340	0.28335	0.00666	0.27915	0.00655	0.0029	0.1367
Amanos	1822	420	0.11367	0.00241	0.11827	0.00252	0.0024	0.1122
Hacıpaşa 1	1872	500	0.03424	0.00070	0.03506	0.00071	0.0020	0.0952
Hacıpaşa 2	1408	710	0.12678	0.00271	0.12444	0.00266	0.0014	0.0681
Hacıpaşa	1408	970	0.07339	0.00152	0.07474	0.00155	0.0010	0.0502

5.7. Background Smoothed-Seismicity

The study which was undertaken by Kafka [159] concluded that seismic hazard assessment for -probably- almost all intraplate regions is based on seismicity in order to estimate locations of future major earthquakes. In this sense, as it is done similarly in the research conducted by Demircioğlu et al. [28], historical and instrumental seismicity have been used to depict the earthquake pattern of the fault zones and determine the small magnitude events happening around the faults. Eventually, in the implementation of background smoothed seismicity, individual sources are considered as point sources, each one of which is described through depth distribution, style of faulting, b value (i.e., recurrence parameters), and lower and upper limit of magnitude. Other than recurrence rates, all characteristics of point sources are the same with corresponding area sources, which are produced by Şeşetyan et al. [64]. b value for each point source is assumed to be equal to the b value of the surrounding fault zones.

In addition to the earthquakes whose epicenters do not fall within the buffer zones of the NAF and EAF, earthquakes with $Mw<6$ inside the buffer zones form background seismicity (i.e., it is assumed that events with $Mw>6$ within the buffer zones happened exactly on the fault sources). Earthquakes that do not meet these magnitude and epicenter criteria are excluded from the catalogue during the calculation of background activity rates. The lower limit for the magnitude of these events, on the other hand, is 4.3. These events are taken into consideration as gridded point sources, created 0.1° x 0.1° intervals, with activity rates calculated using Frankel's smoothed seismicity approach [67]. This approach is based on the premise that future earthquakes will happen in the region where previous earthquakes occurred.

6. SEISMIC HAZARD CALCULATIONS

Sucuoğlu and Akkar have noted that ground-motion prediction models guess the ground-motion intensity parameters (e.g., PGA, PGV, and SA) at a specific site by considering the source, path and site effects. These effects are essentially characterized by independent variables such as magnitude (M), source-to-site distance (R), site class (SC) and style-of-faulting (SoF) [160]. In order to carry out a realistic PSHA, the choice of the most suitable GMM for the studied region is a critical stage [28].Akkar et al. [3] have concluded that Akkar et al. [62], Chiou and Youngs [53], Akkar and Çağnan [54], and Zhao et al. [51] can be used to conduct a PSHA for shallow active crustal regions including Turkey. On the other hand, Zhao et al. [51], Atkinson and Boore [58], Youngs et al. [57] and Lin and Lee [59] exemplify GMMs that can be used for subduction regions. The aim of the present work being the evaluation of the effects of different earthquake recurrence models, a single GMM for each tectonic region was selected for the modeling of the ground motion. As Chiou and Youngs [161] is the updated version of Chiou and Youngs [53] model and is one of the most widely used models for active shallow regions, it has been our preferred model for such regions while Zhao et al. [51] was adopted for subduction regions. Here it should be noted that only the Cyprean Arc is included as a subduction zone for sake of completeness of the final hazard model.

PSHA is performed for 10% and 2% probabilities of exceedance rates in the next 50 years by using OpenQuake Software [29]. During the calculations, Vs30 value has been considered to be equal to 760 m/s. Analyses have been carried out at every 5 km in the studied region, the results of which have been used to show GMIM distributions within the buffer zone of the faults. On the other hand, 13 sites along the faults, seen in Figure 6.1., have been selected to show and compare the results in terms of PGA and 5% damped SA at T = 0.2 s and T = 1.0 s for the return periods of 475 and 2475 years.

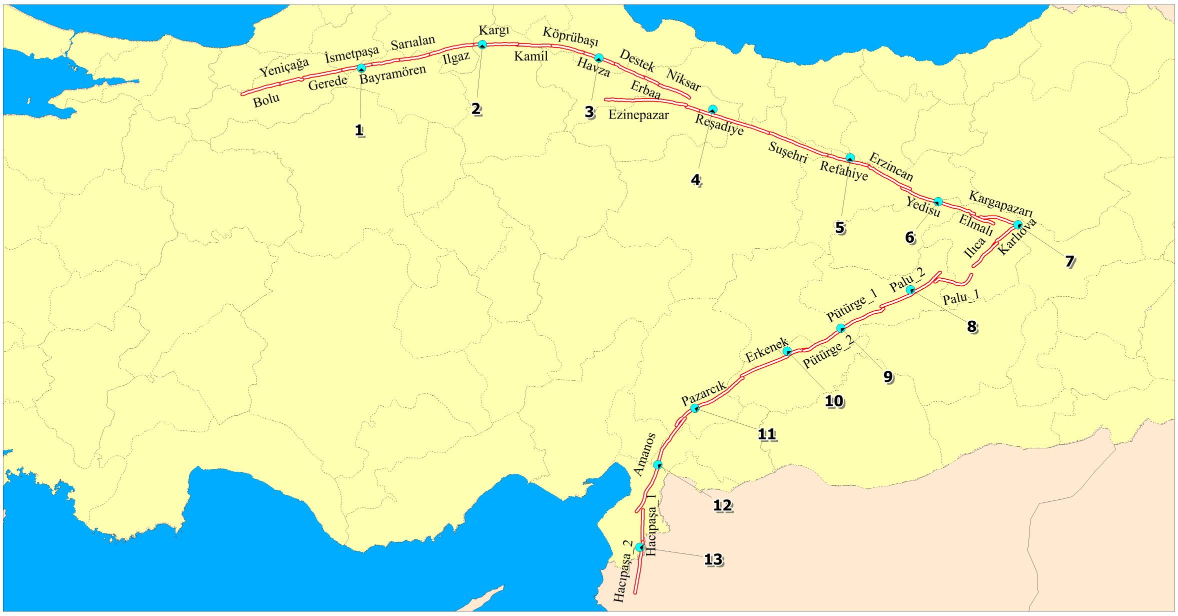

Figure 6.1. Selected points on the NAF and EAF for the computation of PSHA

7. RESULTS AND DISCUSSION

Although the primary objective of this research is to develop a strong hybrid earthquake recurrence relationship for the NAF and EAF, three other earthquake occurrence models have also been built in order to make some comparisons and to put the hybrid model on a rational basis. The models with hazard curves below exclude background smoothed seismicity and surrounding faults because first of all, make sure that the NAF and EAF are modeled properly.

7.1. Hazard Curves of Different Recurrence Models

From Site 1 to Site 13, mean hazard curves of various occurrence models, all of which are being Poissonian, have been presented in Figure 7.1 and 7.2.

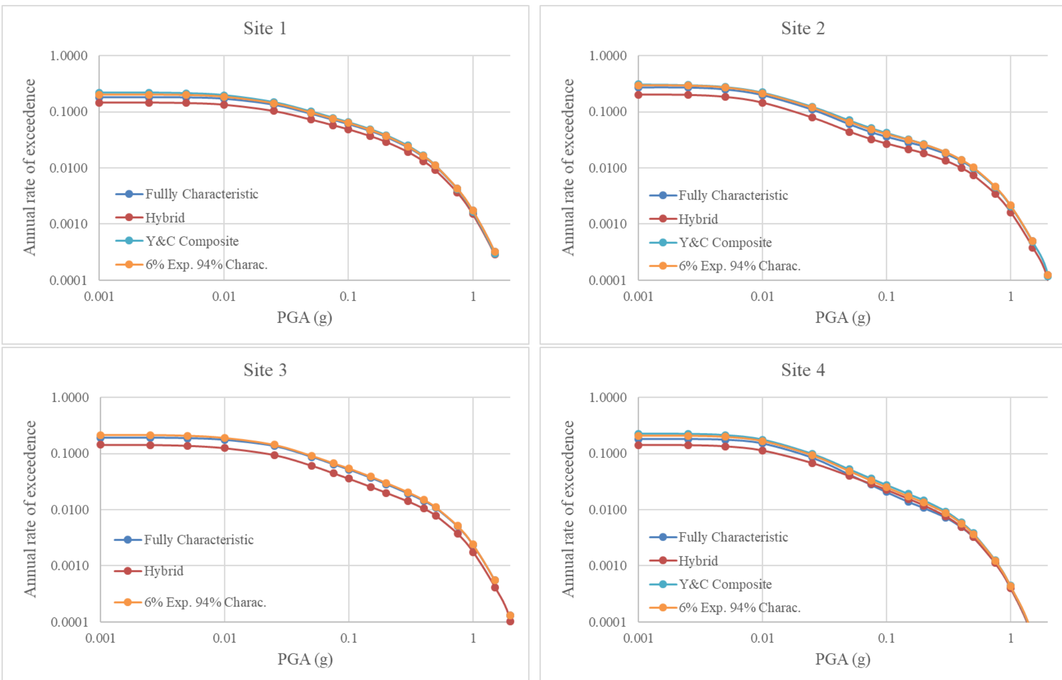

Figure 7.1. Mean hazard curves of different earthquake occurrence models for the site 1, 2, 3, and 4

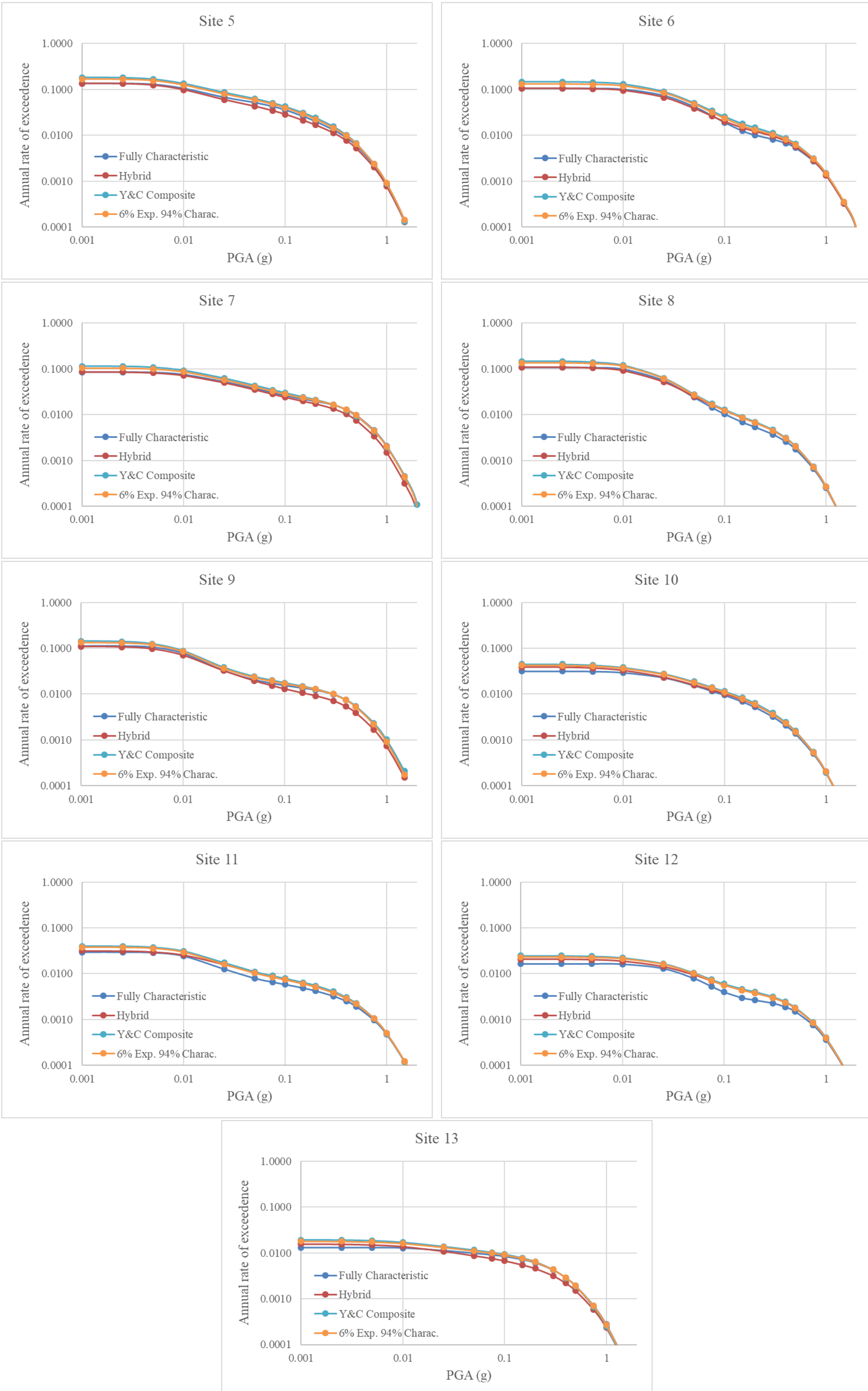

Figure 7.2. Mean hazard curves obtained from different earthquake occurrence models for the site 5, 6, 7, 8, 9, 10, 11, 12, and 13

If all seismic moment accumulated along a fault segment is released by only characteristic earthquakes, it can be claimed that the fault behaves completely characteristicly. By assigning all slip rate of faults to only individual rupture scenarios, the “Fully Characteristic” model in these graphs is obtained. Since the model gives unrelastic results (e.g., an earthquake with Mw$\sim$7 occurs on average every 60-70 years along the NAF), this model has been abandoned. However, the hazard curves of the “Fully Characteristic” model make some inferences possible.

When the total slip rate of a fault segment is split between the exponential tail and the individual rupture scenario of the fault by 6% and 94%, respectively, “6% Exp. 94% Charac.” model is achieved. On the other hand, “Y&C Composite” one, corresponding classical Youngs and Coppersmith composite earthquake recurrence model [25], is obtained automatically by means of OpenQuake software. The “Hybrid” model in the graphs represents the hybrid occurrence model developed in this study.

As seen in the graphs above, the difference between the hazard curves of “6% Exp. 94% Charac.” and “Y&C Composite” models can be neglected. This means that manually allocating 6% of the slip rate to the exponential part of the hybrid model will not lead to erroneous results.

Compared to the EAF, the NAF is more susceptible to the fully characteristic fault source modeling. The results of the “Fully Characteristic” model are more dominant along the NAF. This is because earthquake recurrence intervals of the NAF’s segments are smaller especially for the western side. In other words, as the slip rate of the faults decreases, the results of the “Fully Characteristic” model converge to those obtained from the other models.

While the hybrid recurrence model gives the smallest results along the NAF, the discrepancy between results of the hybrid model and the others becomes negligible on the EAF. The reason for this case is that the hybrid model is the only one involving the possibility of occurring combined rupture, and the NAF is much richer in terms of the variety of combined rupture scenarios compared to the EAF.

Regardless of the model, annual rates of exceedance ground motion levels are lower on the EAF because annual seismic moment accumulated along the EAF is less than that stored along the NAF. Moreover, the difference between the results of the recurrence models disappears at larger PGAs.

7.2. Hazard Curves of the Hybrid Model and Its Components

Here, the hazard contribution of the exponential tail and combined - characteristic part of the hybrid model will be discussed separately. The relation between the hybrid model and its components in terms of the hazard contribution are presented for each site in the figure 7.2.1.

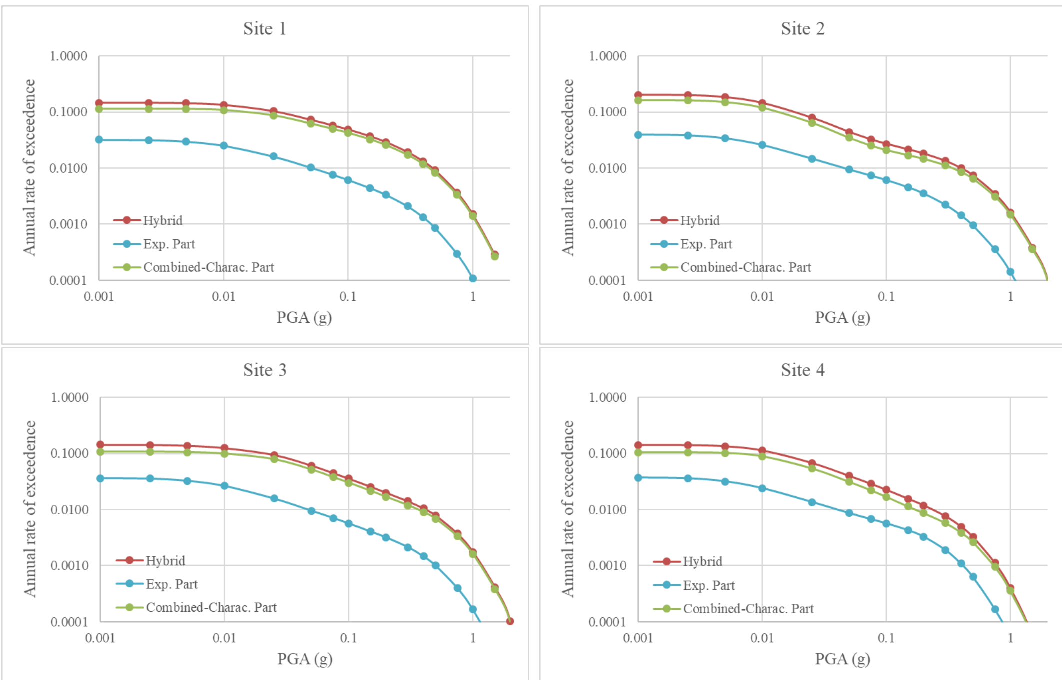

Figure 7.3. Mean hazard curves obtained from the hybrid earthquake occurrence model and the contribution of the different components for the site 1, 2, 3, and 4

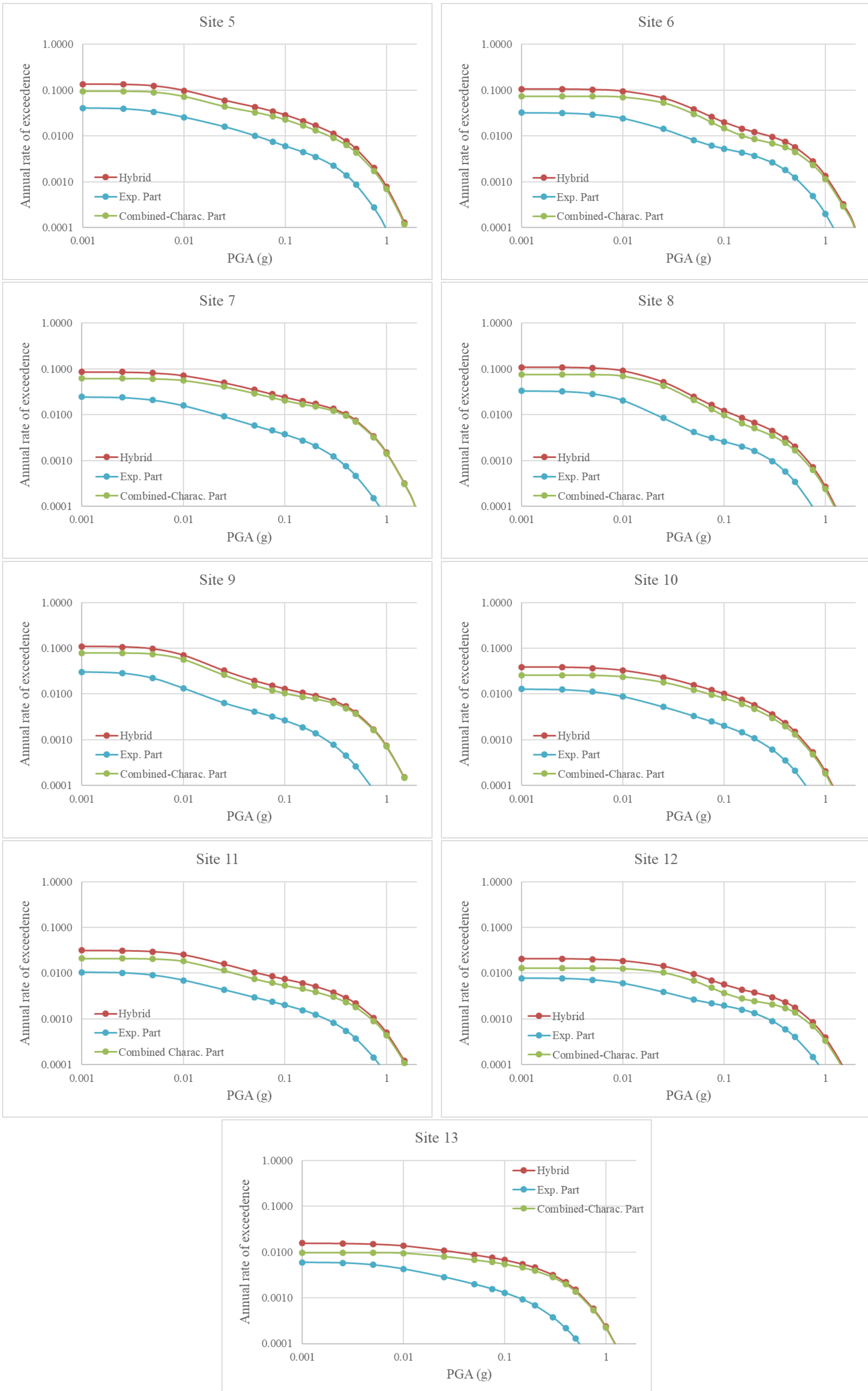

Figure 7.4. Mean hazard curves obtained from the hybrid earthquake occurrence model and the contribution of the different components for the site 5, 6, 7, 8, 9, 10, 11, 12, and 13

In the graphs, while the exponential tail of the hybrid model is named “Exp. Part”, combined - characteristic portion is called “Combined-Charac. Part”.

It has been observed that the hazard contribution of the exponential tail is smallest at all sites. On the other hand, the difference between exponential tail and combined - characteristic part in terms of the hazard contribution becomes minimum on the EAF especially for the southern section of it. This is also because of the amount of slip rate. As it decreases, the hazard contribution of the combined characteristic part is decaying, and thus, the relative contribution of exponential tail becomes dominant. It should also be pointed out although only 6% of the total seismic moment is allocated to the exponential tail, the hazard contribution of it cannot be disregarded for all sites.

For greater PGA values, the results of the hybrid model are almost equal to the results of the combined - characteristic part, which implies the combined - characteristic part of the hybrid model governs the overall hazard for larger PGAs.

7.3. GMIMs and Elastic Design Spectra for the Selected Sites

After concluding that the hybrid earthquake occurrence model of the NAF and EAF produces logical results to represent the intrinsic behavior of these faults, information of surrounding (i.e., secondary) faults and background smoothed seismicity are added to the hybrid model. Thus, the results of the hybrid model become comparable to the results of the fully exponential recurrence model developed for the same faults by Demircioğlu et al. [28]. The results are given in Table 7.1, 7.2, and 7.3 in terms of PGA and SA at T=0.2 and 1.0 s for the return periods of 475 and 2475 years.

Elastic design spectra for the all sites are also presented to give civil engineers insight into the effect of different modeling types on seismic hazard. Thus, the information given in the following tables will have a more practical meaning. Equation 2.2 and 2.3 in Turkish Earthquake Building Code (2018) have been used to plot the elastic design spectra. These spectra are drawn for the return periods of 475 and 2475 years and shown in Figure 7.5 to 7.17.

Table 7.1. Comparison of the results in terms of PGA.

Sites	Fully Exponential Model		Hybrid Model (Poissonian)		Hybrid Model (Renewal)	
	PGA(g) (RP=475 yr)	PGA(g) (RP=2475 yr)	PGA(g) (RP=475 yr)	PGA(g) (RP=2475 yr)	PGA(g) (RP=475yr)	PGA(g) (RP=2475 yr)
1	1.04	1.66	0.90	1.38	0.85	1.31
2	1.08	1.73	0.90	1.48	0.83	1.37
3	1.04	1.71	0.93	1.51	0.86	1.41
4	1.03	1.66	0.59	1.00	0.54	0.91
5	1.02	1.66	0.73	1.16	0.67	1.09
6	1.29	2.04	0.84	1.41	0.91	1.50
7	1.13	1.74	0.97	1.47	1.06	1.57
8	0.92	1.52	0.55	0.93	0.62	1.03
9	1.02	1.66	0.71	1.18	0.71	1.21
10	0.82	1.39	0.56	0.94	0.55	0.91
11	0.73	1.28	0.52	1.06	0.76	1.32
12	0.83	1.47	0.48	1.00	0.49	1.01
13	0.40	0.77	0.49	0.86	0.55	0.98

Table 7.2. Comparison of the results in terms of SA for RP=475 years.

Sites	Fully Exponential Model		Hybrid Model (Poissonian)		Hybrid Model (Renewal)	
	SA(g) (T=0.2 s)	SA(g) (T=1.0 s)	SA(g) (T=0.2 s)	SA(g) (T=1.0 s)	SA(g) (T=0.2 s)	SA(g) (T=1.0 s)
1	2.559	0.722	2.34	0.79	2.22	0.73
2	2.659	0.769	2.32	0.82	2.13	0.73
3	2.524	0.726	2.39	0.84	2.21	0.75
4	2.521	0.737	1.53	0.50	1.35	0.43
5	2.466	0.724	1.89	0.62	1.73	0.55
6	3.191	0.905	2.16	0.76	2.33	0.84
7	2.842	0.755	2.56	0.86	2.87	0.98
8	2.259	0.605	1.41	0.40	1.61	0.50
9	2.469	0.670	1.82	0.58	1.82	0.59
10	1.995	0.528	1.44	0.42	1.40	0.41
11	1.734	0.463	1.28	0.41	1.91	0.66
12	1.983	0.544	1.15	0.35	1.18	0.37
13	0.945	0.252	1.25	0.37	1.41	0.44

Table 7.3. Comparison of the results in terms of SA for RP=2475 years.

Sites	Fully Exponential Model		Hybrid Model (Poissonian)		Hybrid Model (Renewal)	
	SA(g) (T=0.2 s)	**SA(g) (T=1.0 s)**	**SA(g) (T=0.2 s)**	**SA(g) (T=1.0 s)**	**SA(g) (T=0.2 s)**	**SA(g) (T=1.0 s)**
1	4.273	1.254	3.86	1.35	3.68	1.25
2	4.441	1.340	4.05	1.52	3.77	1.35
3	4.332	1.320	4.15	1.53	3.89	1.36
4	4.233	1.287	2.66	0.95	2.43	0.84
5	4.207	1.324	3.22	1.13	3.01	1.02
6	5.168	1.561	3.87	1.45	4.11	1.57
7	4.497	1.249	4.11	1.46	4.45	1.60
8	3.830	1.076	2.49	0.81	2.78	0.94
9	4.188	1.204	3.24	1.14	3.32	1.20
10	3.488	0.963	2.50	0.82	2.44	0.79
11	3.214	0.901	2.80	1.02	3.60	1.35
12	3.648	1.073	2.57	0.93	2.61	0.95
13	1.863	0.478	2.29	0.77	2.59	0.90

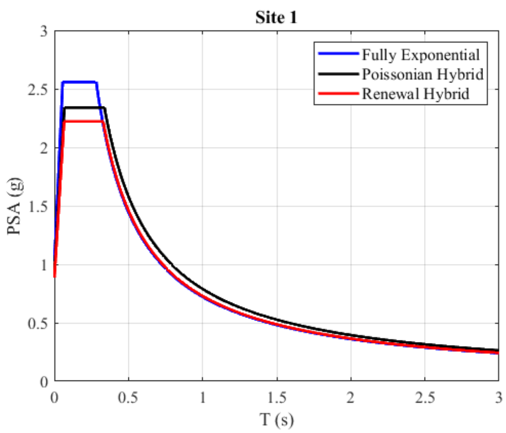

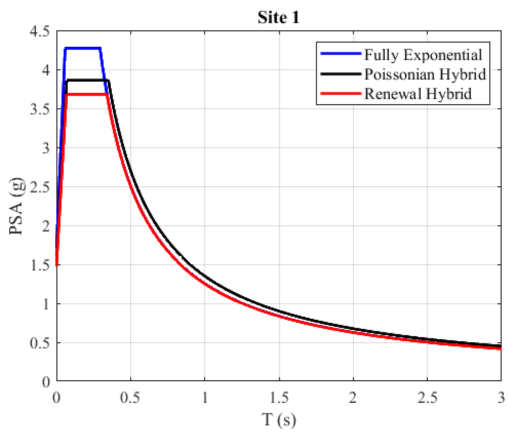

Figure 7.5. Elastic design spectra for Site 1 for the return periods of 475 (left) and 2475 (right) years

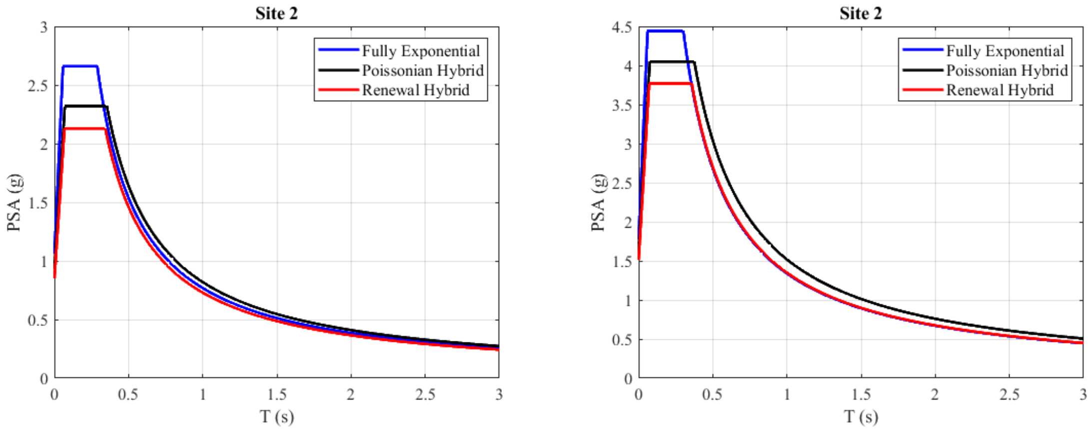

Figure 7.6. Elastic design spectra for Site 2 for the return periods of 475 (left) and 2475 (right) years

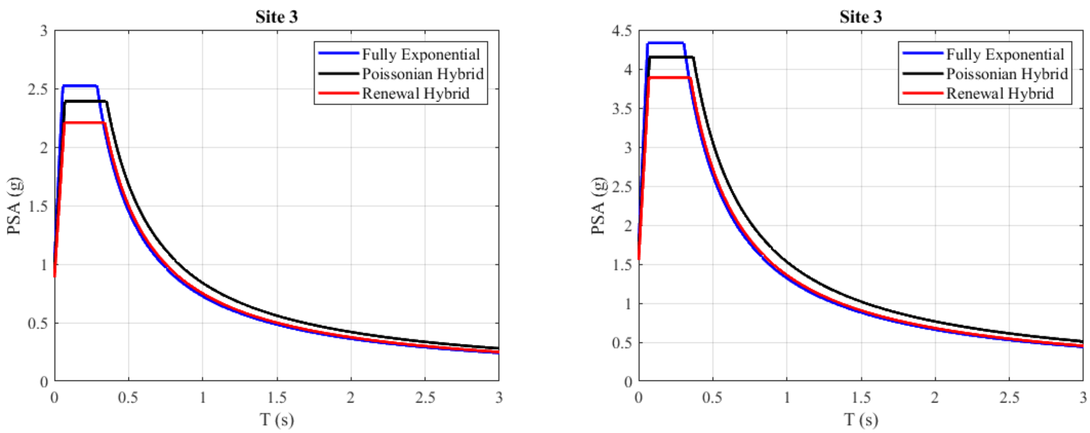

Figure 7.7. Elastic design spectra for Site 3 for the return periods of 475 (left) and 2475 (right) years

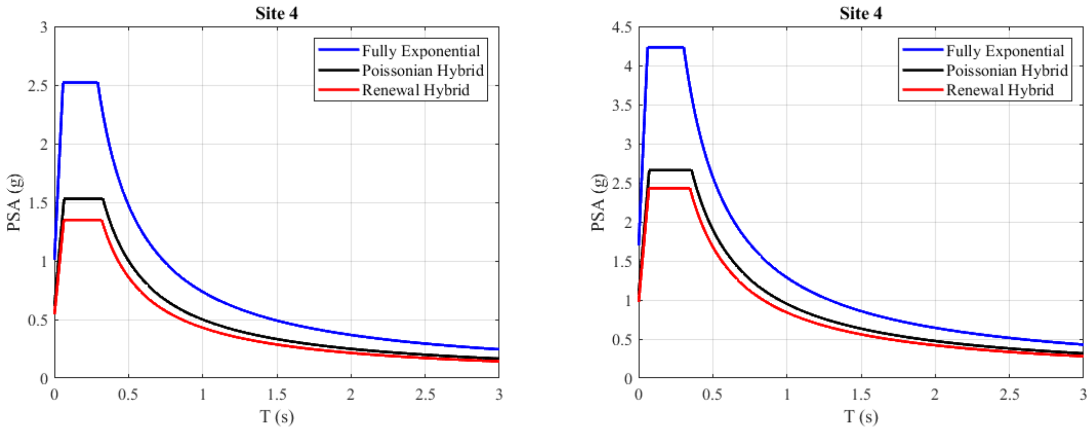

Figure 7.8. Elastic design spectra for Site 4 for the return periods of 475 (left) and 2475 (right) years

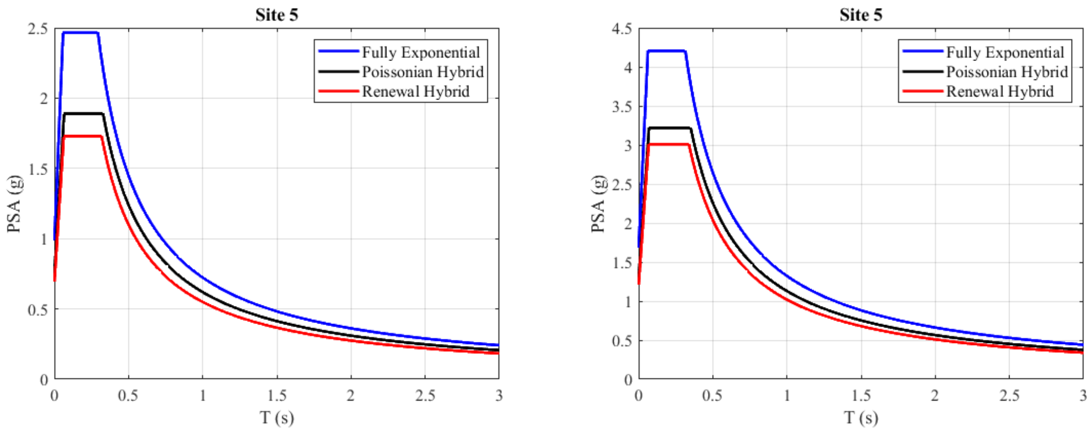

Figure 7.9. Elastic design spectra for Site 5 for the return periods of 475 (left) and 2475 (right) years

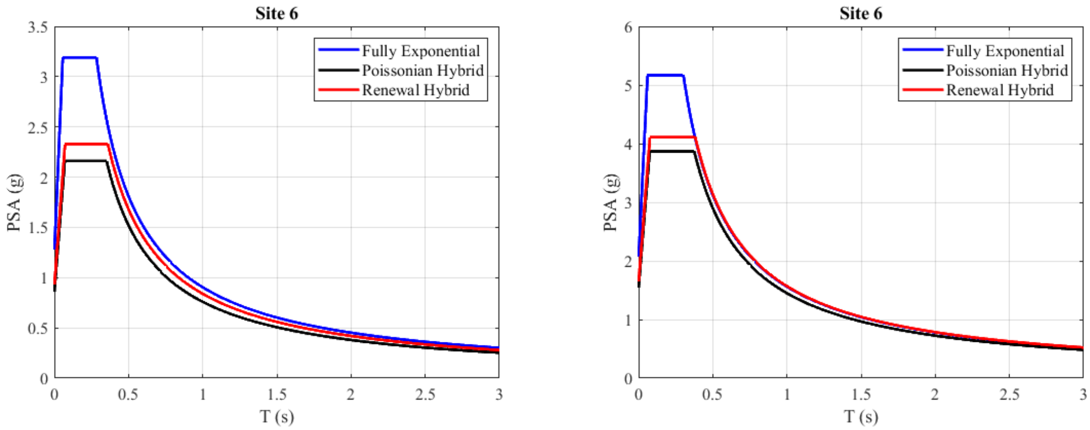

Figure 7.10. Elastic design spectra for Site 6 for the return periods of 475 (left) and 2475 (right) years

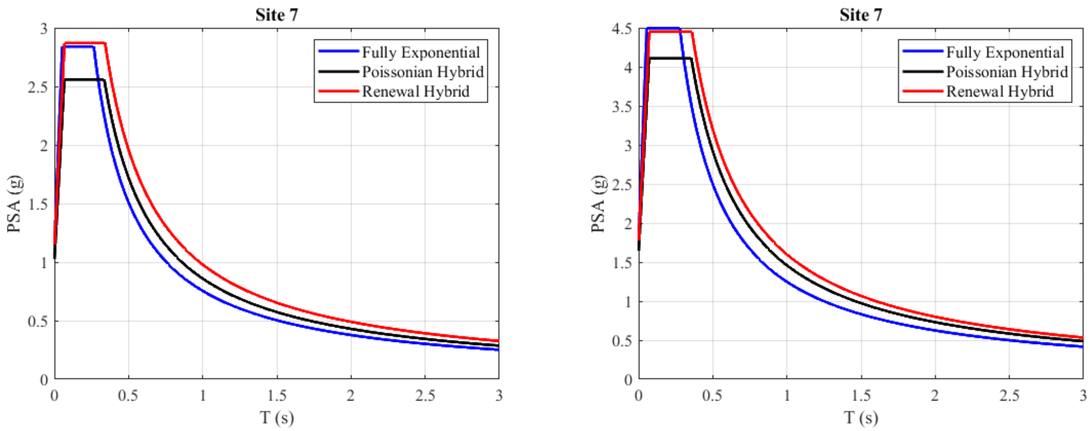

Figure 7.11. Elastic design spectra for Site 7 for the return periods of 475 (left) and 2475 (right) years

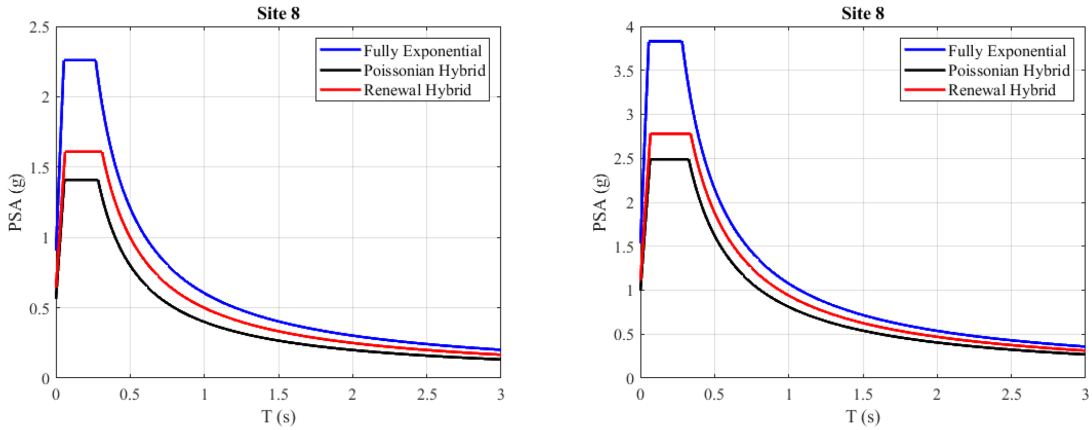

Figure 7.12. Elastic design spectra for Site 8 for the return periods of 475 (left) and 2475 (right) years

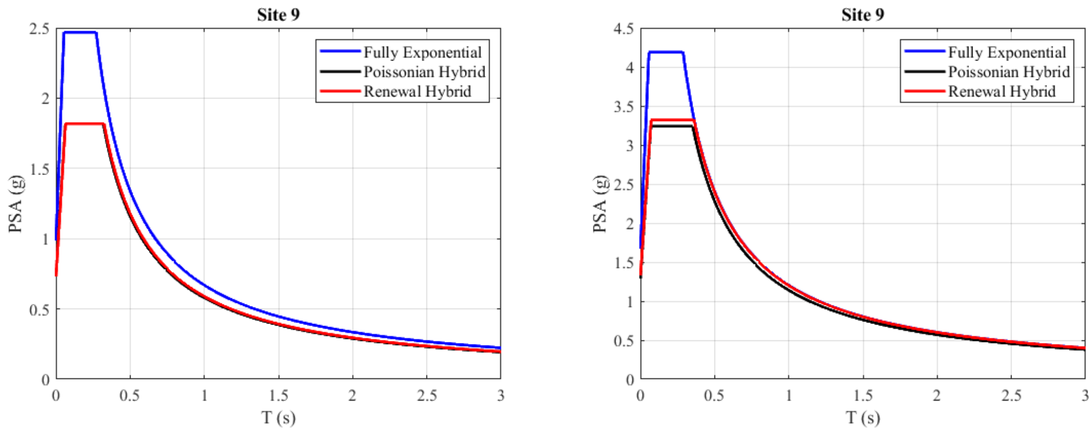

Figure 7.13. Elastic design spectra for Site 9 for the return periods of 475 (left) and 2475 (right) years

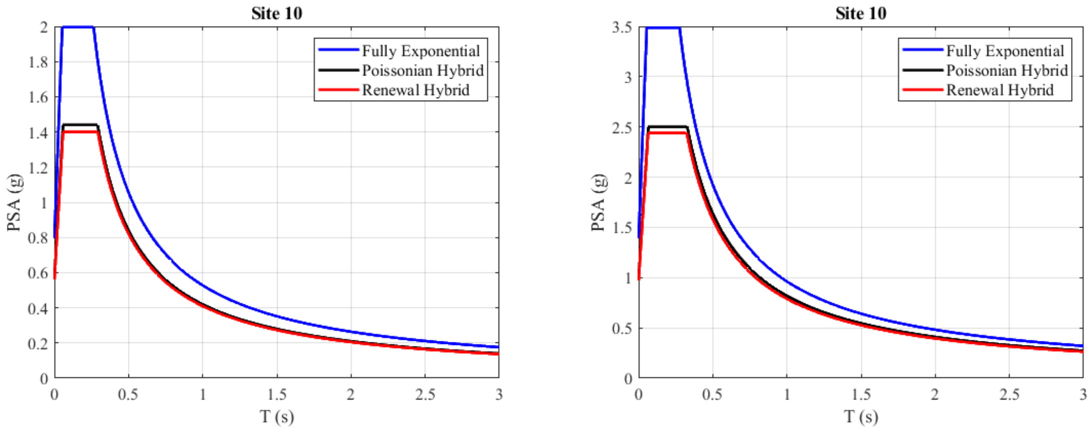

Figure 7.14. Elastic design spectra for Site 10 for the return periods of 475 (left) and 2475 (right) years

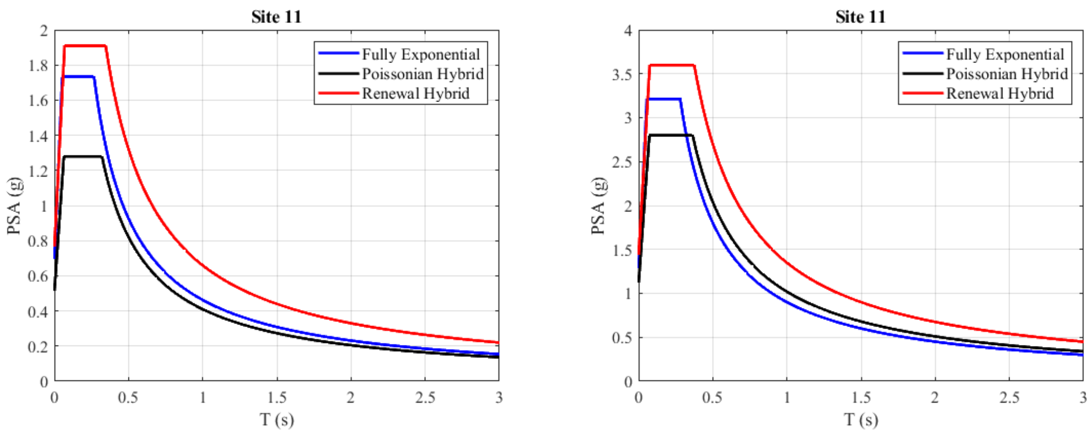

Figure 7.15. Elastic design spectra for Site 11 for the return periods of 475 (left) and 2475 (right) years

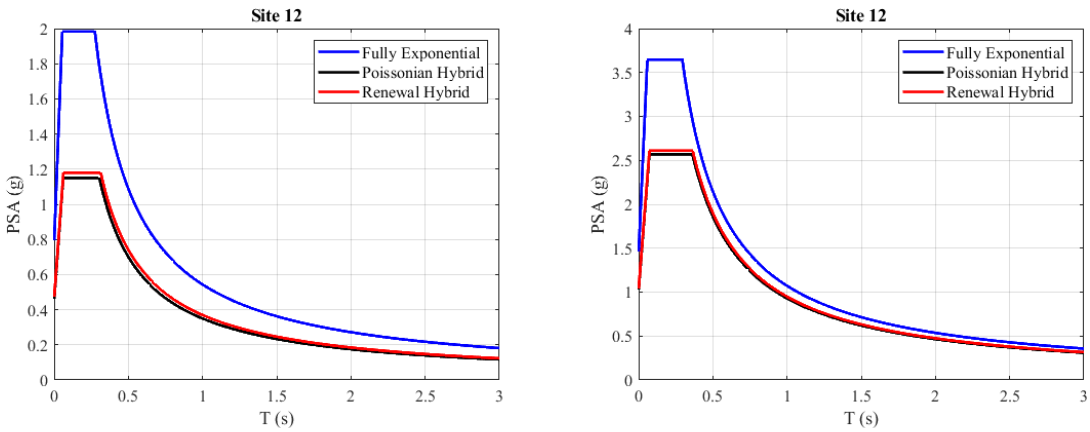

Figure 7.16. Elastic design spectra for Site 12 for the return periods of 475 (left) and 2475 (right) years

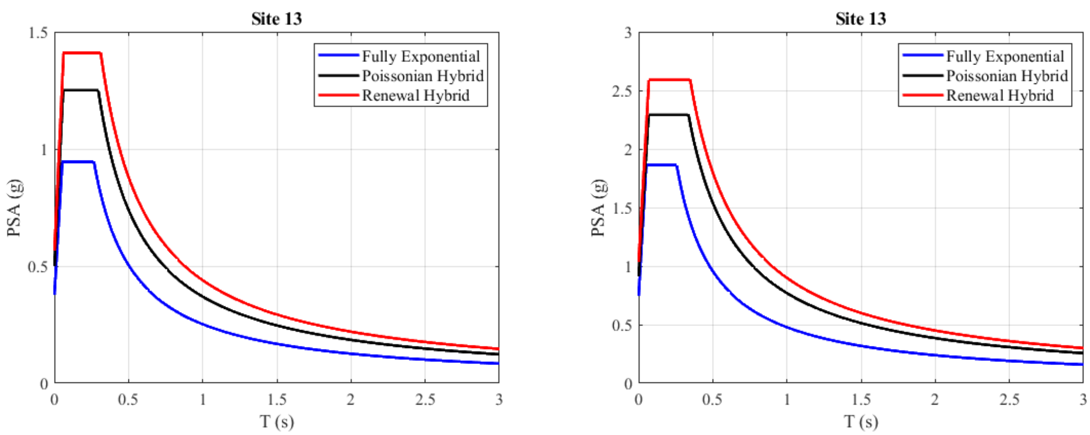

Figure 7.17. Elastic design spectra for Site 13 for the return periods of 475 (left) and 2475 (right) years

Discussion will be made over the fault zones and segments where the sites are located. Thus, the sites 1, 2,3,4,5, and 6 represent the NAF while the others –except for 7- symbolize the EAF. The Site 7 is under the effect of both fault zones. In addition, the inferences that will be drawn are valid for the two return periods.

First of all, looking at the results of the Poissonian and renewal hybrid models along the NAF, it is seen that the GMIMs are the lowest on the site 4 (Reşadiye segment) and they increase towards the point 7. Among the NAF's segments corresponding to the selected sites, the ones with the lowest annual rate of earthquake occurrences are Yedisu and Reşadiye, respectively. While the EAF can contribute the hazard on the site 6 (Yedisu segment), its effect on the site 4 becomes to be neglected. Therefore, the minimum seismic hazard is observed on the point 4 along the NAF.

When the fully exponential model and Poissonian hybrid model are compared in terms of PGA, Poissonian hybrid model gives smaller results. The site 13 is the exception to this situation. On this site, PGA values originated in the Poissonian hybrid model are higher.

SA at T= 1 s values obtained from the fully exponential model do not always higher than those obtained from Poissonian hybrid model. They do not follow the same trend with PGA and SA at T=0.2 s. That is, the results of the fully exponential model converge to the results of Poissonian hybrid model for SA values at higher natural periods.

The comparison between the Poissonian and Renewal hybrid models leads us to the following conclusions:

- Other than site 6, corresponding Yedisu segment, the renewal model produces smaller results along the NAF because there is a seismic gap on the Yedisu segment and the NAF discharged its accumulated strain energy in the 20th century by characteristic earthquakes.
- For the Karlıova triple junction, represented by the site 7, the time - dependent model yields higher PGA and SA.
- Although it is stated in the literature that there is a slip deficit on the Erkenek segment (Site 10), the renewal model does not produce higher results. Contrarily, the time - independent model produces greater GMIMs.

- For site 8, 11, 12, and 13, the renewal model yields higher results. This is an anticipated outcome since there are seismic gaps on the Pazarcık (Site 11), Amanos (Site 12) and Hacıpaşa segments (Site 13). The sharp difference is on the site 11 because the last characteristic earthquake on that segment was occurred in 1513. On the other hand, the difference between the results of both model can be neglected for the site 12. In other words, the slip deficit on the Amanos segment do not control the seismic hazard.
- In all cases, the two models give approximately same results at the site 9. Due to the fact that Pütürge 2 segment released its accumulated strain energy during the 2020 Elazığ earthquake, the renewal hybrid model does not yield greater GMIMs at site 9.

As fully exponential model gives overestimated results compared to the Poissonian hybrid model, it can be asserted that the fully exponential model is safe for all cases –except for SA values at T=1 s-. However, when the results of the time - dependent model is compared with those obtained from the fully exponential one, it is observed that for site 7, 11, and 13, the fully exponential model yields smaller spectral accelerations. Therefore, even fully exponential model may not produce safe results if there is a large quantity of slip deficit on a fault segment. It is a pragmatic approach to construct time - dependent seismic hazard models for such faults.

7.4. Ground Motion Distributions within the Buffer Zone

Time – independent and time – dependent seismic hazard maps are produced for the buffer zone of the faults. Analyses are performed based on 10% and 2% probabilities of exceedance in 50 years for each modeling type. Finally, a comparison between the results of the two model is drawn for each recurrence period.

For return periods of 475 and 2475 years, the distributions of mean GMIMs in the region are illustrated as time – independent seismic hazard maps in Figure 7.18 to 7.23. Time – dependent ones, on the other hand, are shown in Figure 7.24 to 7.29 for the same recurrence periods.

The ratios between the results of the Poissonian and renewal models are also presented as maps in Figure 7.30 to 7.35 for the return periods of 475 and 2475 years. With respect to the magnitude of this ratio, the results are colored from blue to red in these maps.

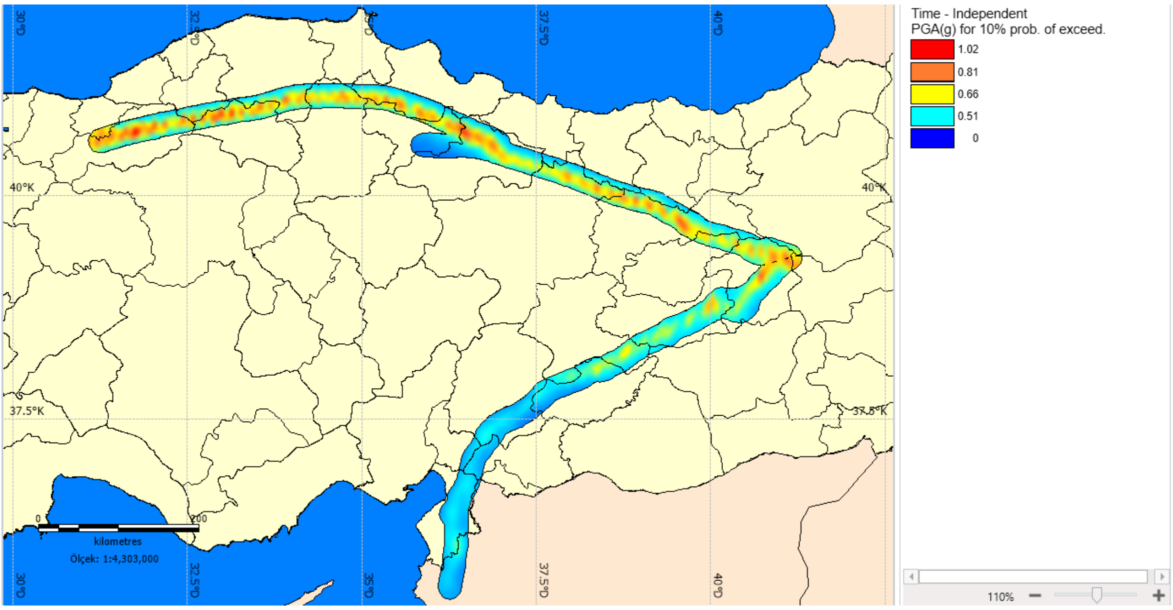

Figure 7.18. PGA distribution for RP = 475 years within the buffer zone (Time – Independent)

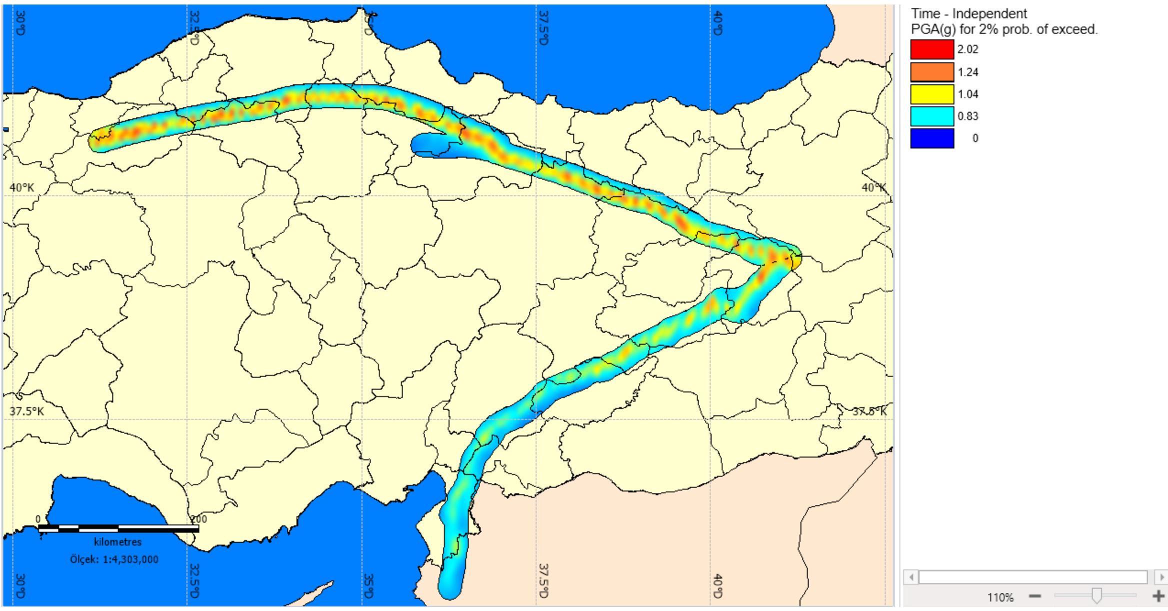

Figure 7.19. PGA distribution for RP = 2475 years within the buffer zone (Time – Independent)

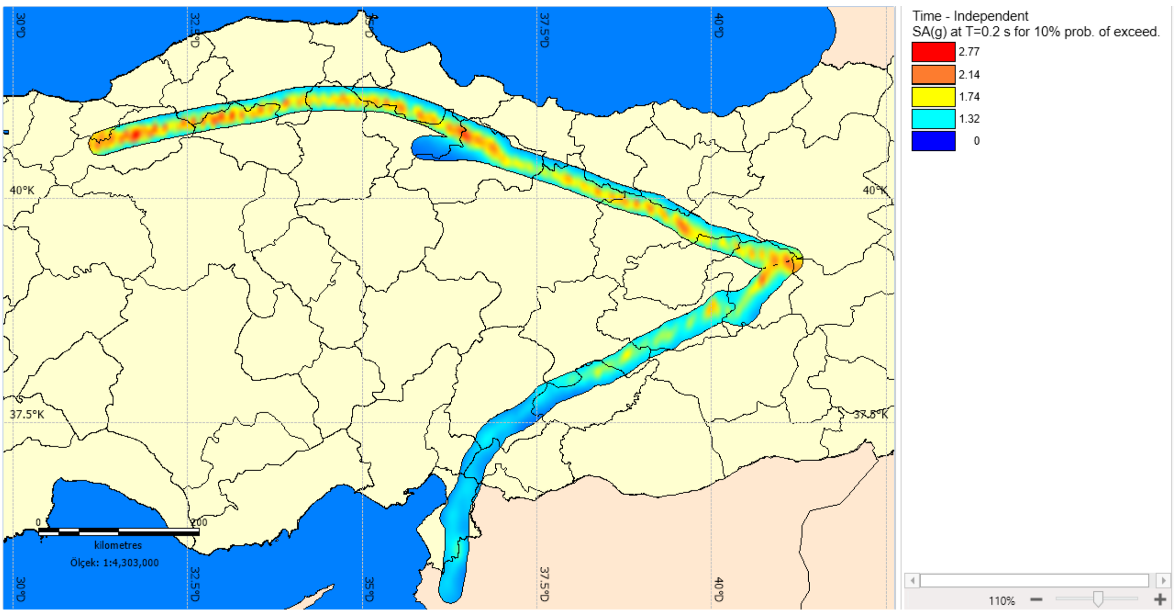

Figure 7.20. SA at T=0.2 s distribution for RP = 475 years within the buffer zone (Time – Independent)

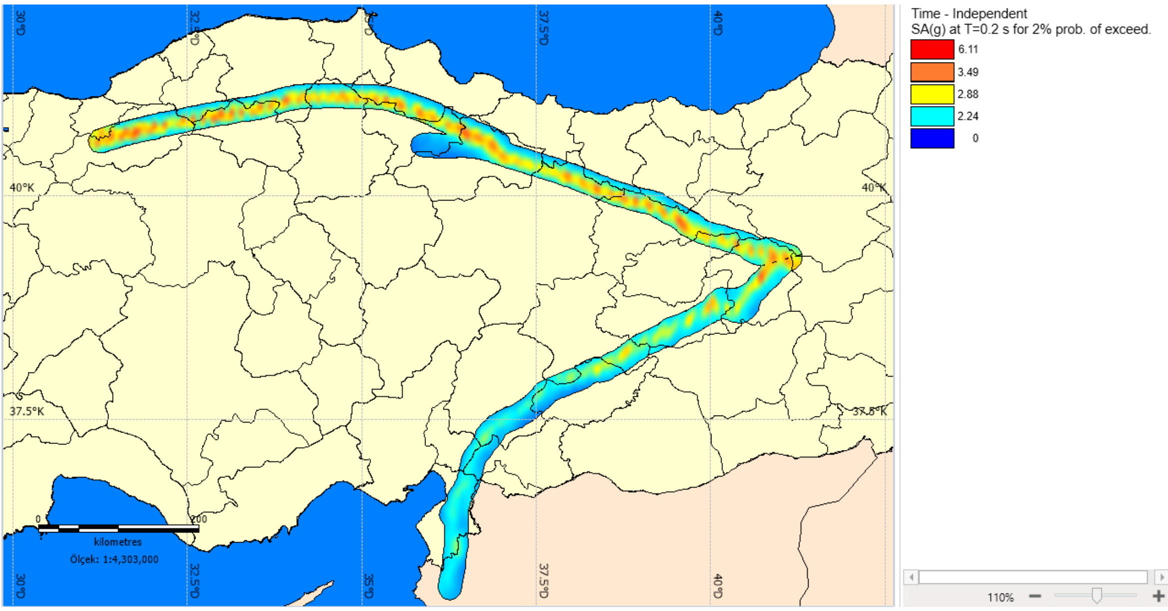

Figure 7.21. SA at T=0.2 s distribution for RP = 2475 years within the buffer zone (Time – Independent)

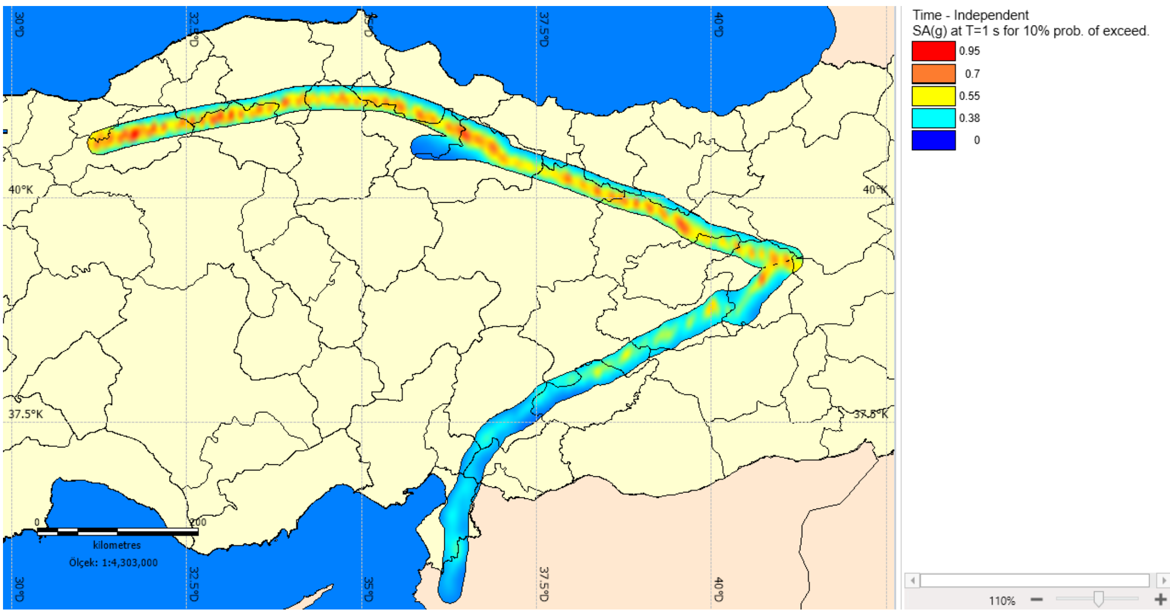

Figure 7.22. SA at T=1 s distribution for RP = 475 years within the buffer zone (Time – Independent)

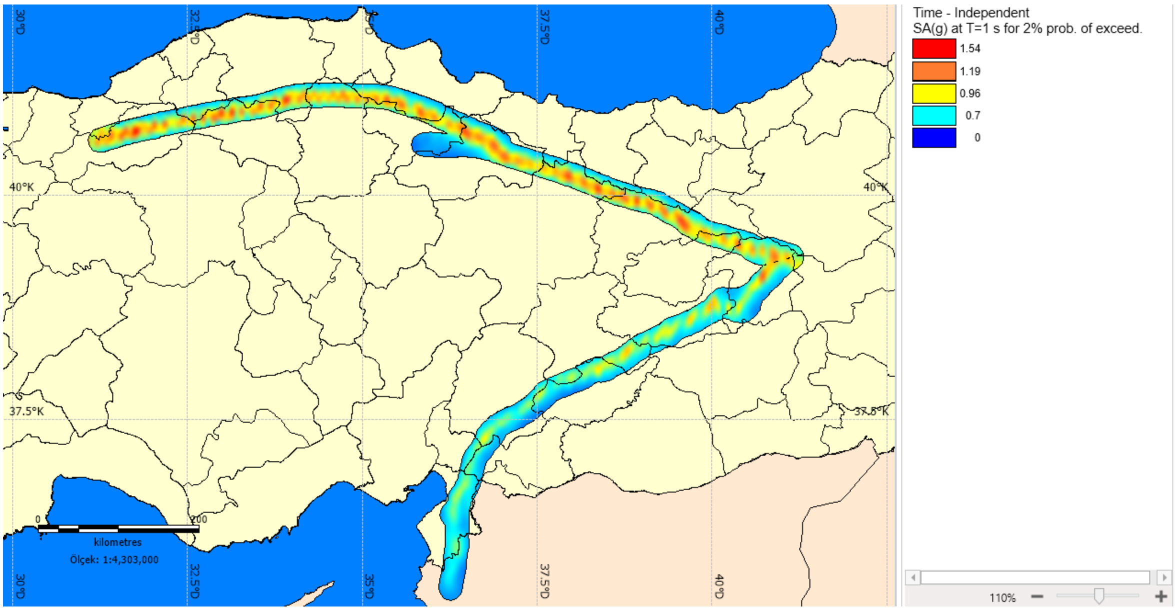

Figure 7.23. SA at T=1 s distribution for RP = 2475 years within the buffer zone (Time – Independent)

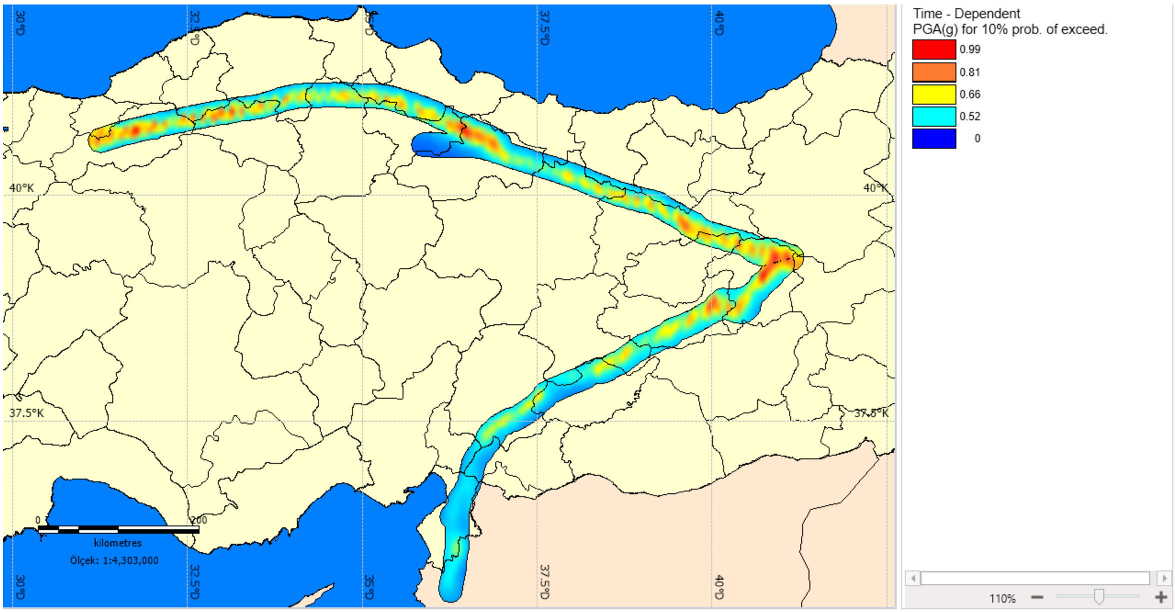

Figure 7.24. PGA distribution for RP = 475 years within the buffer zone (Time – Dependent)

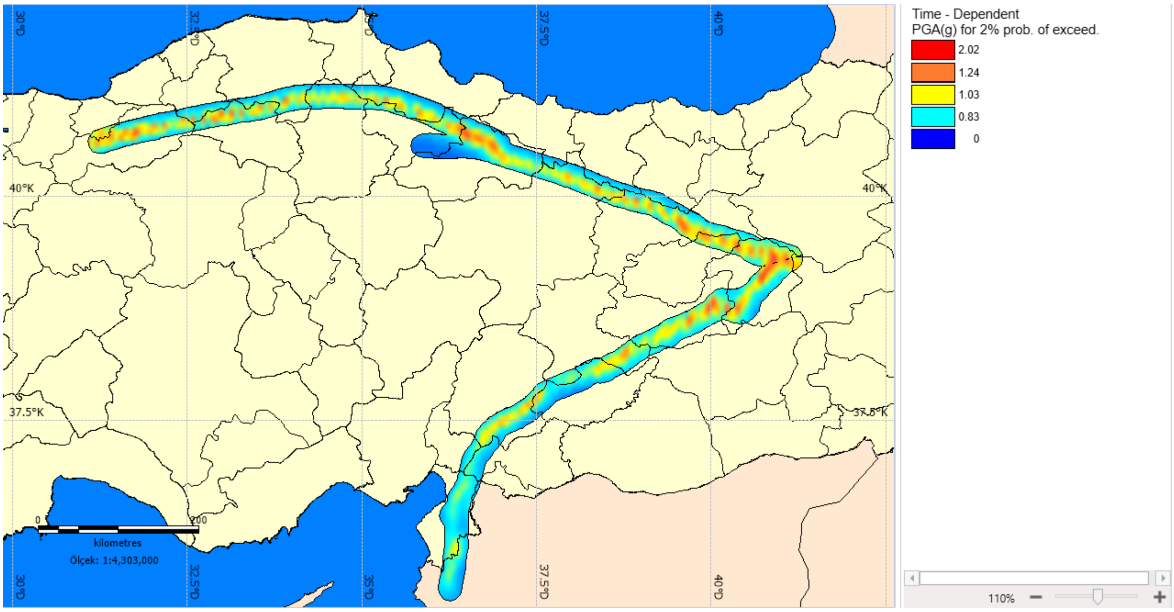

Figure 7.25. PGA distribution for RP = 2475 years within the buffer zone (Time – Dependent)

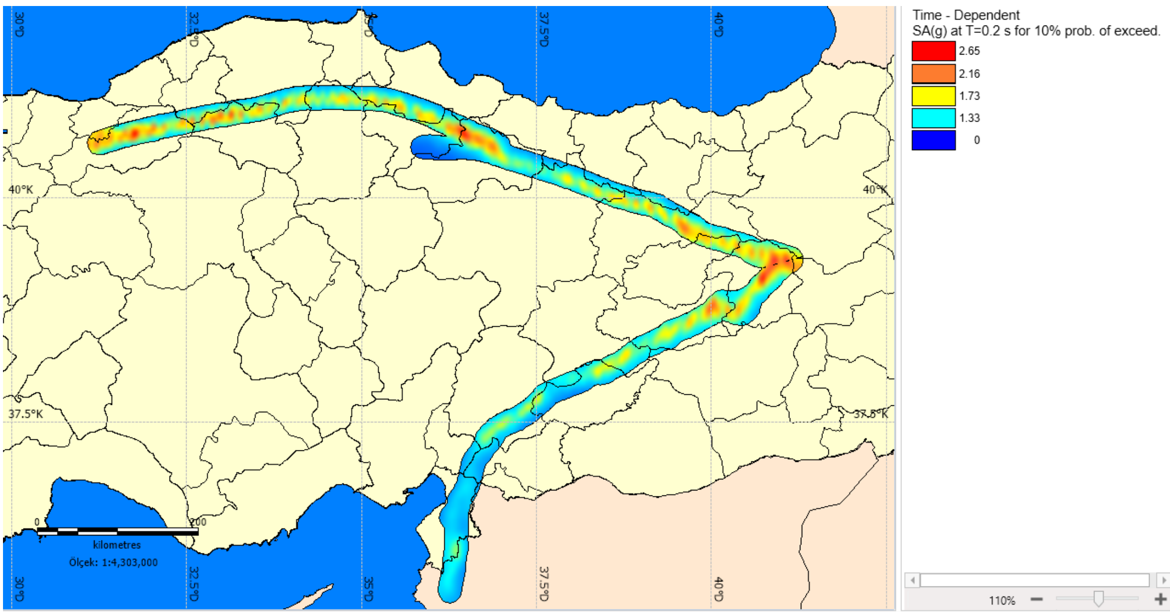

Figure 7.26. SA at T=0.2 s distribution for RP = 475 years within the buffer zone (Time – Dependent)

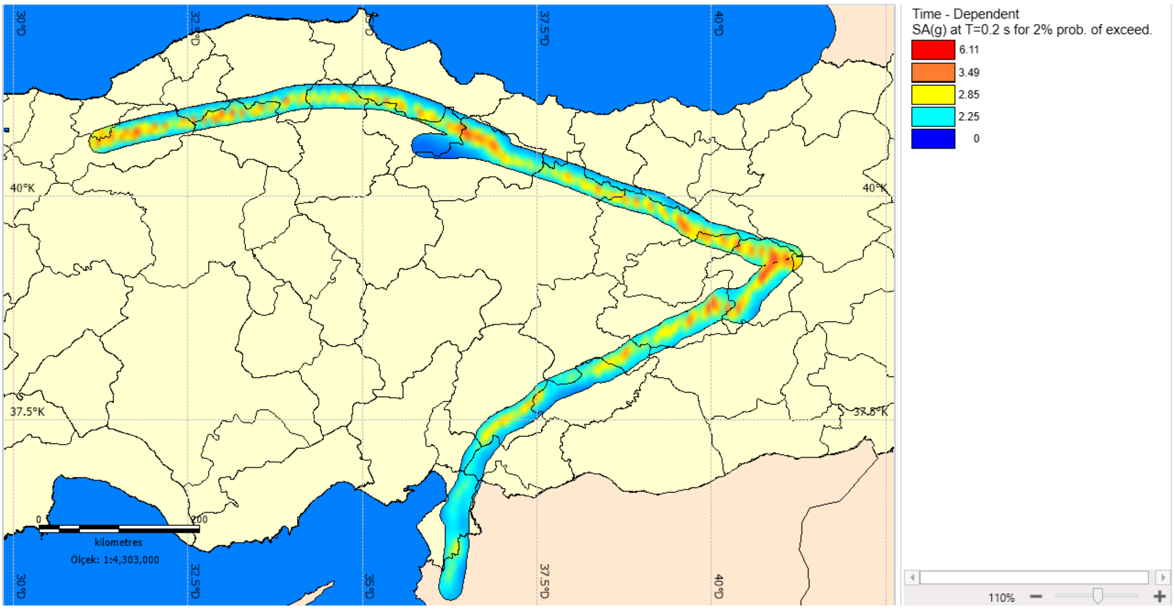

Figure 7.27. SA at T=0.2 s distribution for RP = 2475 years within the buffer zone (Time – Dependent)

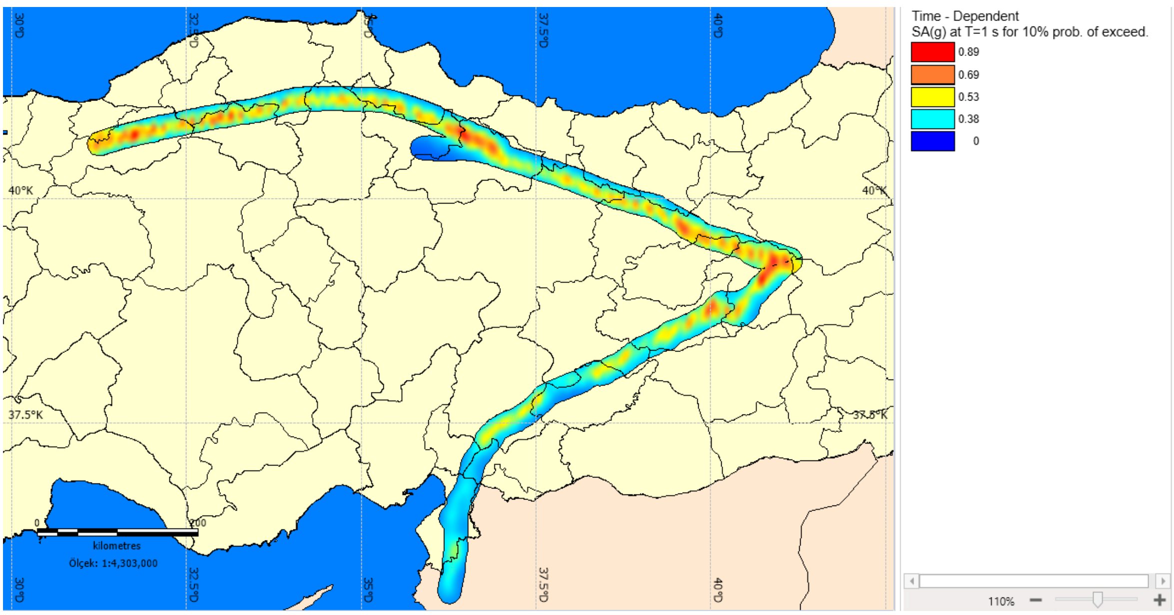

Figure 7.28. SA at T=1 s distribution for RP = 475 years within the buffer zone (Time – Dependent)

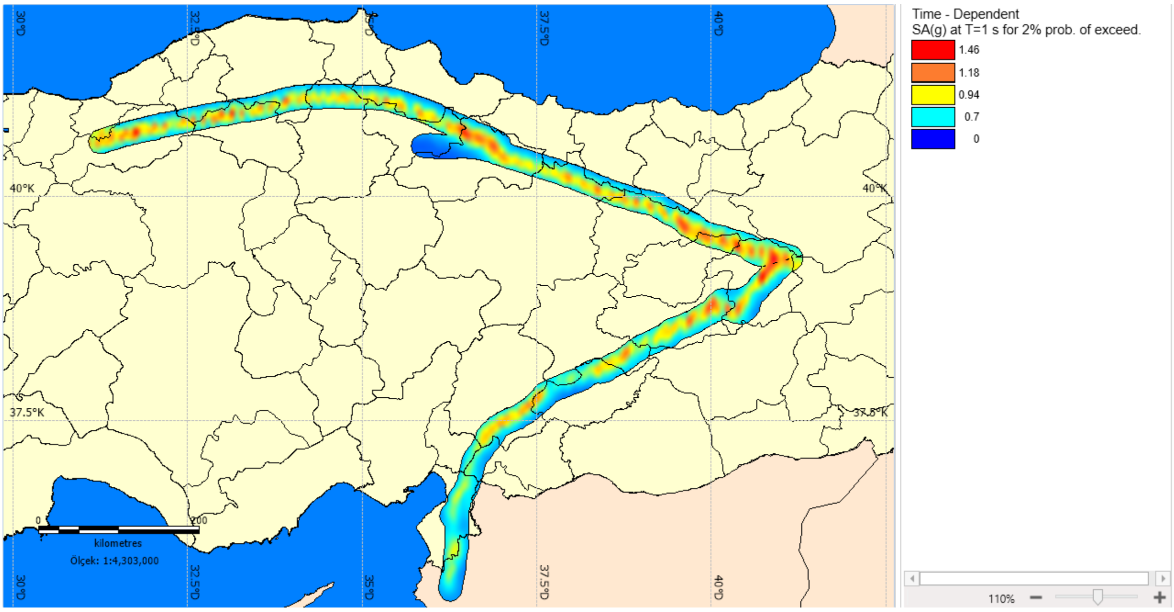

Figure 7.29. SA at T=1 s distribution for RP = 2475 years within the buffer zone (Time – Dependent)

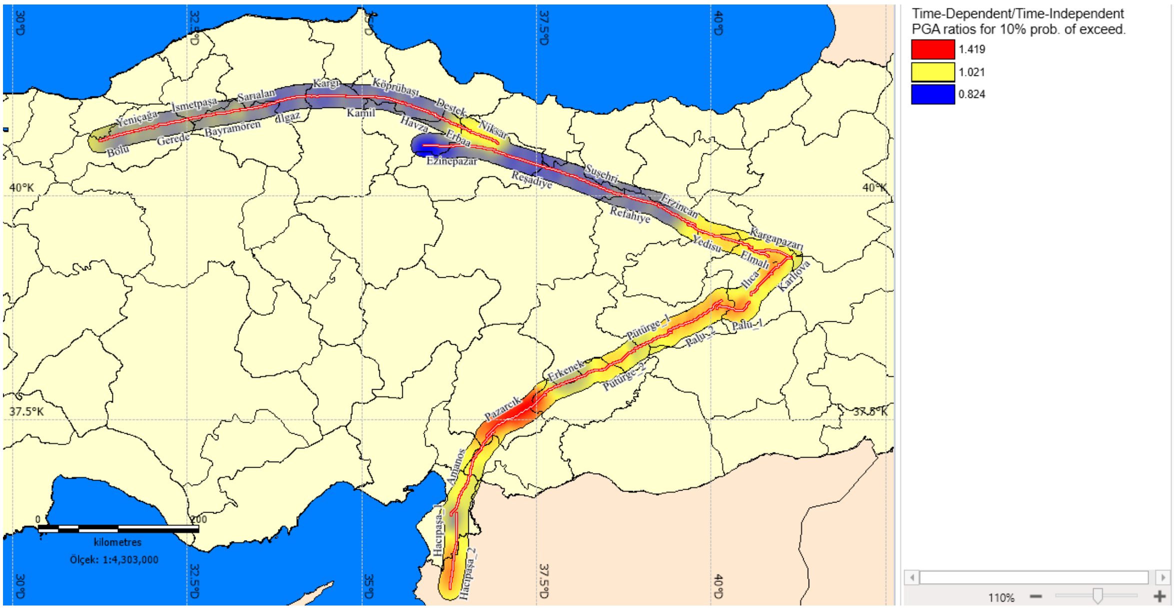

Figure 7.30. The PGA ratios between the Renewal and Poissonian Hybrid Models for RP = 475 years within the buffer zone

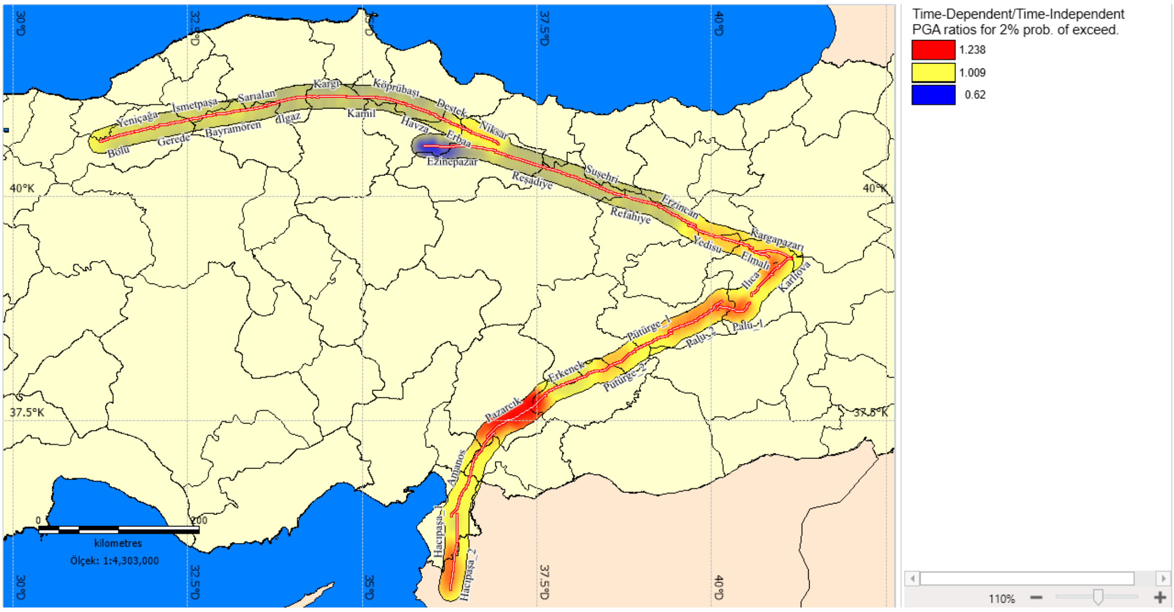

Figure 7.31. The PGA ratios between the Renewal and Poissonian Hybrid Models for RP = 2475 years within the buffer zone

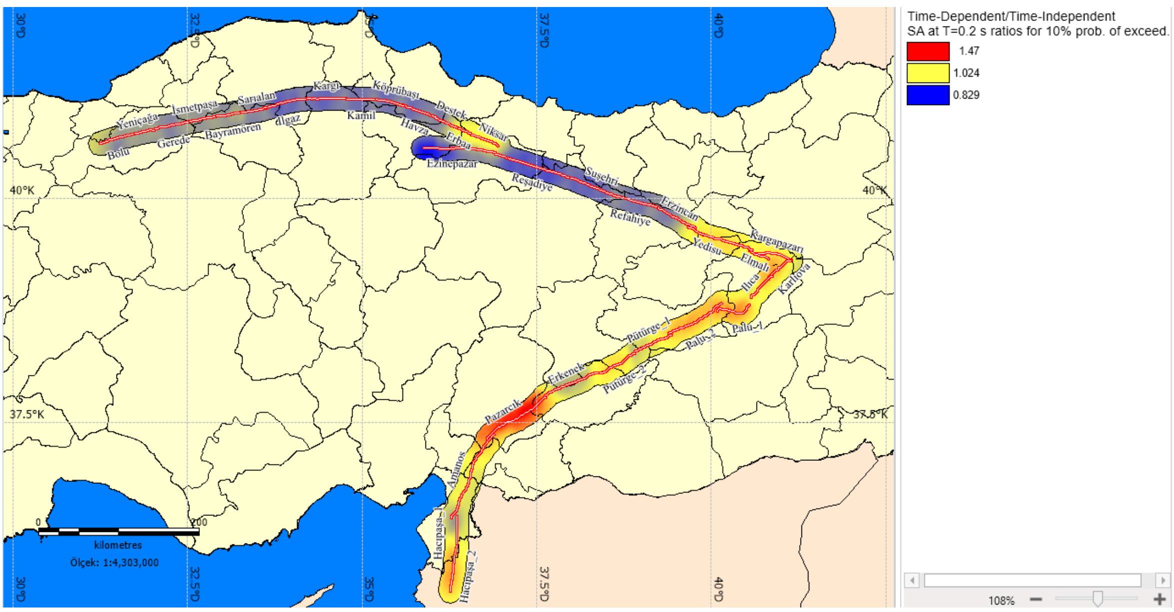

Figure 7.32. The SA at T=0.2 s ratios between the Renewal and Poissonian Hybrid Models for RP = 475 years within the buffer zone

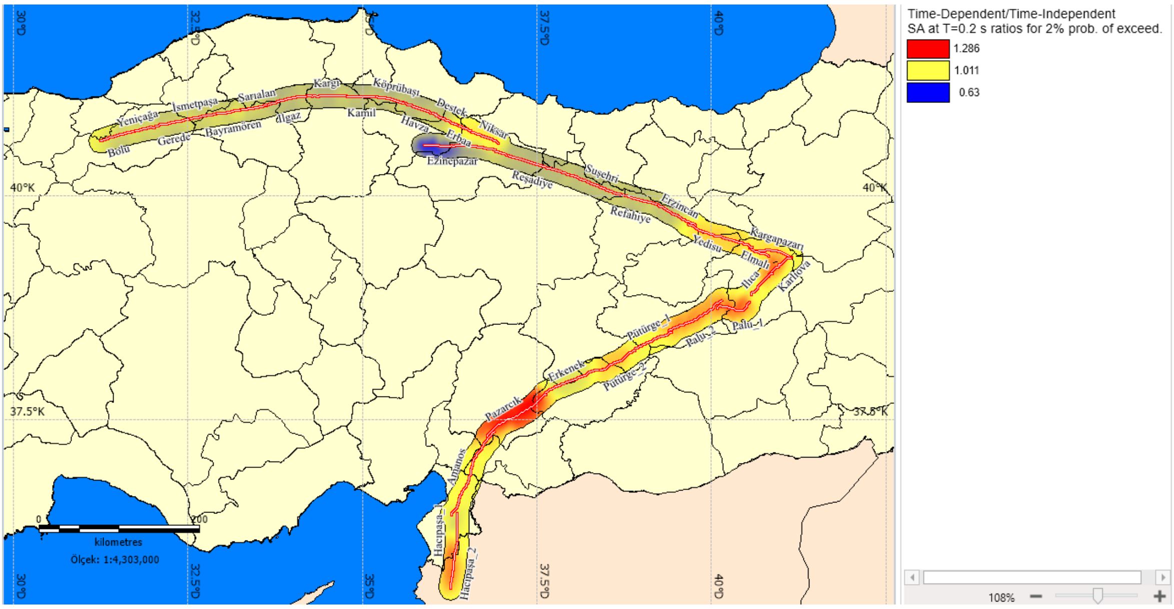

Figure 7.33. The SA at T=0.2 s ratios between the Renewal and Poissonian Hybrid Models for RP = 2475 years within the buffer zone

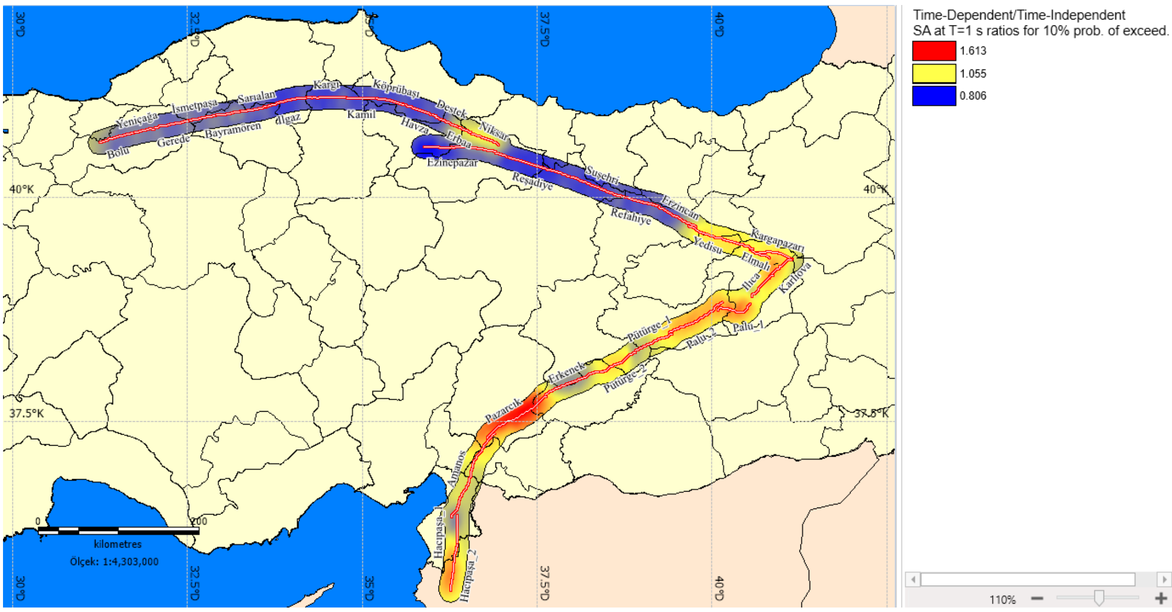

Figure 7.34. The SA at T=1 s ratios between the Renewal and Poissonian Hybrid Models for RP = 475 years within the buffer zone

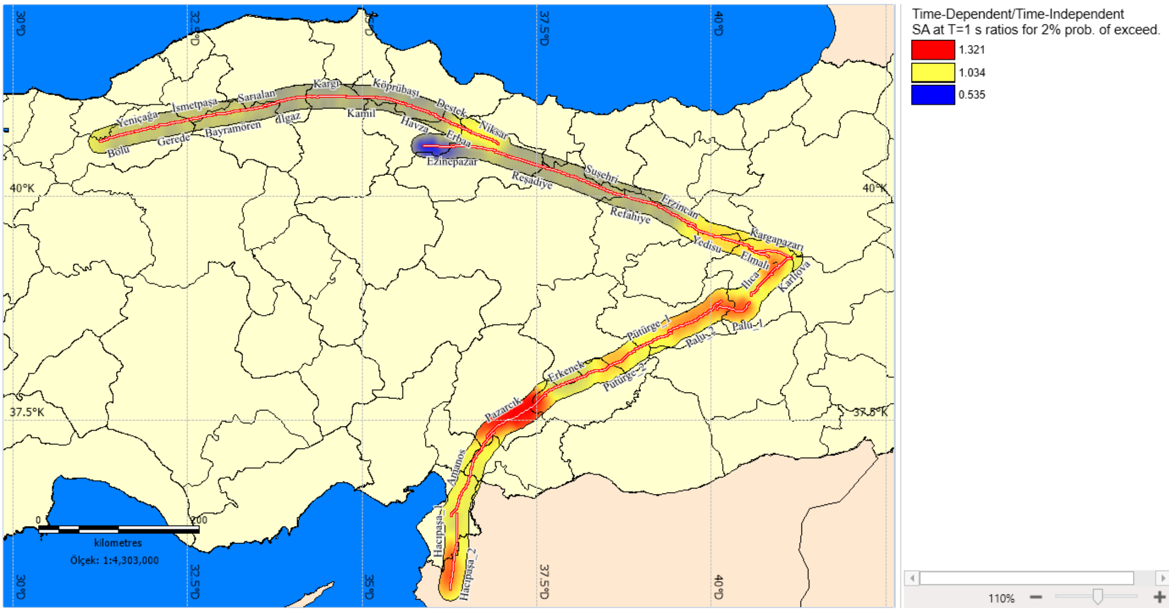

Figure 7.35. The SA at T=1 s ratios between the Renewal and Poissonian Hybrid Models for RP = 2475 years within the buffer zone

The following results are obtained from the comparison of the GMIM distributions of the time - dependent and independent models.

- The difference between the results of both models is greater for 10% probability of exceedance in 50 years. That is, the results of the time – dependent model converge to those of time – independent one as the return period increases.
- For both probabilities of exceedance, the renewal model yields smaller results along the NAF. Yedisu and Kargapazarı segments are exceptions to this case. The slip deficits on these segments cause higher hazard around eastern part of the NAF. Moreover, although Niksar & Erbaa segments discharged their accumulated seismic energy in the recent past, the hazard obtained from the renewal model is also higher around these segments.
- The time – dependent model generally gives greater results throughout the EAFZ. Around the Karlıova, Palu 1, Palu 2, Pazarcık, and Hacıpaşa 2 segments, the places where the renewal model produces higher results can be easily noticed.

Along the EAF, the time – dependent seismic hazard hits peak on the Pazarcık segment and surrounding region. On the other hand, the difference between the GMIMs produced by both models is subtle on the Ilıca, Pütürge 1, Erkenek, Amanos and Hacıpaşa 1 segments, which means the Poissonian model is adequate to depict seismic hazard around these sections of the EAF.

- If the time – dependent model is considered as more realistic or accurate, the time – independent model produces overestimated GMIMs for most of the NAFZ. Contrarily, it usually yields underestimated results along the EAFZ.

8. CONCLUSIONS

This thesis, which presents a hybrid-characteristic fault source modeling of the NAF and EAF, creates the opportunity to judge whether fully exponential earthquake occurrence model of the NAF and EAF yields overestimated results or not. Because characteristic fault source modeling is based on Reid's theory [115] (i.e., a physically-motivated fault source modeling type), the hybrid recurrence model, developed within the scope of this study, is the basis for this evaluation. A major advantage of this type of modelling is that it also forms the basis for a time - dependent seismic hazard model. Thus, the first time – dependent seismic hazard model for the NAF and EAF is built and the effect of slip deficits along these faults on the seismic hazard has been examined.

Analyses are made for 10% and 2% probabilities of exceedance in the next 50 years. The results of the seismic hazard calculations are presented in the form of the mean PGA and 5% damped mean SA at T = 0.2 and 1 s. In order to assess results, 13 specific locations are selected throughout the faults and GMIMs on those sites are compared. Furthermore, the distributions of GMIMs are shown as seismic hazard maps, which make it possible to assess hazard level at locations other than the selected points. When all the analyses' results are evaluated, the following conclusions can be drawn:

- The fully exponential fault source model of the NAF and EAF, developed by Demircioğlu et al. [28], yields overestimated GMIMs compared to the time – independent hybrid characteristic earthquake recurrence model, built in this thesis. On the other hand, the difference between two models decreases with higher return periods and natural periods.
- Since the NAF mostly released its accumulated seismic energy in the 20th century, the renewal hybrid model produces smaller GMIMs compared to the Poissonian one. Nonetheless, around the Niksar & Erbaa segments, the time – dependent model slightly gives higher GMIMs contrary to expectation.

- The slip deficit on the Yedisu & Kargapazarı segments causes the time – dependent model to produce higher seismic hazard than that of Poissonian hybrid model.
- Along the EAF, the renewal hybrid model generally yields greater hazard compared to the Poissonian one. However, this case is reversed around the Erkenek and Hacıpaşa 1 segments. This is an unexpected outcome because these sections of the EAF accommodate seismic gaps.
- Around the Palu 2, Pazarcık and Hacıpaşa 2 segments, which involve seismic gaps, the seismic hazard based on the time – dependent hybrid model is higher than that of the time – independent model. When the GMIM values produced by the renewal model are divided by those obtained from Poissonian one, the ratio of SA at T=1 s for the recurrence period of 475 years reaches 1.66 around the Pazarcık segment.
- Despite the fact that there is a slip deficit on the Amanos segment, both time – dependent and independent hybrid model give approximately the same results.
- Although Pütürge 1 segment discharged its accumulated strain energy during the 2020 Elazığ earthquake, the GMIM values obtained by two hybrid model are almost identical. The renewal model does not yield considerably lower GMIMs compared to the Poissonian model.
- The renewal model yields greater seismic hazard than Poissonian model around the Karlıova and Palu 1 segments.
- In the vicinity of the Pütürge 2 and Ilıca segments, both hybrid models give almost the same GMIMs.
- As is shown in the elastic design spectra, the time – dependent hybrid model yields highest spectral accelerations around the Karlıova triple junction, Pazarcık and Hacıpaşa 2 segments. Since the latest Turkish Seismic Hazard Map combines the results of area source model [64] and fault source model [28] with equal weights, it should be indicated that design spectral acceleration values taken from AFAD are considerably lower than those given in this study. This should be a point of consideration especially for the design of important structures in the region.

- The overestimated results of the fully exponential earthquake recurrence model with respect to both hybrid models can be adopted to design safe structures. In other words, the results of the fully exponential model do not lead to the design of structures that cannot resist earthquakes. However, in cases where the slip deficit on a fault segment is large, the results of the time - dependent hybrid model may exceed the results of the exponential model (e.g., around the Hacıpaşa 2 and Pazarcık segments). Therefore, the time – dependent seismic hazard models of such faults should be developed in the construction procedure of special structures (e.g., nuclear power plants) so as to account for the worst case.

Issues that are beyond the scope of this study and that need to be investigated are as follows:

- Since the fully exponential model of the NAF and EAF yields mostly overestimated results compared to the Poissonian and renewal hybrid models, the financial effect of its results on the structural design should be evaluated.
- The comparison between the results of Poissonian and renewal models shows that the time – independent one yields overestimated GMIMs along most of the NAF. The economic impact of this situation on structural design should also be explored.
- If there is a substantial slip deficit on a fault segment, this situation may adversely affect the target performance level of structures located in the vicinity of that fault. Therefore, in locations where the renewal hybrid model gives greater seismic hazard than that of Poissonian model, performance based design should be done for such structures in order to estimate the effect of the higher seismic hazard on structural safety.
- Uncertainties are not considered within the present study. Slip rates along the fault segments are one of the primary factors affecting the earthquake productivity. The fault database of Emre et al. [14], which has been used as the basis of fault parametrization, provides very small uncertainty for the slip rates along the NAF and EAF. However, based on different studies, larger uncertainties may

be associated with the slip rates along the segments of these two fault zones, especially if differences between geologic and geodetic estimations are considered. These issues may further be explored. Another uncertainty, especially for the EAF, is the association of historical earthquakes with the different segments of the fault. As new data and studies permitting, alternative models can be developed.

- 20th century ruptures occupy central role to draw combined rupture scenarios for the NAF. As for the EAF, the scenarios are determined more arbitrarily. For both fault zones, different combined - rupture scenarios can also be taken into account to account for the epistemic uncertainties regarding the multi-segment rupture configurations.
- So as to characterize the moderate periodic behavior of the NAF and EAF, CoV is chosen 0.5. Analyses can be performed by using a set of CoV values (e.g., 0.3, 0.5, 0.7), which considers the possibility of faults to behave more periodically or aperiodically.

REFERENCES

1. Sieberg, A., “Erdbebengeographie, vol Band IV, Lieferung 3”, *Verlag von Gebrüder Borntraeger, Berlin*, 1932.

2. Özmen, B., “Türkiye Deprem Bölgeleri Haritalarının Tarihsel Gelişimi”, *Türkiye Jeoloji Bülteni*, Vol. 55, No. 1, 2012.

3. Akkar, S., T. Azak, T. Can, U. Çeken, D. Tümsa, T. Duman, M. Erdik, S. Ergintav, F. Kadirioğlu, D. Kalafat *et al.*, “Evolution of Seismic Hazard Maps in Turkey”, *Bulletin of Earthquake Engineering*, Vol. 16, No. 8, pp. 3197–3228, 2018.

4. Fraser, J., K. Vanneste and A. Hubert-Ferrari, “Recent Behavior of the North Anatolian Fault: Insights from An Integrated Paleoseismological Data Set”, *Journal of Geophysical Research: Solid Earth*, Vol. 115, No. B9, 2010.

5. Barka, A. A., “The North Anatolian Fault Zone”, *Annales Tectonicae*, Vol. 6, pp. 164–195, 1992.

6. Sengor, A., O. Tuysuz, C. Imren, M. Sakinc, H. Eyidogan, N. Gorur, X. Le Pichon and C. Rangin, “The North Anatolian Fault: A New Look”, *Annual Review of Earth and Planetary Sciences*, Vol. 33, No. 1, pp. 37–112, 2005.

7. Erdik, M., M. Demircioglu, K. Sesetyan, E. Durukal and B. Siyahi, “Earthquake Hazard in Marmara Region, Turkey”, *Soil Dynamics and Earthquake Engineering*, Vol. 24, No. 8, pp. 605–631, 2004.

8. Iacoletti, S., G. Cremen and C. Galasso, “Advancements in Multi-Rupture Time-Dependent Seismic Hazard Modeling, Including Fault Interaction”, *Earth-Science Reviews*, Vol. 220, p. 103650, 2021.

9. Basili, R., G. Valensise, P. Vannoli, P. Burrato, U. Fracassi, S. Mariano, M. M.

Tiberti and E. Boschi, "The Database of Individual Seismogenic Sources (DISS), Version 3: Summarizing 20 Years of Research on Italy's Earthquake Geology", *Tectonophysics*, Vol. 453, No. 1-4, pp. 20–43, 2008.

10. Ambraseys, N., "The Little-Known Earthquakes of 1866 and 1916 in Anatolia (Turkey)", *Journal of Seismology*, Vol. 1, No. 3, pp. 289–299, 1997.

11. Ambraseys, N., "Temporary Seismic Quiescence: SE Turkey", *Geophysical Journal International*, Vol. 96, No. 2, pp. 311–331, 1989.

12. Kadirioğlu, F., R. F. Kartal, T. Kılıç, D. Kalafat, T. Y. Duman, T. Eroğlu Azak, S. Özalp and Ö. Emre, "An Improved Earthquake Catalogue (M$\geq$ 4.0) for Turkey and Its Near Vicinity (1900–2012)", *Bulletin of Earthquake Engineering*, Vol. 16, No. 8, pp. 3317–3338, 2018.

13. McKenna, P., "Earthquake Engineer: Earthquakes Don't Kill, but Buildings Do", *New Scientist*, Vol. 210, No. 2813, p. 23, 2011.

14. Emre, Ö., T. Y. Duman, S. Özalp, F. Şaroğlu, Ş. Olgun, H. Elmacı and T. Çan, "Active Fault Database of Turkey", *Bulletin of Earthquake Engineering*, Vol. 16, No. 8, pp. 3229–3275, 2018.

15. Hsu, C.-C., M.-Y. Chong, P. Yang and C.-F. Yen, "Posttraumatic Stress Disorder among Adolescent Earthquake Victims in Taiwan", *Journal of the American Academy of Child & Adolescent Psychiatry*, Vol. 41, No. 7, pp. 875–881, 2002.

16. Abali, O., ü. Tüzün, ü. Göktürk, K. An gürkan, B. Alyanak and I. Görker, "Acute Psychological Reactions of Children and Adolescents After the Marmara Earthquake: A Brief Preliminary Report", *Clinical Child Psychology and Psychiatry*, Vol. 7, No. 2, pp. 283–287, 2002.

17. Kılıç, C. and M. Ulusoy, "Psychological Effects of the November 1999 Earthquake in Turkey: An Epidemiological Study", *Acta Psychiatrica Scandinavica*, Vol. 108,

No. 3, pp. 232–238, 2003.

18. Azarian, A., V. Skriptchenko-Gregorian, T. W. Miller and R. F. Kraus, "Childhood Trauma in Victims of the Armenian Earthquake", *Journal of Contemporary Psychotherapy*, Vol. 24, No. 2, pp. 77–85, 1994.

19. Şalcıoğlu, E. and M. Başoğlu, "Psychological Effects of Earthquakes in Children: Prospects for Brief Behavioral Treatment", *World Journal of Pediatrics*, Vol. 4, No. 3, pp. 165–172, 2008.

20. Yarar, R., O. Ergünay, M. Erdik and P. Gülkan, "A Preliminary Probabilistic Assessment of the Seismic Hazard in Turkey", *Proc. 7th World Conf. Earthquake Eng., Istanbul*, Vol. 309, p. 316, 1980.

21. Erdik, M., V. Doyuran, N. Akkaş and P. Gülkan, "A Probabilistic Assessment of the Seismic Hazard in Turkey", *Tectonophysics*, Vol. 117, No. 3-4, pp. 295–344, 1985.

22. Woessner, J., D. Laurentiu, D. Giardini, H. Crowley, F. Cotton, G. Grünthal, G. Valensise, R. Arvidsson, R. Basili, M. B. Demircioglu *et al.*, "The 2013 European Seismic Hazard Model: Key Components and Results", *Bulletin of Earthquake Engineering*, Vol. 13, No. 12, pp. 3553–3596, 2015.

23. Anderson, J. G. and J. E. Luco, "Consequences of Slip Rate Constraints on Earthquake Occurrence Relations", *Bulletin of the Seismological Society of America*, Vol. 73, No. 2, pp. 471–496, 1983.

24. Şeşetyan, K., L. Danciu, M. B. Demircioğlu Tümsa, D. Giardini, M. Erdik, S. Akkar, L. Gülen, M. Zare, S. Adamia, A. Ansari *et al.*, "The 2014 Seismic Hazard Model of the Middle East: Overview and Results", *Bulletin of Earthquake Engineering*, Vol. 16, No. 8, pp. 3535–3566, 2018.

25. Youngs, R. R. and K. J. Coppersmith, "Implications of Fault Slip Rates and

Earthquake Recurrence Models to Probabilistic Seismic Hazard Estimates", *Bulletin of the Seismological Society of America*, Vol. 75, No. 4, pp. 939–964, 1985.

26. Gülerce, Z. and S. Ocak, "Probabilistic Seismic Hazard Assessment of Eastern Marmara Region", *Bulletin of Earthquake Engineering*, Vol. 11, No. 5, pp. 1259–1277, 2013.

27. Şeşetyan, K., M. B. Demircioğlu Tümsa and A. Akinci, "Evaluation of the Seismic Hazard in the Marmara Region (Turkey) Based on Updated Databases", *Geosciences*, Vol. 9, No. 12, p. 489, 2019.

28. Demircioğlu, M. B., K. Şeşetyan, T. Y. Duman, T. Can, S. Tekin and S. Ergintav, "A Probabilistic Seismic Hazard Assessment for the Turkish Territory: Part II—Fault Source and Background Seismicity Model", *Bulletin of Earthquake Engineering*, Vol. 16, No. 8, pp. 3399–3438, 2018.

29. Pagani, M., D. Monelli, G. Weatherill, L. Danciu, H. Crowley, V. Silva, P. Henshaw, L. Butler, M. Nastasi, L. Panzeri *et al.*, "OpenQuake Engine: An Open Hazard (and Risk) Software for the Global Earthquake Model", *Seismological Research Letters*, Vol. 85, No. 3, pp. 692–702, 2014.

30. Schwartz, D. P. and K. J. Coppersmith, "Fault Behavior and Characteristic Earthquakes: Examples from the Wasatch and San Andreas Fault Zones", *Journal of Geophysical Research: Solid Earth*, Vol. 89, No. B7, pp. 5681–5698, 1984.

31. Clark, C. E., "Science, Reason, and an Angry God: The Literature of an Earthquake", *New England Quarterly*, pp. 340–362, 1965.

32. Harris, L., "The God of the Gaps", *JASA*, Vol. 15, No. 4, pp. 101–104, 1963.

33. Cornell, C. A., "Engineering Seismic Risk Analysis", *Bulletin of the Seismological Society of America*, Vol. 58, No. 5, pp. 1583–1606, 1968.

34. Corotis, R. B., R. K. McGuire and G. B. Baecher, "Eminent Structural Engineer: Dr C. Allin Cornell (1938–2007)", *Structural Engineering International*, Vol. 19, No. 2, pp. 220–221, 2009.

35. Erdik, M. and S. Mathur, "Evaluation of Earthquake Hazards-Correlation of Seismic Activity and Tectonic Elements of Turkey", *Bulletin of the International Association of Engineering Geology-Bulletin de l'Association Internationale de Géologie de l'Ingénieur*, Vol. 19, No. 1, pp. 145–152, 1979.

36. Gülkan, P., A. Koçyiğit, M. Yücemen, V. Doyuran and N. Başöz, "En Son Verilere Göre hazırlanan Türkiye Deprem bölgeleri Haritası", *Rapor no: METU/EERC*, Vol. 93, No. 01, 1993.

37. Erdik, M. and S. Öner, "A Rational Approach for the Probabilistic Assessment of the Seismic Risk Associated with the North Anatolian Fault", *Multidisciplinary Approach to Earthquake Prediction*, pp. 115–127, Springer, 1982.

38. Onur, T., *Earthquake Hazard in Turkey Based on Spectral Acceleration Amplitudes*, Master's Thesis, Kandilli Rasathanesi ve Deprem Araştırma Enstitüsü, 1997.

39. Bommer, J., R. Spence, M. Erdik, S. Tabuchi, N. Aydinoglu, E. Booth, D. Del Re and O. Peterken, "Development of an Earthquake Loss Model for Turkish Catastrophe Insurance", *Journal of seismology*, Vol. 6, No. 3, pp. 431–446, 2002.

40. Jimenez, M.-J., D. Giardini, G. Grünthal, S. W. Group *et al.*, "Unified Seismic Hazard Modelling throughout the Mediterranean Region", *Bollettino di Geofisica Teorica ed Applicata*, Vol. 42, No. 1-2, pp. 3–18, 2001.

41. Demircioglu, M., K. Sesetyan, E. Durukal and M. Erdik, "Assessment of Earthquake Hazard in Turkey", *Proceedings of the 4th International Conference on Earthquake Geotechnical Engineering*, pp. 25–28, 2007.

42. Danciu, L., K. Şeşetyan, M. Demircioglu, L. Gülen, M. Zare, R. Basili, A. Elias, S. Adamia, N. Tsereteli, H. Yalçın *et al.*, "The 2014 Earthquake Model of the Middle East: Seismogenic Sources", *Bulletin of Earthquake Engineering*, Vol. 16, No. 8, pp. 3465–3496, 2018.

43. Erdik, M., V. Doyuran, P. Gülkan and G. Akçora, "Probabilistic Assessment of the Seismic Intensity in Turkey for the Siting of Nuclear Power Plants", *Proceedings of the 2nd CSNI Meeting on Probabilistic Methods in Seismic Risk Assessment for Nuclear Power Plants. Lawrence Livermore National Laboratory, Livermore*, 1983.

44. Schnabel, P. B. and H. Bolton Seed, "Accelerations in Rock for Earthquakes in the Western United States", *Bulletin of the Seismological Society of America*, Vol. 63, No. 2, pp. 501–516, 1973.

45. Campbell, K. W., "Near-Source Attenuation of Peak Horizontal Acceleration", *Bulletin of the Seismological Society of America*, Vol. 71, No. 6, pp. 2039–2070, 1981.

46. Joyner, W. B. and D. M. Boore, "Peak Horizontal Acceleration and Velocity from Strong-Motion Records Including Records from the 1979 Imperial Valley, California, Earthquake", *Bulletin of the Seismological Society of America*, Vol. 71, No. 6, pp. 2011–2038, 1981.

47. Ambraseys, N. N., K. u. Simpson and J. J. Bommer, "Prediction of Horizontal Response Spectra in Europe", *Earthquake Engineering & Structural Dynamics*, Vol. 25, No. 4, pp. 371–400, 1996.

48. Campbell, K. W., "Empirical Near-source Attenuation Relationships for Horizontal and Vertical Components of Peak Ground Acceleration, Peak Ground Velocity, and Pseudo-Absolute Acceleration Response Spectra", *Seismological Research Letters*, Vol. 68, No. 1, pp. 154–179, 1997.

49. Boore, D. M., W. B. Joyner and T. E. Fumal, “Equations for Estimating Horizontal Response Spectra and Peak Acceleration from Western North American Earthquakes: A Summary of Recent Work”, *Seismological Research Letters*, Vol. 68, No. 1, pp. 128–153, 1997.

50. Sadigh, K., C.-Y. Chang, J. Egan, F. Makdisi and R. R. Youngs, “Attenuation Relationships for Shallow Crustal Earthquakes Based on California Strong Motion Data”, *Seismological Research Letters*, Vol. 68, No. 1, pp. 180–189, 1997.

51. Zhao, J. X., J. Zhang, A. Asano, Y. Ohno, T. Oouchi, T. Takahashi, H. Ogawa, K. Irikura, H. K. Thio, P. G. Somerville *et al.*, “Attenuation Relations of Strong Ground Motion in Japan Using Site Classification Based on Predominant Period”, *Bulletin of the Seismological Society of America*, Vol. 96, No. 3, pp. 898–913, 2006.

52. Cauzzi, C. and E. Faccioli, “Broadband (0.05 to 20 s) Prediction of Displacement Response Spectra Based on Worldwide Digital Records”, *Journal of Seismology*, Vol. 12, No. 4, pp. 453–475, 2008.

53. Chiou, B.-J. and R. R. Youngs, “An NGA Model for the Average Horizontal Component of Peak Ground Motion and Response Spectra”, *Earthquake Spectra*, Vol. 24, No. 1, pp. 173–215, 2008.

54. Akkar, S. and J. J. Bommer, “Empirical Equations for the Prediction of PGA, PGV, and Spectral Accelerations in Europe, the Mediterranean Region, and the Middle East”, *Seismological Research Letters*, Vol. 81, No. 2, pp. 195–206, 2010.

55. Toro, G. R., “Modification of the Toro et al.(1997) Attenuation Equations for Large Magnitudes and Short Distances”, *Risk Engineering Technical Report*, Vol. 10, 2002.

56. Campbell, K. W., “Prediction of Strong Ground Motion Using the Hybrid Empirical Method and Its Use in the Development of Ground-Motion (Attenuation) Relations in Eastern North America”, *Bulletin of the Seismological Society of*

America, Vol. 93, No. 3, pp. 1012–1033, 2003.

57. Youngs, R., S.-J. Chiou, W. Silva and J. Humphrey, "Strong Ground Motion Attenuation Relationships for Subduction Zone Earthquakes", *Seismological Research Letters*, Vol. 68, No. 1, pp. 58–73, 1997.

58. Atkinson, G. M. and D. M. Boore, "Empirical Ground-Motion Relations for Subduction-Zone Earthquakes and Their Application to Cascadia and Other Regions", *Bulletin of the Seismological Society of America*, Vol. 93, No. 4, pp. 1703–1729, 2003.

59. Lin, P.-S. and C.-T. Lee, "Ground-Motion Attenuation Relationships for Subduction-Zone Earthquakes in Northeastern Taiwan", *Bulletin of the Seismological Society of America*, Vol. 98, No. 1, pp. 220–240, 2008.

60. Faccioli, E., M. Villani, M. Vanini and C. Cauzzi, "Mapping Seismic Hazard for the Needs of Displacement-Based Design: the Case of Italy", *Advances in Performance-Based Earthquake Engineering*, pp. 3–14, Springer, 2010.

61. Akkar, S. and Z. Çağnan, "A local Ground-Motion Predictive Model for Turkey, and Its Comparison with Other Regional and Global Ground-Motion Models", *Bulletin of the Seismological Society of America*, Vol. 100, No. 6, pp. 2978–2995, 2010.

62. Akkar, S., M. A. Sandıkkaya and J. J. Bommer, "Empirical Ground-Motion Models for Point-and Extended-Source Crustal Earthquake Scenarios in Europe and the Middle East", *Bulletin of Earthquake Engineering*, Vol. 12, No. 1, pp. 359–387, 2014.

63. Atkinson, G. M. and D. M. Boore, "Earthquake Ground-Motion Prediction Equations for Eastern North America", *Bulletin of the Seismological Society of America*, Vol. 96, No. 6, pp. 2181–2205, 2006.

64. Sesetyan, K., M. B. Demircioglu, T. Y. Duman, T. Can, S. Tekin, T. E. Azak and Ö. Z. Fercan, "A Probabilistic Seismic Hazard Assessment for the Turkish Territory—Part I: the Area Source Model", *Bulletin of Earthquake Engineering*, Vol. 16, No. 8, pp. 3367–3397, 2018.

65. Emre, Ö., T. Duman, S. Özalp, H. Elmacı, Ş. Olgun and F. Şaroğlu, "Active Fault Map of Turkey with Explanatory Text", *General Directorate of Mineral Research and Exploration Special Publication Series*, Vol. 30, 2013.

66. Duman, T. Y., T. Çan, Ö. Emre, F. Kadirioğlu, N. Başarır Baştürk, T. Kılıç, S. Arslan, S. Özalp, R. F. Kartal, D. Kalafat *et al.*, "Seismotectonic Database of Turkey", *Bulletin of Earthquake Engineering*, Vol. 16, No. 8, pp. 3277–3316, 2018.

67. Frankel, A. *et al.*, "Mapping Seismic Hazard in the Central and Eastern United States", *Seismological Research Letters*, Vol. 66, No. 4, pp. 8–21, 1995.

68. Megawati, K. and T.-C. Pan, "Ground-Motion Attenuation Relationship for the Sumatran Megathrust Earthquakes", *Earthquake Engineering & Structural Dynamics*, Vol. 39, No. 8, pp. 827–845, 2010.

69. García, D., S. K. Singh, M. Herráiz, M. Ordaz and J. F. Pacheco, "Inslab Earthquakes of Central Mexico: Peak Ground-Motion Parameters and Response Spectra", *Bulletin of the Seismological Society of America*, Vol. 95, No. 6, pp. 2272–2282, 2005.

70. Şengör, A., N. Görür and F. Şaroğlu, "Strike-Slip Faulting and Related Basin Formation in Zones of Tectonic Escape: Turkey as a Case Study", *SEPM Spec. Publ*, Vol. 17, pp. 227–264, 1985.

71. Barka, A. and K. Kadinsky-Cade, "Strike-Slip Fault Geometry in Turkey and Its Influence on Earthquake Activity", *Tectonics*, Vol. 7, No. 3, pp. 663–684, 1988.

72. Reilinger, R., S. McClusky, P. Vernant, S. Lawrence, S. Ergintav, R. Cakmak, H. Ozener, F. Kadirov, I. Guliev, R. Stepanyan *et al.*, "GPS Constraints on Continental Deformation in the Africa-Arabia-Eurasia Continental Collision Zone and Implications for the Dynamics of Plate Interactions", *Journal of Geophysical Research: Solid Earth*, Vol. 111, No. B5, 2006.

73. Aktug, B., J. Nocquet, A. Cingöz, B. Parsons, Y. Erkan, P. England, O. Lenk, M. Gürdal, A. Kilicoglu, H. Akdeniz *et al.*, "Deformation of Western Turkey from a Combination of Permanent and Campaign GPS data: Limits to Block-Like Behavior", *Journal of Geophysical Research: Solid Earth*, Vol. 114, No. B10, 2009.

74. Aktug, B., U. Dikmen, A. Dogru and H. Ozener, "Seismicity and Strain Accumulation Around Karliova Triple Junction (Turkey)", *Journal of Geodynamics*, Vol. 67, pp. 21–29, 2013.

75. Aktuğ, B., E. Parmaksız, M. Kurt, O. Lenk, A. Kılıçoğlu, M. A. Gürdal and S. Özdemir, "Deformation of Central Anatolia: GPS Implications", *Journal of Geodynamics*, Vol. 67, pp. 78–96, 2013.

76. Ketin, I., "Über die Tektonisch-Mechanischen Folgerungen aus den Grossen Anatolischen Erdbeben des Letzten Dezenniums", *Geologische Rundschau*, Vol. 36, No. 1, pp. 77–83, 1948.

77. McKenzie, D., "Active Tectonics of the Mediterranean Region", *Geophysical Journal International*, Vol. 30, No. 2, pp. 109–185, 1972.

78. McKenzie, D., "The East Anatolian Fault: A Major Structure in Eastern Turkey", *Earth and Planetary Science Letters*, Vol. 29, No. 1, pp. 189–193, 1976.

79. Sengör, A., "The North Anatolian Transform Fault: Its Age, Offset and Tectonic Significance", *Journal of the Geological Society*, Vol. 136, No. 3, pp. 269–282, 1979.

80. Şengör, A. M. C., "Türkiye'nin Neotektoniğinin Esasları", *Türkiye Jeoloji Kurumu Yayını*, Vol. 40, 1980.

81. Jackson, J. and D. McKenzie, "Active Tectonics of The Alpine—Himalayan Belt between Western Turkey and Pakistan", *Geophysical Journal International*, Vol. 77, No. 1, pp. 185–264, 1984.

82. Dewey, J., M. Hempton, W. Kidd, F. Saroglu and A. Şengör, "Shortening of Continental Lithosphere: the Neotectonics of Eastern Anatolia — A Young Collision Zone", *Geological Society, London, Special Publications*, Vol. 19, No. 1, pp. 1–36, 1986.

83. Arpat, E., "Nereden Çıktı Şimdi Bu Fay? Doğu Anadolu Fayı'nın İlginç Öyküsü", *Jeodergi*, Vol. 19, No. 19, pp. 15–20, 2020.

84. Arpat, E., *22 Mayıs 1971 Bingöl Depremi-Ön Rapor, Rept. 4697*, Tech. rep., Institute of Mineral Research and Exploration (in Turkish), 1971.

85. Ketin, İ., "Türkiye'nin Genel Tektonik Durumu ile Başlıca Deprem Bölgeleri Arasındaki İlişkiler", *Maden Tetkik ve Arama Dergisi*, Vol. 71, No. 71, 1968.

86. Allen, C. R., "Active Faulting in Northern Turkey, Division of Geological Science", *Calif. Inst. Technol. Contrib.*, Vol. 1577, p. 32, 1969.

87. Arpat, E. and F. Şaroğlu, "Doğu Anadolu Fayi ile İlgili Bazi gözlemler ve Düşünceler", *MTA Dergisi*, Vol. 78, pp. 33–39, 1972.

88. Duman, T. Y. and Ö. Emre, "The East Anatolian Fault: Geometry, Segmentation and Jog Characteristics", *Geological Society, London, Special Publications*, Vol. 372, No. 1, pp. 495–529, 2013.

89. Arpat, E. and F. Şaroğlu, "Türkiye'deki Bazı önemli Genç Tektonik Olaylar", *Türkiye Jeoloji Kurumu Bülteni*, Vol. 18, No. 1, pp. 91–101, 1975.

90. Taymaz, T., H. Eyidoğan and J. Jackson, “Source Parameters of Large Earthquakes in the East Anatolian Fault Zone (Turkey)”, *Geophysical Journal International*, Vol. 106, No. 3, pp. 537–550, 1991.

91. Westaway, R. and J. Arger, “The Gölbaºi basin, Southeastern Turkey: A Complex Discontinuity in A Major Strike-Slip Fault Zone”, *Journal of the Geological Society*, Vol. 153, No. 5, pp. 729–744, 1996.

92. Westaway, R., “Kinematics of the Middle East and Eastern Mediterranean Updated”, *Turkish Journal of Earth Sciences*, Vol. 12, No. 1, pp. 5–46, 2003.

93. Karabacak, V. and Ö. Yönlü, “Paleoseismic Behavior of the East Anatolian Fault Zone Between Gölbaşı and Türkoğlu: Implications on 900 Years of Seismic Quiescence”, *International Earth Science Colloquium on the Aegean Region, IESCA-2012*, p. 110, 2012.

94. Hubert-Ferrari, A., L. Lamair, S. Hage, S. Schmidt, M. N. Çağatay and U. Avşar, “A 3800 Yr Paleoseismic Record (Lake Hazar Sediments, Eastern Turkey): Implications for the East Anatolian Fault Seismic Cycle”, *Earth and Planetary Science Letters*, Vol. 538, p. 116152, 2020.

95. Westaway, R. and J. Arger, “Kinematics of the Malatya–Ovacik Fault Zone”, *Geodinamica Acta*, Vol. 14, No. 1-3, pp. 103–131, 2001.

96. Şaroğlu, F., Ö. Emre and A. Boray, “Türkiye’nin diri fayları ve Depremsellikleri”, *MTA. Rap*, Vol. 394, 1987.

97. Şaroğlu, F., Ö. Emre and İ. Kuşçu, “The East Anatolian Fault Zone of Turkey”, *Annales Tectonicae, Special Issue, VI*, pp. 99–125, 1992.

98. Barka, A., “Slip Distribution Along the North Anatolian Fault Associated with the Large Earthquakes of the Period 1939 to 1967”, *Bulletin of the Seismological Society of America*, Vol. 86, No. 5, pp. 1238–1254, 1996.

99. Kondo, H., Y. Awata, O. Emre, A. Dogan, S. Ozalp, F. Tokay, C. Yıldırım, T. Yoshioka and K. Okumura, "Slip Distribution, Fault Geometry, and Fault Segmentation of the 1944 Bolu-Gerede Earthquake Rupture, North Anatolian Fault, Turkey", *Bulletin of the Seismological Society of America*, Vol. 95, No. 4, pp. 1234–1249, 2005.

100. Lettis, W., J. Bachhuber, R. Witter, C. Brankman, C. Randolph, A. Barka, W. Page and A. Kaya, "Influence of Releasing Step-Overs on Surface Fault Rupture and Fault Segmentation: Examples from the 17 August 1999 Izmit Earthquake on the North Anatolian Fault, Turkey", *Bulletin of the Seismological Society of America*, Vol. 92, No. 1, pp. 19–42, 2002.

101. Hempton, M., J. Dewey and F. Şaroğlu, "The East Anatolian Transform Fault: Along Strike Variations in Geometry and Behavior", *EOS Trans.*, Vol. 62, p. 393, 1981.

102. Herece, E., "Dogu Anadolu Fayı (DAF) Atlası (Atlas of the East Anatolian Fault (EAF))", *General Directorate of Mineral research and Exploration (MTA)*, 2008.

103. Gülen, L., A. Barka and M. Toksöz, "Continental Collision and Related Complex Deformation: Maras Triple Junction and Surrounding Structures, SE Turkey", *Hacettepe University Earth Science Journal*, Vol. 14, pp. 319–336, 1987.

104. Karig, D. and H. KOZLU, "Late Palaeogene-Neogene Evolution of the Triple Junction Region near Maraş, South-Central Turkey", *Journal of the Geological Society*, Vol. 147, No. 6, pp. 1023–1034, 1990.

105. Perinçek, D. and I. Çemen, "The Structural Relationship Between the East Anatolian and Dead Sea Fault Zones in Southeastern Turkey", *Tectonophysics*, Vol. 172, No. 3-4, pp. 331–340, 1990.

106. Cetin, H., H. Güneyli and L. Mayer, "Paleoseismology of the Palu–Lake Hazar Segment of the East Anatolian Fault Zone, Turkey", *Tectonophysics*, Vol. 374,

No. 3-4, pp. 163–197, 2003.

107. Karabacak, V., E. Altunel, M. Meghraoui and H. Akyüz, "Field Evidences from Northern Dead Sea Fault Zone (South Turkey): New Findings for the Initiation Age and Slip Rate", *Tectonophysics*, Vol. 480, No. 1-4, pp. 172–182, 2010.

108. Akyuz, H. S., E. Altunel, V. Karabacak and C. C. Yalciner, "Historical Earthquake Activity of the Northern Part of the Dead Sea Fault Zone, Southern Turkey", *Tectonophysics*, Vol. 426, No. 3-4, pp. 281–293, 2006.

109. McGuire, R. K., *Seismic Hazard and Risk Analysis*, Earthquake Engineering Research Institute, Boulder, Colorado, 2004.

110. Baker, J. W., "An Introduction to Probabilistic Seismic Hazard Analysis", *White Paper Version*, Vol. 2, No. 1, p. 79, 2013.

111. Allin Cornell, C. and S. R. Winterstein, "Temporal and Magnitude Dependence in Earthquake Recurrence Models", *Bulletin of the Seismological Society of America*, Vol. 78, No. 4, pp. 1522–1537, 1988.

112. Field, E. H., G. P. Biasi, P. Bird, T. E. Dawson, K. R. Felzer, D. D. Jackson, K. M. Johnson, T. H. Jordan, C. Madden, A. J. Michael *et al.*, "Long-Term Time-Dependent Probabilities for the Third Uniform California Earthquake Rupture Forecast (UCERF3)", *Bulletin of the Seismological Society of America*, Vol. 105, No. 2A, pp. 511–543, 2015.

113. Gutenberg, B. and C. F. Richter, "Frequency of Earthquakes in California", *Bulletin of the Seismological society of America*, Vol. 34, No. 4, pp. 185–188, 1944.

114. Akinci, A., D. Perkins, A. M. Lombardi and R. Basili, "Uncertainties in Probability of Occurrence of Strong Earthquakes for Fault Sources in the Central Apennines, Italy", *Journal of seismology*, Vol. 14, No. 1, pp. 95–117, 2010.

115. Reid, H. F., "The Mechanics of the earthquake, in The California Earthquake of April 18, 1906", *Report of the State Earthquake Investigation Commission*, Vol. 2, pp. 16–28, 1910.

116. Field, E. H., K. R. Milner, J. L. Hardebeck, M. T. Page, N. van der Elst, T. H. Jordan, A. J. Michael, B. E. Shaw and M. J. Werner, "A Spatiotemporal Clustering Model for the Third Uniform California Earthquake Rupture Forecast (UCERF3-ETAS): Toward An Operational Earthquake Forecast", *Bulletin of the Seismological Society of America*, Vol. 107, No. 3, pp. 1049–1081, 2017.

117. Hagiwara, Y., "Probability of Earthquake Occurrence As Obtained from a Weibull Distribution Analysis of Crustal Strain", *Tectonophysics*, Vol. 23, No. 3, pp. 313–318, 1974.

118. Nishenko, S. P. and R. Buland, "A Generic Recurrence Interval Distribution for Earthquake Forecasting", *Bulletin of the Seismological Society of America*, Vol. 77, No. 4, pp. 1382–1399, 1987.

119. Ellsworth, W. L., M. V. Matthews, R. M. Nadeau, S. P. Nishenko, P. A. Reasenberg and R. W. Simpson, "A Physically-Based Earthquake Recurrence Model for Estimation of Long-Term Earthquake Probabilities", *US Geological Survey Open-File Report*, Vol. 99, No. 522, p. 22, 1999.

120. Matthews, M. V., W. L. Ellsworth and P. A. Reasenberg, "A Brownian Model for Recurrent Earthquakes", *Bulletin of the Seismological Society of America*, Vol. 92, No. 6, pp. 2233–2250, 2002.

121. Abrahamson, N. A., "State of the Practice of Seismic Hazard Evaluation", *ISRM International Symposium*, OnePetro, 2000.

122. Convertito, V., L. Faenza, M. Beer, I. Kougioumtzoglou, E. Patelli and I. Au, "Earthquake Recurrence", *Encyclopedia of Earthquake Engineering; Beer, M., Kougioumtzoglou, IA, Patelli, E., Au, SK, Eds*, 2014.

123. Field, E. H., T. E. Dawson, K. R. Felzer, A. D. Frankel, V. Gupta, T. H. Jordan, T. Parsons, M. D. Petersen, R. S. Stein, R. Weldon *et al.*, "Uniform California Earthquake Rupture Forecast, Version 2 (UCERF 2)", *Bulletin of the Seismological Society of America*, Vol. 99, No. 4, pp. 2053–2107, 2009.

124. Weichert, D. H., "Estimation of the Earthquake Recurrence Parameters for Unequal Observation Periods for Different Magnitudes", *Bulletin of the Seismological Society of America*, Vol. 70, No. 4, pp. 1337–1346, 1980.

125. Molnar, P., "Earthquake Recurrence Intervals and Plate Tectonics", *Bulletin of the Seismological Society of America*, Vol. 69, No. 1, pp. 115–133, 1979.

126. Anderson, J. G., S. G. Wesnousky and M. W. Stirling, "Earthquake Size As A function of Fault Slip Rate", *Bulletin of the Seismological Society of America*, Vol. 86, No. 3, pp. 683–690, 1996.

127. Stirling, M., T. Goded, K. Berryman and N. Litchfield, "Selection of Earthquake Scaling Relationships for Seismic-Hazard analysis", *Bulletin of the Seismological Society of America*, Vol. 103, No. 6, pp. 2993–3011, 2013.

128. Hofmann, R. B., "Individual Faults Can't Produce A Gutenberg-Richter Earthquake Recurrence", *Engineering geology*, Vol. 43, No. 1, pp. 5–9, 1996.

129. Wesnousky, S., C. Scholz, K. Shimazaki and T. Matsuda, "Earthquake Frequency Distribution and the Mechanics of Faulting", *Journal of Geophysical Research: Solid Earth*, Vol. 88, No. B11, pp. 9331–9340, 1983.

130. Bungum, H., "Numerical Modelling of Fault Activities", *Computers & geosciences*, Vol. 33, No. 6, pp. 808–820, 2007.

131. Weatherill, G., *OpenQuake Hazard Modeller's Toolkit - User Guide*, Tech. rep., Global Earthquake Model (GEM), 2014.

132. Hanks, T. C. and H. Kanamori, "A Moment Magnitude Scale", *Journal of Geophysical Research: Solid Earth*, Vol. 84, No. B5, pp. 2348–2350, 1979.

133. Hamiel, Y. and Y. Fialko, "Structure and Mechanical Properties of Faults in the North Anatolian Fault System from InSAR Observations of Coseismic Deformation Due to the 1999 Izmit (Turkey) Earthquake", *Journal of Geophysical Research: Solid Earth*, Vol. 112, No. B7, 2007.

134. Stirling, M., G. McVerry, M. Gerstenberger, N. Litchfield, R. Van Dissen, K. Berryman, P. Barnes, L. Wallace, P. Villamor, R. Langridge *et al.*, "National Seismic Hazard Model for New Zealand: 2010 Update", *Bulletin of the Seismological Society of America*, Vol. 102, No. 4, pp. 1514–1542, 2012.

135. Kagan, Y., D. D. Jackson, R. J. Geller *et al.*, "Characteristic Earthquake Model, 1884–2011, RIP", *arXiv preprint arXiv:1207.4836*, 2012.

136. Geller, R. J., F. Mulargia and P. B. Stark, "Why We Need A New Paradigm of Earthquake Occurrence", *Subduction Dynamics: from Mantle Flow to Mega Disasters*, pp. 183–191, 2015.

137. Mulargia, F., P. B. Stark and R. J. Geller, "Why Is Probabilistic Seismic Hazard Analysis (PSHA) Still Used?", *Physics of the Earth and Planetary Interiors*, Vol. 264, pp. 63–75, 2017.

138. Ishibe, T. and K. Shimazaki, "Characteristic Earthquake Model and Seismicity Around Late Quaternary Active Faults in Japan", *Bulletin of the Seismological Society of America*, Vol. 102, No. 3, pp. 1041–1058, 2012.

139. Field, E. H., R. J. Arrowsmith, G. P. Biasi, P. Bird, T. E. Dawson, K. R. Felzer, D. D. Jackson, K. M. Johnson, T. H. Jordan, C. Madden *et al.*, "Uniform California Earthquake Rupture Forecast, Version 3 (UCERF3)—The Time-Independent Model", *Bulletin of the Seismological Society of America*, Vol. 104, No. 3, pp. 1122–1180, 2014.

140. Boncio, P., G. Lavecchia and B. Pace, "Defining a Model of 3D Seismogenic Sources for Seismic Hazard Assessment Applications: the Case of Central Apennines (Italy)", *Journal of Seismology*, Vol. 8, No. 3, pp. 407–425, 2004.

141. Pace, B., F. Visini and L. Peruzza, "FiSH: MATLAB Tools to Turn Fault Data into Seismic-Hazard Models", *Seismological Research Letters*, Vol. 87, No. 2A, pp. 374–386, 2016.

142. Visini, F., A. Valentini, T. Chartier, O. Scotti and B. Pace, "Computational Tools for Relaxing the Fault Segmentation in Probabilistic Seismic Hazard Modelling in Complex Fault Systems", *Pure and Applied Geophysics*, Vol. 177, No. 5, pp. 1855–1877, 2020.

143. Parsons, T. and E. L. Geist, "Is There A Basis for Preferring Characteristic Earthquakes Over A Gutenberg–Richter Distribution in Probabilistic Earthquake Forecasting?", *Bulletin of the Seismological Society of America*, Vol. 99, No. 3, pp. 2012–2019, 2009.

144. DePolo, C. M., D. G. Clark, D. B. Slemmons and A. R. Ramelli, "Historical Surface Faulting in the Basin and Range Province, Western North America: Implications for Fault Segmentation", *Journal of structural Geology*, Vol. 13, No. 2, pp. 123–136, 1991.

145. Schwartz, D. P., P. J. Haeussler, G. G. Seitz and T. E. Dawson, "Why the 2002 Denali Fault Rupture Propagated Onto the Totschunda Fault: Implications for Fault Branching and Seismic Hazards", *Journal of Geophysical Research: Solid Earth*, Vol. 117, No. B11, 2012.

146. Iezzi, F., G. Roberts, J. F. Walker and I. Papanikolaou, "Occurrence of Partial and Total Coseismic Ruptures of Segmented Normal Fault Systems: Insights from the Central Apennines, Italy", *Journal of Structural Geology*, Vol. 126, pp. 83–99, 2019.

147. Murru, M., A. Akinci, G. Falcone, S. Pucci, R. Console and T. Parsons, "M≥ 7 Earthquake Rupture Forecast and Time-Dependent Probability for the Sea of Marmara Region, Turkey", *Journal of Geophysical Research: Solid Earth*, Vol. 121, No. 4, pp. 2679–2707, 2016.

148. Doğru, A., F. Bulut, C. Yaltırak and B. Aktuğ, "Slip Distribution of the 2020 Elazığ Earthquake (M w 6.75) and Its Influence on Earthquake Hazard in the Eastern Anatolia", *Geophysical Journal International*, Vol. 224, No. 1, pp. 389–400, 2021.

149. Wells, D. L. and K. J. Coppersmith, "New Empirical Relationships among Magnitude, Rupture Length, Rupture Width, Rupture Area, and Surface Displacement", *Bulletin of the Seismological Society of America*, Vol. 84, No. 4, pp. 974–1002, 1994.

150. Leonard, M., "Earthquake Fault Scaling: Self-Consistent Relating of Rupture Length, Width, Average Displacement, and Moment Release", *Bulletin of the Seismological Society of America*, Vol. 100, No. 5A, pp. 1971–1988, 2010.

151. Hanks, T. C. and W. H. Bakun, "M–log A Models and Other Curiosities", *Bulletin of the Seismological Society of America*, Vol. 104, No. 5, pp. 2604–2610, 2014.

152. Ambraseys, N. and J. Jackson, "Faulting Associated with Historical and Recent Earthquakes in the Eastern Mediterranean Region", *Geophysical Journal International*, Vol. 133, No. 2, pp. 390–406, 1998.

153. Nalbant, S. S., J. McCloskey, S. Steacy and A. A. Barka, "Stress Accumulation and Increased Seismic Risk in Eastern Turkey", *Earth and Planetary Science Letters*, Vol. 195, No. 3-4, pp. 291–298, 2002.

154. Emre, Ö., S. Özalp, C. Yıldırım, V. Özaksoy and A. Doğan, "12 ve 14 Mart 2005 Karlıova Depremlerinin Değerlendirilmesi", *Maden Tetkik Arama Enstitüsü, Ankara*, 12.

155. Seymen, İ. and A. Aydin, "Bingöl Deprem Fayı ve Bunun Kuzey Anadolu Fay Zonu ile İlişkisi (The Bingöl Earthquake Fault and Its Relation to the North Anatolian Fault)", *MTA Dergisi*, Vol. 79, 1976.

156. Aktug, B., H. Ozener, A. Dogru, A. Sabuncu, B. Turgut, K. Halicioglu, O. Yilmaz and E. Havazli, "Slip Rates and Seismic Potential on the East Anatolian Fault System Using an Improved GPS Velocity Field", *Journal of Geodynamics*, Vol. 94, pp. 1–12, 2016.

157. Abou Karaki, N., *Synthèse et Carte Sismotectonique des Pays de la Bordure Orientale de la Méditerranée: sismicité du système de Failles du Jourdain-Mer Morte*, Ph.D. Thesis, Université Louis Pasteur (Strasbourg)(1971-2008), 1987.

158. Khair, K., G. F. Karakaisis and E. E. Papadimitriou, "Seismic Zonation of the Dead Sea Transform Fault Area", *Annali di Geofisica*, Vol. 43, No. 1, pp. 61–79, 2000.

159. Kafka, A. L., "Does Seismicity Delineate Zones Where Future Large Earthquakes Are Likely to Occur in Intraplate Environments?", *Special Papers-Geological Society of America*, Vol. 425, p. 35, 2007.

160. Sucuoğlu, H. and S. Akkar, *Basic Earthquake Engineering*, Springer Cham, Switzerland, 2014.

161. Chiou, B. S.-J. and R. R. Youngs, "Update of the Chiou and Youngs NGA Model for the Average Horizontal Component of Peak Ground Motion and Response Spectra", *Earthquake Spectra*, Vol. 30, No. 3, pp. 1117–1153, 2014.